The circumstellar environment of eruptive young stars

PhD thesis

Nikoletta Sipos

submitted to

PhD School of Physics,
Particle- and Astrophysics Programme,
Eötvös Loránd University, Faculty of Science

Head of PhD School: Prof. Ferenc Csikor
Head of PhD Programme: Prof. Ferenc Csikor

Thesis supervised by:
Mária Kun, DSc (scientific advisor)

Advised by:
Péter Ábrahám, DSc (scientific advisor, director)

Konkoly Observatory of the Hungarian Academy of Sciences
Budapest, 2011

Foreword

The birth process of stars and planets, including our Solar-system, has always puzzled astronomers and non-astronomers alike. Recently, this topic has become probably the most dynamically developing field in astronomy. Driven by the incredible improvement of infrared observational techniques in the past two–three decades, advances of interpretation methods, and elaboration of computer-based models, a general qualitative picture of early stellar and planetary evolution arose. Still, we are left with many riddles and unresolved details.

This thesis contributes to the study of an important phase of the star formation process. During my PhD research I investigated the structure and evolution of circumstellar disk–envelope systems. Especially, I focused on the circumstellar environment of the class of low-mass eruptive young stars.

Solar-type stars collect their material from the parental cloud mostly through a circumstellar accretion disk, which together with the surrounding remains of the natal cloud or envelope, determines the conditions for the evolution of the stellar system. Besides governing stellar build-up, accretion disks also provide the birth-place for planets. The dramatic and rather spectacular outbursts of young eruptive systems, the main objects of interest in this thesis, are attributed to runaway mass-accretion. This indicates that the accumulation of stellar material is an episodic process and for limited time periods, a significant amount of material is delivered onto the stellar surface. The outbursts have a major effect on the evolution of stars, and also modify the structure and dust composition of the circumstellar disk, affecting planet formation. The nature of changes during the outbursts was one of the main topics of my research.

The other question I examined was whether young eruptive stars are exceptional among regular low-mass T Tauri stars, which would yield that eruptive phenomena are only important in the evolution of a subclass of stars. On the other hand, if they show no distinct properties in quiescence, it indicates, that they are indeed typical among young stars, and eruptive phases occur during the early evolution of all Sun-like stars. In this case, eruptions have a general significance in the birth process of all low-mass stars and their planets. In the hope of finding answers to these still open issues, I analyzed systems on different spatial scales both in outburst and quiescence, and examined their basic properties and evolutionary states.

Contents

Chapter 1

Introduction

In this introduction I briefly describe star formation with an emphasis on the early evolution of circumstellar disks and envelopes. I summarize the basic properties of eruptive stars and theoretical models for the outburst mechanism.

1.1 The early evolution of Sun-like stars

Young stars are born inside huge clouds of interstellar gas and dust, mainly consisting of molecular hydrogen. Sizes and masses of these star-forming regions, called molecular clouds, vary greatly. The smallest are $\leq 1\,\mathrm{pc}$ and $\leq 10\,\mathrm{M}_\odot$, while giant molecular clouds and molecular cloud complexes have sizes of $\sim$100 pc and masses of $\sim 10^6\,\mathrm{M}_\odot$ (Hartmann, 2009). Some examples of the closest, and most studied star forming regions are presented in Fig. 1.1. Namely, they are Taurus, Orion and Lupus, at a distance of $\sim$ 100–400 pc containing the objects discussed in later chapters. We can see that the spatial structure of the clouds is not homogeneous. They contain clumps and filaments of dense gas and dust, which appear to be dark bands at optical wavelengths due to the obscuration of dust. However in the infrared, where we can see thermal radiation of the dust, these dense regions are bright. Star-birth is clearly localized into these structures (Fig. 1.1 bottom panel). The possible seeds of protostars are some of the densest and coldest clumps, called molecular cloud cores, that become self-gravitating. They typically have temperatures of 10–20 K and densities of 2×10^3–$10^5\,\mathrm{cm}^{-3}$. The number of cloud cores differs from cloud to cloud, and core properties also vary. As a result stars of different nature are born.

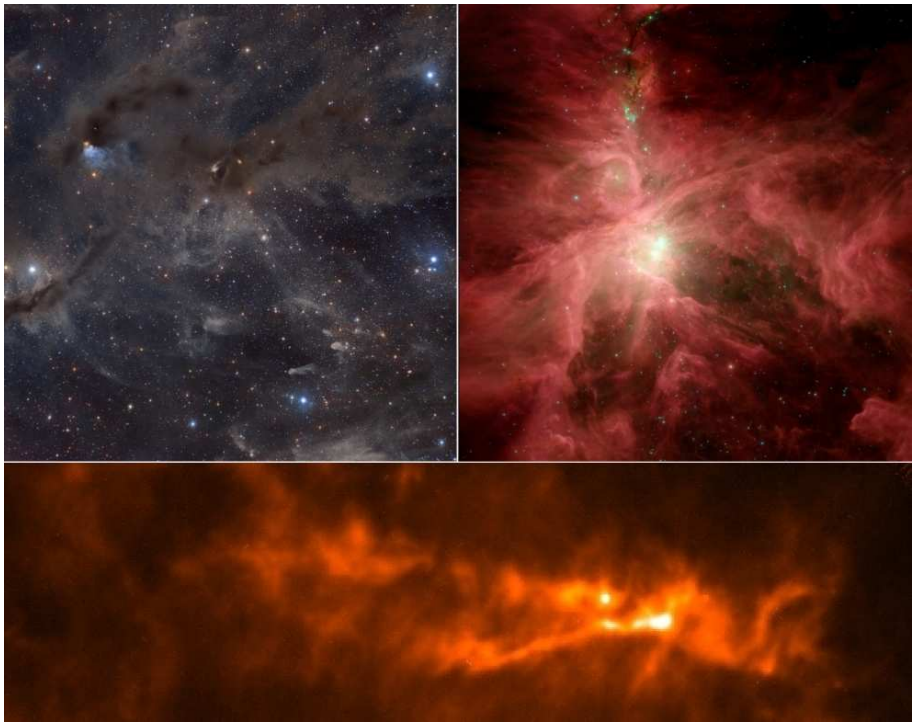

Figure 1.1 – Three of the best studied and nearest star forming regions seen at various wavelengths. Objects discussed in the thesis are located in these star forming regions. *Upper left:* Dust complex in the Taurus cloud (Credit: John Davis, astrophotographer). Dark regions in the image mark dense, obscuring dust. *Upper right:* Mid-infrared view of the Orion Nebula taken with the IRAC instrument of Spitzer Space Telescope (credit: NASA/JPL-Caltech/Harvard-Smithsonian CfA). Reddish colors show dense, dusty birthplace of young stars still embedded, bluish stars are more evolved and already got rid of their natal cloud. *Bottom:* Far-infrared image of the Lupus III complex taken by ESA's Herschel Space Observatory (credit: Pezzuto et al. 2010). The bright regions show the filamentary structure of the cloud. The brightest source is a deeply embedded very young object.

In the following I summarize the steps of star-birth in a nutshell, mostly based on the textbook of Hartmann (2009) and recent excellent reviews of Armitage (2011), Williams & Cieza (2011), Dullemond & Monnier (2010), and McKee & Ostriker (2007).

Evolution and also the early life of stars strongly depend on their mass. High-mass stars ($\geq 8\,M_\odot$), born out of massive cores, pass through the initial stages of their formation rapidly, and exhaust their hydrogen resources quickly. While for a star of $1\,M_\odot$ it takes about 50 million years to reach the main-sequence, a $10\,M_\odot$ star reaches it in only 100,000 years. Meanwhile, at the other end of the stellar

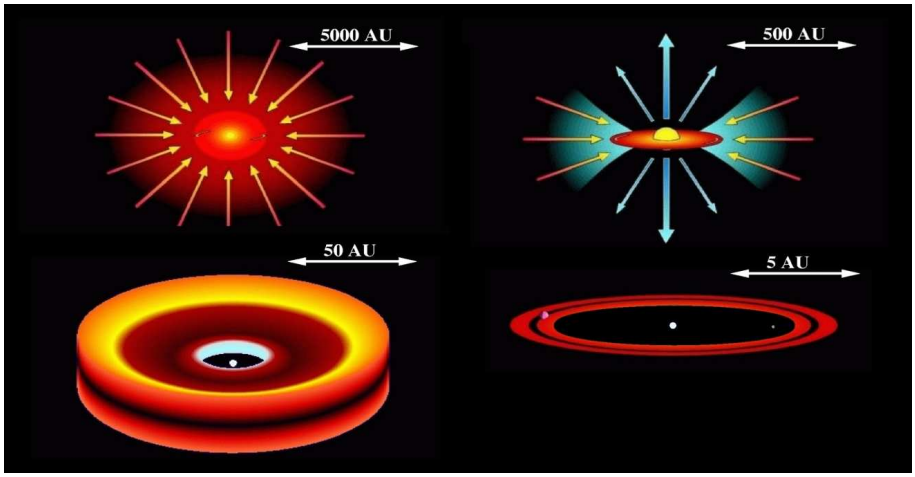

Figure 1.2 – Sketch of different stages of star formation and approximate spatial scales for a solar-type star. Collapse begins at t=0, the embedded accretion phase with outflows lasts roughly from 10^4 yr to a couple of times 10^5 yr, the main accretion phase on average lasts for 3 Myr, but individual objects show large variations from these timescales. (Image credit: A. Natta, M. McCraughrean, C. Dominik, V. Icke)

mass-range, brown dwarfs (0.08–0.01 $M_\odot$) evolve on a much longer timescale and they never heat up enough to be able to start hydrogen fusion. Even though details differ, it seems that the most important steps of the formation process are similar for stars with intermediate and low masses (2–8 $M_\odot$, called Herbig Ae/Be stars and 0.08–2 $M_\odot$, called T Tauri stars, respectively) and brown dwarfs. In the following, I will describe the star formation process for low-mass stars as our Sun. The star formation process is best understood in case of these stars, and also the objects discussed in this thesis belong to this category.

Molecular cloud cores are often found in clusters, and asymmetric cores may fragment during their collapse phase. As a result, most stars form in groups or clusters rather than in isolation. Also they are often members of binaries or multiple stellar systems. The early evolution of stars, however is most well-known in the simple case of isolated star formation, so in the following I will describe the birth of isolated low-mass stars. The process is likely similar in cluster environments as well, though interaction among members makes it more complex. A sketch of the steps of the star formation process is presented in Fig. 1.2.

Low-mass stars are born from cloud fragments of a few solar masses and sizes of a few times 0.1 pc, where turbulent motion is reduced, compared to the mostly

supersonic turbulence in the cloud. The molecular cloud cores become unstable, gravity is no longer balanced by the internal pressure forces of thermal gas pressure, turbulent motions and magnetic fields. As a result, material falls almost at free-fall velocities towards the centre, the core collapses. At the beginning, the collapse is isothermal. However, during this process the optical depth increases, until eventually material becomes opaque enough to trap its own radiation in the inner regions, at $\sim 10^4$ yr after the onset of the collapse. Due to the released gravitational energy during the collapse gas and dust in the central region heat up. As a consequence, the thermal pressure overcomes gravity, and the collapse in the center stops, the first core forms. The mass of the first core is $\sim 5 \times 10^{-2}\,\mathrm{M}_\odot$, still very small compared to the final mass of the star. On the other hand, its radius of $\sim 5\,\mathrm{AU}$ is still much larger than that of a typical Sun-like star. Subsequently, the core slowly contracts, while its temperature continues to increase. When the temperature becomes high enough to dissociate hydrogen molecules ($\sim 2000\,\mathrm{K}$), the core becomes unstable, and a second collapse results in a protostar to form, having radii of a couple of $\mathrm{R}_\odot$, high central temperatures of $\sim 10^5\,\mathrm{K}$ and densities of $\sim 10^{-2}\,\mathrm{gcm}^{-3}$.

The above presented picture however is modified by rotational effects. Cores have an initial rotation and due to the very quick collapse, angular momentum cannot be transferred efficiently. Soon after the start of the collapse, insufficient angular momentum transfer and angular momentum conservation causes a flattened structure, a disk to form in the midplane (perpendicular to the rotational axis), along with the stellar core. Disks are already present within 10^4 yr after the start of the collapse, deep inside the remains of the natal cloud surrounding the star–disk system, the so-called envelope. After the disk is formed, infalling material reaches the disk first, and it is accreted onto the star through the disk, while angular momentum is transported to external regions. The future star gathers most of its mass through this protoplanetary accretion disk. At the beginning of the protostellar phase the disk-mass grows rapidly.

After the disk forms, it remains embedded in the envelope for a typical period of 0.1–0.5 Myr. Contrary to initial theoretical assumptions, observations show that during the embedded phase, disk masses do not increase steadily with time. It seems that disks form quickly, within $\sim 10^4$ yr and later their masses remain constant

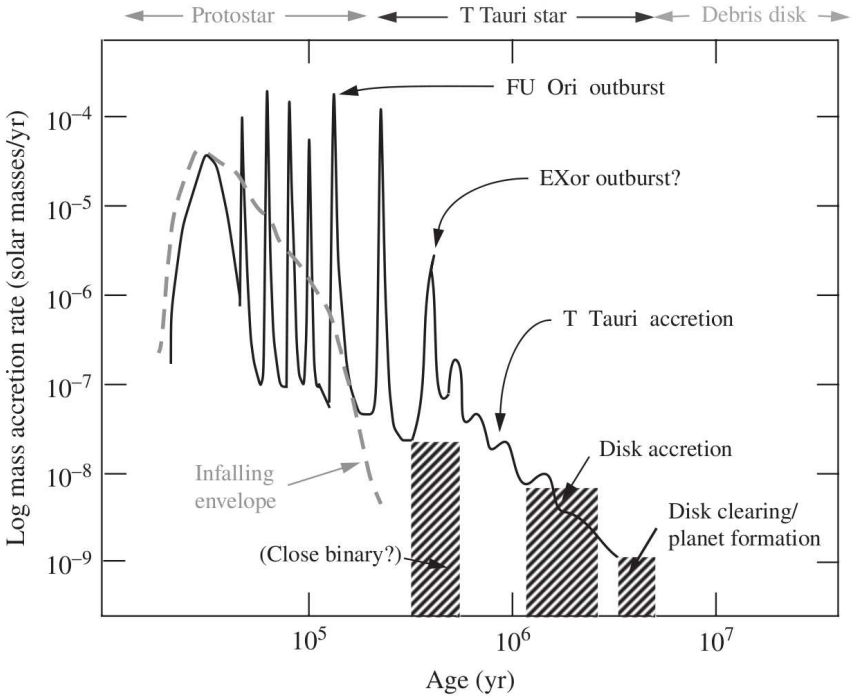

Figure 1.3 – Sketch of estimated mass accretion rates during the early evolution of a solar-type star. Individual objects, however may have very different accretion history, and there is a large uncertainity in characteristic ages as well. (Image credit: Hartmann 2009.)

through the early evolution. This would imply that material is transported onto the star at the same rate as infall happens onto the disk. However, observations do not support this assumption. If accretion was as rapid as mass infall on the disk, young systems would be about an order of magnitude more luminous, than what is actually observed. Supposing that mass transfer to the star is episodic resolves this problem. In this picture, the rate at which material is accumulated in the disk is larger than the accretion rate from the disk onto the star, resulting in piled-up matter in the disk. This might lead to disk instabilities and sporadic runaway accretion events (Fig. 1.3). The idea, besides the observed generally low luminosities among young stellar objects is also supported by the observed random high-accretion activities seen as FU Orionis-type (FUor) outbursts (see details in Sect. 1.2). During these periods the typical accretion rates of 10^{-9}–$10^{-7}\,\mathrm{M_\odot yr^{-1}}$ may rise up to $10^{-4}\,\mathrm{M_\odot yr^{-1}}$, thus during an eruption a significant amount of matter, $10^{-2}\,\mathrm{M_\odot}$ may be transported onto the star.

During the embedded phase, as a result of strong accretion, young stellar objects (YSOs) might develop bipolar outflows, in which material is ejected from the inner disk surface, and starts clearing away polar regions of the dusty circumstellar envelope, and forms an outflow cavity. The density and mass of the envelope gradually decreases, it feeds the disk until its material is completely used up or diminishes. Simultaneously, the star is built up and once it becomes hot enough ($T \sim 10^6$ K), it starts to burn deuterium. The young pre-main sequence star becomes visible, and appears on the Hertzsprung-Russell diagram (HRD) at the birth-line.

After the circumstellar envelope diminishes, infall onto the disk ceases due to the lack of a reservoir of material. At this time, the mass of the disk is only a small fraction of that of the young star. During this phase the disk goes through an evolution. Accretion onto the central star continues, and at the same time the primordial disk (the gas-rich circumstellar disk composed of matter originating in the interstellar medium but processed through the star/disk-forming accretion shock (Evans et al., 2009)) slowly starts to dissipate and first large grains, then seeds of planets start to form within it. Disk evolution and dispersal is driven by several different mechanisms, which are described below. The main steps of disk evolution are presented in Fig. 1.4.

1. *Accretion from the disk onto the star* — Viscous accretion is generally the most relevant process during primordial disk evolution. During accretion, mass spirals inwards onto the pre-main sequence star, and in the meantime angular momentum needs to be transported to larger radii. The simplest model for disk accretion is that of a geometrically thin disk treated as a viscous fluid, where the vertical scale height h in a geometrically thin disk is much smaller than the outer radius of the disk r_{out}. This approximation predicts, that while accreting material onto the star, the disk is constantly spreading outwards. The source of viscosity is still subject to debate, candidates include magneto-rotational instability of weakly magnetized disks, self-gravity, and hydrodynamic instabilities possibly contribute as well. The most widely used classical approach of Shakura & Sunyaev (1973), commonly referred to as the 'α-prescription', does not specify the source of viscosity ν, only treats it as $\nu = \alpha c_s h$, where c_s is the isothermal sound speed and α is a dimensionless

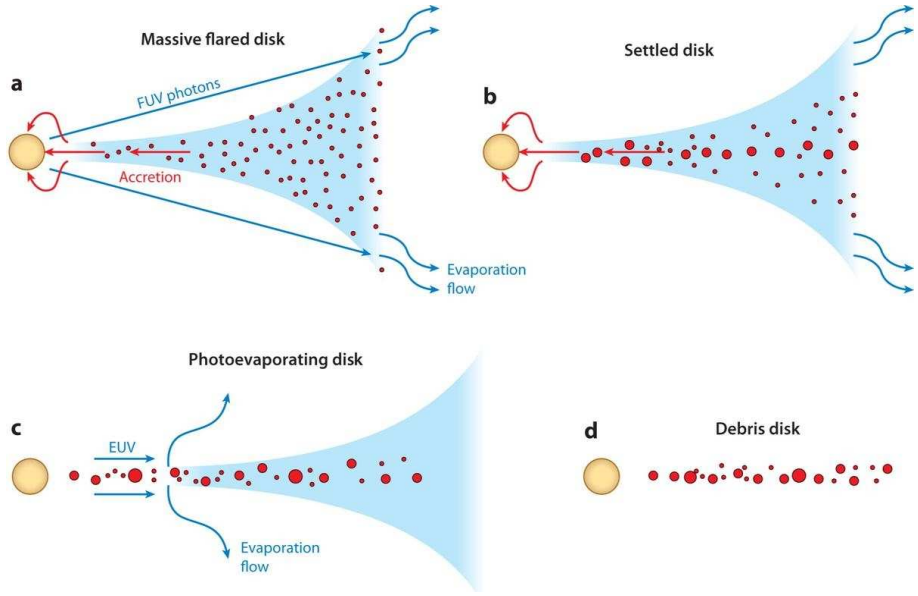

Figure 1.4 – Evolutionary phases of protoplanetary disks. *(a)* main accreting phase of the disk, having a typical flaring shape *(b)* dust particles coagulate and larger grains settle towards the mid-plane, causing the scale height of the disk to reduce *(c)* at sufficiently low accretion rates the innner disk is dissipated by photoevaporation, accretion stops *(d)* a debris disk forms from dust due to collisions of larger bodies. (Image credit: Williams & Cieza 2011.)

constant, introduced to represent the uncertainties. The parameter is often taken to be of the order of 10^{-2}. The great advantage of this model is its simplicity, though it seems that none of the processes actually driving viscosity behaves accordingly. However, by taking α to be constant, the evolution of the disks and their thermal structure is easy to describe. The temperature structure of an α-disk is

$$T_{eff}^4 = \frac{3GM_\star \dot{M}}{8\pi\sigma r^3}\left[1-\sqrt{\frac{r_{in}}{r}}\right], \tag{1.1}$$

which is widely used to model observations, including the models used in later chapters. In the most widely accepted picture of magnetospheric accretion, the accretion disk does not extend in to the stellar surface. It is truncated by the magnetic field and inward of this truncation radius of typically a couple of stellar radii (Calvet & Gullbring, 1998), accreted material reaches the stellar surface along the magnetic field lines, producing hot spots covering a varying fraction of 0.1–20% of the stellar surface (Calvet & Gullbring, 1998). A schematic structure of a typical disk during the main accretion phase is

presented in Fig. 1.5.

2. *Photoevaporation of the disk* — Photoevaporation is driven by energetic X-ray and UV photons originating either from the central star or from nearby massive stars outside of the system. Photons coming from the central star start eroding the inner disk, while photons from outside sources act on the outer disk. Photoevaporation from the central young star becomes important, once the viscous accretion rate drops below $\sim 10^{-10} - 10^{-9}\,\mathrm{M}_{\odot}/\mathrm{yr}$ and energetic photons become capable of entering the inner disk. As a result, an inner hole forms in the disk around the young star, which makes it possible for the high-energy photons to act on the outer disk as well. This process completely stops accretion, and after a short transitional phase, a gas-poor optically thin disk is left behind (Fig. 1.4, *c*).

3. *Grain growth, dust settling and coagulation of larger particles/bodies* — Simultaneously with the evolution of the gas content of the circumstellar disk, solid particles also change. Dust provides material for the build-up of planets and smaller bodies found in planetary systems. There is observational evidence for grain growth within the protoplanetary disks from sub-micron sizes to millimeter-centimeter range (Fig. 1.4, *b*). As grains grow to larger bodies, they settle towards the midplane, where they grow to rocks and planetesimals and eventually they might become planets.

4. *Dynamical interaction with sub-stellar companions* — In case a (sub)stellar or planetary companion is present in the system they also contribute to the dissipation of the disk. Companions clear up regions within the disk due to dynamical interaction.

The accretion phase lasts on average 2–3 Myr, however there is a large scatter from star to star. About half of the stars at the age of 1 Myr are without disks, while a few percent of them exhibit optically thick disks even at the age of 10 Myr. In the majority, though not in all of the young stellar objects, accretion signatures correlate well with the presence of dusty inner disks (e.g. Nguyen et al. 2009; Sicilia-Aguilar et al. 2006), indicating that the accretion process proceeds parallel to dusty

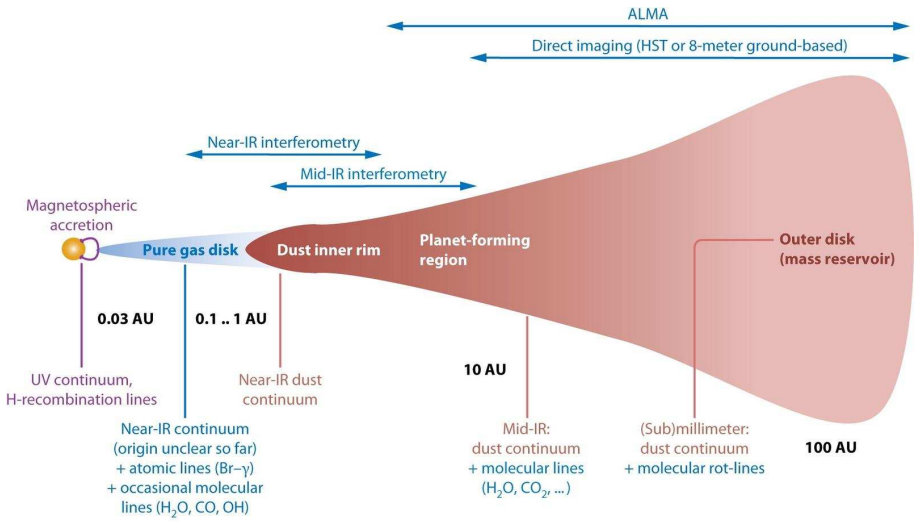

Figure 1.5 – Regions of the circumstellar disk are shown along with typical spatial scales (the figure is not to scale). The wavelength ranges where the different regions emit at are indicated below the disk. Observational techniques used to probe the different disk regions are shown above (Dullemond & Monnier, 2010)

.

disk evolution. However, Fedele et al. (2010) found that the fraction of accreting systems is systematically lower than those having optically thick inner disks and they give slightly different timescales for mass accretion (2.3 Myr) and inner disk dissipation (2.9 Myr).

At the end of the accreting phase, during a transition period that is significantly shorter than the main accretion phase, the disk loses its gas content due to photoevaporation. After gas is removed from the disk by photoevaporation, the star is left with an optically thin disk containing coagulated dust grains, rocks, or planetesimals. These smaller and larger bodies may remain and through collisions may produce secondary dust of the debris disks found around many main-sequence stars (Fig. 1.4, *d*).

1.2 Eruptive young stars

Means and timing of the accumulation of mass in stars during the star formation process is of fundamental importance. Mass accretion rates during the early stellar evolution generally decrease with time, however it seems there are episodes of sud-

den, short-timescale bursts, when mass is transferred onto the young star at rates several orders of magnitude higher than usual (see Fig. 1.3, Vorobyov & Basu 2006; Hartmann 2009). The eruptions of the FU Orionis- and EX Lupi- type variable stars (FUors and EXors, respectively) may represent the most intense bursts (e.g., Hartmann & Kenyon 1996; Herbig 2007 and references therein). The outburst events are observed as sporadic, spectacular brightenings of several magnitudes, lasting for diverse periods of time. The shorter flare-ups, typical of EXors, are only a couple of months – years long, while among FUors we know of objects being in a high state for almost a century, and all of them have spent several decades in outburst.

Altogether we know about somewhat less then 30 EXors/FUors. Still, eruptive phenomena cannot be considered rare. If we take into account the short-lived nature of the bursts, then according to statistical considerations we expect that most young stars may undergo these stages during their evolution, and furthermore the bursts have to be repetitive with at least ∼4 recurrences for every object (Hartmann, 2009), and more if not all stars show eruptive phenomena.

Eruptive phases play a very important role in the early evolution of stellar systems. They affect the stars themselves, their circumstellar environments, and consequently also the formation of their planetary systems. During the high state, the accretion rate increases to 10^{-7}–$10^{-4}\,M_{\odot}$/yr. The extra accretion energy heats up the whole system, and the increased accretion is accompanied by powerful winds and outflows. These events can modify both the circumstellar structure and the dust composition of YSO systems on the time-scales of weeks – months. In Chapters 5 and 4 we follow with the help of detailed models for the first time what changes occurred in the circumstellar environment during the recent flare-up of two sources: V1647 Ori and EX Lupi.

In Chapter 3, the quiescent properties of EXors are examined, with the aim of clarifying their nature and evolutionary status. Until recently we had no detailed information about the pre-outburst or quiescent conditions in their circumstellar environments. In this thesis I check if they have special, distinctive features that may cause the eruptions and, may make them atypical among young stars or they are non-exceptional among regular YSOs in their low-state.

In the following I give a brief summary about the observational properties of the

two classes of eruptive stars.

1.2.1 FUors

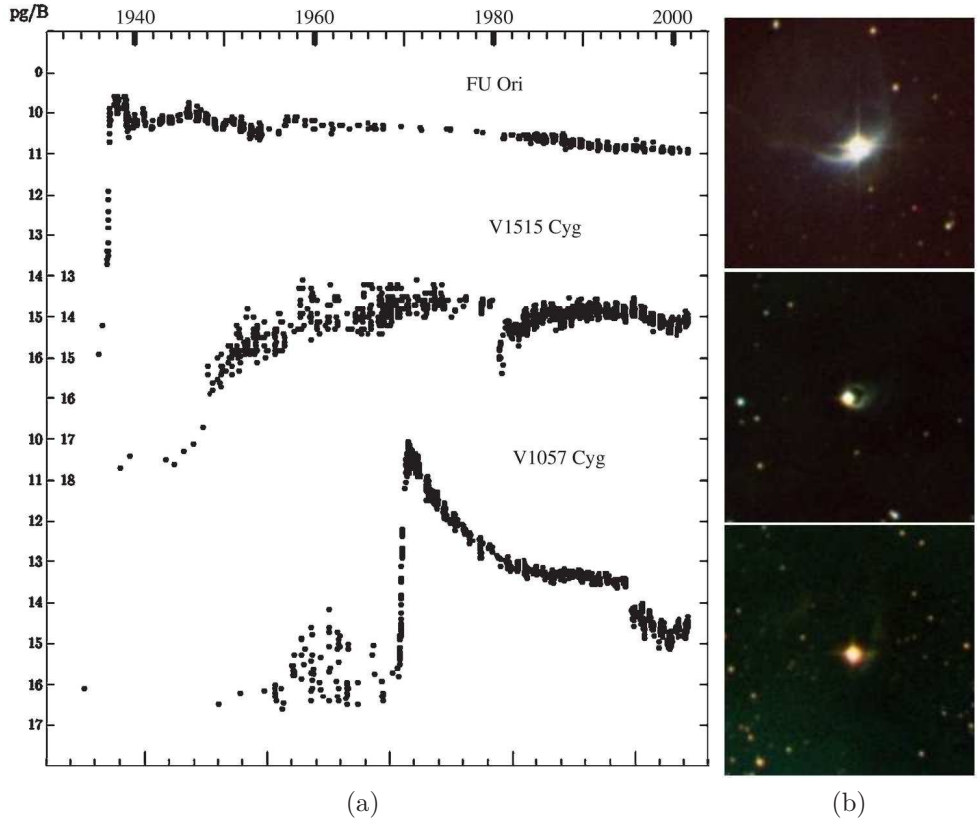

Figure 1.6 – *(a)* Light curves of the FUors FU Ori, V1515 Cyg, and V1057 Cyg. Historical data are photographic photometry, recent is in the B-band. (Credit: Hartmann 2009) *(b) RGB* color-composite POSS2 images of the same objects in the same order (infrared (R), red (G) and blue (B)).

FUors originally drew attention to themselves by their unusual brightening of 4–6 mag. The class was named after FU Orionis, which brightened by 5 mag in 1936, compared to its previous brightness of ~ 16 mag, and provided the first observation of such an event (Herbig, 1977, 1989). In Fig. 1.6, light curves of the three first-discovered and thus best studied examples are shown. Although the amplitude of the increase in brightness is similar, the timescales for rising and fading vary. FU Ori and V1057 Cyg reached their maximum brightness in less than a year, whereas the luminosity of V1515 Cyg was continuously increasing for more than a decade. Fading characteristics also differ. FU Ori has been fading very slowly for $\sim$80 yr,

the brightness of V1057 Cyg first dropped quickly, then its light curve became much flatter. V1515 Cyg has remained around its maximum brightness since the 1960s. The eruptive phenomena is supposed to be repetitive, however no one has ever seen a FUor outburst twice, or even returning to the quiescent phase.

FUors share distinctive spectroscopic features, and several members of the class were identified as FUors based only on their spectra. While their optical spectra resemble those of a fast rotating late F–G type supergiant star, their near-infrared (NIR) spectral characteristics indicate M giant–supergiant atmospheres. FUors do not show spectra typical of T Tauri stars.

FUors are young stellar systems. All of them are found within star-forming regions, they are surrounded by reflection nebulae and their spectral energy distributions (SEDs) show a considerable amount of infrared excess at longer wavelengths, typical of embedded young stellar systems. Besides this, the Li I 6707 Å absorption line is always present in their spectrum, characteristic of young stars. The only FUor spectrum taken during a pre-outburst phase was that of V1057 Cyg. Before the onset of the burst, it showed emission lines usually observed in accreting T Tauri stars, however, after the start of the outburst a typical FUor spectrum could be observed, first with an effective temperature of ~ 9000 K and later cooler. Spectral information about the quiescent source provides further evidence for FUors being pre-main sequence stars.

1.2.2 EXors

Members of the EXor subclass of young low-mass stars show less dramatic flare-ups, thus sometimes they are mentioned as the 'downscaled version of FUors' and referred to as 'subfuors' (Herbig, 1989). The EXor name was given after the example first recognized showing this behavior, EX Lupi.

The amplitudes of these bursts are generally smaller, ranging between 1–5 mag in the optical wavelengths. The sudden, repetitive eruptions typically last for a couple of months or a few years and are separated by intervals of quiescent periods (Herbig, 1989). Between two eruptions the systems spend several years in a low-state. Some typical light curves are shown in Fig. 1.7.

Spectra of EXors are clearly different from FUor spectra. In quiescence they

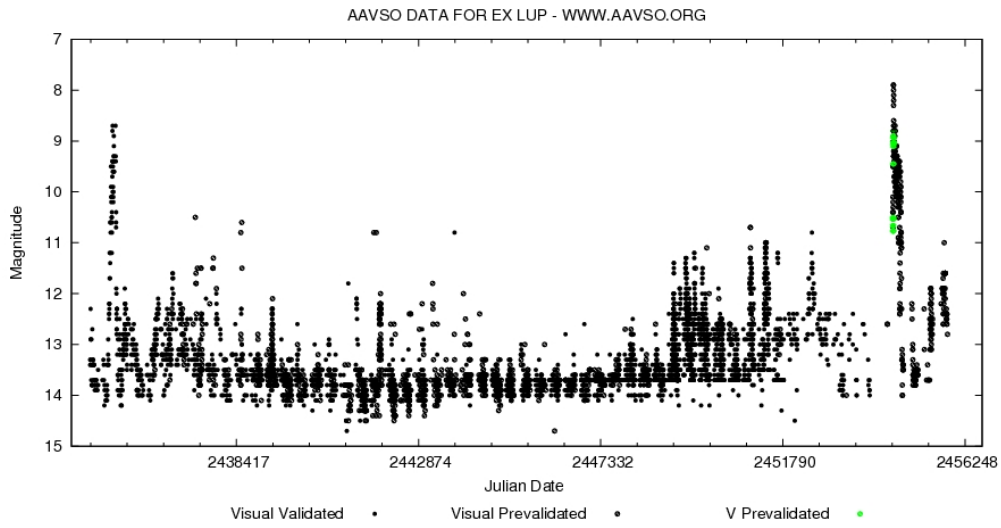

(a)

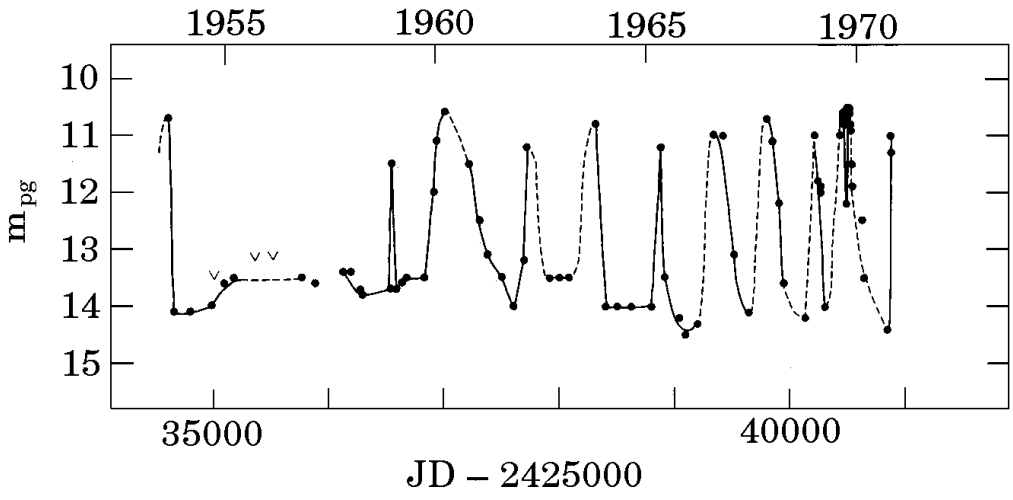

(b)

Figure 1.7 – Optical light curves of two EXors: *(a)* EX Lupi and *(b)* VY Tau. Both objects have shown several sporadic flare-ups of 1 – 3 mag. Measurements are shown from 1950s until 2011 Sept in the case of EX Lup and 1972 in the case of VY Tau. VY Tau has been in quiescence since then. The large 4 – 5 magnitude outbursts of EX Lup happened in 1955-1956 and 2008. (Image credit: AAVSO International Database (*www.aavso.org*) for EX Lup and Herbig (1977) for VY Tau)

resemble K- or early M-type dwarfs, and in addition they show T Tauri-like emission lines (e.g., Sipos et al. 2009). No spectral feature was found that would set them aside from normal T Tauri stars (Herbig, 2007, 2008). During an outburst a hot

continuum appears in the spectrum, reversed P Cygni absorption components are present at several emission lines, and the spectra show great variability on short timescales.

Similarly to FUors, they are also associated with star-forming regions, they also show infrared excess emission, though less than what is observed in the case of FUors. EXors are generally considered to be in the early phase of the T Tauri stage, though in a more evolved state than FUors. They do not necessarily have extended envelopes around them, they have a disk-only circumstellar environment.

Categorization of eruptive objects into the two subclasses is not straightforward. Recently several objects (including V1647 Ori, analysed in Chapter 5) were found showing in-between properties. They show repetitive outbursts, like EXors, that last for a few years with ∼4–5 mag increase in the luminosity, which values are more typical in the case of FUors. They are embedded in an envelope (Kóspál et al., 2007; Acosta-Pulido et al., 2007).

1.2.3 Outburst mechanism

Despite all the differences that EXor and FUor outbursts have, both are considered to be the result of the same process. Eruptive phenomena are generally associated with an enhancement of several orders of magnitude in mass accretion rate from the circumstellar disk to the young star (from typical values of 10^{-9}–$10^{-7}\,M_\odot$/yr for normal YSOs to 10^{-7}–$10^{-4}\,M_\odot$/yr). Due to the increased accretion rate, the accretion luminosities become much higher than that of the central star. As a result, the circumstellar environment heats up, and the emitted flux rises both at optical and infrared wavelengths. However, relying on NIR and optical color changes, several authors suggested that the optical brightening of the objects cannot be attributed to the change of accretion exclusively, but extinction may also play a role (Acosta-Pulido et al., 2007; Kun et al., 2011; Aspin et al., 2008), and contribute at least partly to the brightening during the outburst. This question I revisit in Chapter 5.

There is no consensus so far about what the triggering mechanism of the runaway accretion is. The sudden dramatic increase of the accretion rate is explained as being the result of some kind of instability in the disk. Possible mechanisms are listed below.

(a) *Gravitational instability* – A gravitational instability in the inner circumstellar disk may induce accretion bursts (Vorobyov & Basu, 2006, 2010). Following the collapse phase of star formation, disks may fragment, depending on the conditions defined by the natal core, with a higher probability of fragmentation for larger mass and angular momentum. The fragments, or concentrations in young massive disks move to inner regions. As some of these clumps are randomly accreted onto the star, they trigger bursts sporadically. The model can account for accretion rates of highly variable values ranging from 10^{-8} to $10^{-4}\,\mathrm{M}_{\odot}/\mathrm{yr}$. For this scenario, the disk has to be still in the embedded phase, as constant replenisment of material from the envelope is necessary, and also the disks must fragment.

(b) *Thermal instability* – A thermal instability caused either by the presence of a planetary companion (Lodato & Clarke, 2004), or happening in the disk alone (Hartmann & Kenyon, 1996) provides further possibilities for a triggering mechanism. According to the thermal instability model, we expect that material is still infalling from the envelope to the young disk. Accretion rates from the disk onto the star, and from the envelope onto the disk do not necessarily match, the infall from the envelope can be higher. As a result, matter piles up in the disk. In this state, temperatures are low even in the regions very close to the star. At low temperatures turbulent motions in the disk and thus viscosity, responsible for angular momentum transport, is also low. Because of the slow angular momentum transport, accretion rates onto the star remain also low, and mass piles up in the disk, close to its inner edge. Due to mass accumulation, the density and thus opacity in the disk grows, until the disk will be opaque enough to trap heat. As a result, the temperature increases rapidly. Opacity in the $\sim$ 3000–10000 K temperature range varies very steeply with temperature due to the ionization of hydrogen. Consequently, in this temperature range, which corresponds to a typical maximum radial distance of ~ 0.1 AU from the star, small temperature fluctuations switch on thermal instability. This results in ionisation of the inner regions of the disk. This increases viscosity, which eventually results in runaway accretion. Lodato & Clarke (2004) suggested that planetary companions in the disk help producing circumstances necessary for

the thermal instability. The thermal instability explanation for the onset of the eruption can account for the observed high accretion rates, both the rapid and the slow rise-time of the FUors and also recurrence. This made it for a long time the most widely accepted model. However, recent observations from Spitzer Space Telescope do not confirm this model. High-accretion regions seem to reach much further out, to distances of 0.5–1 AU, than the very small inner radii of ~ 0.1 AU predicted by the thermal instability model. (Hartmann, 2009).

(c) *A combination of magnetic and gravitational instability* – A modification to the thermal instability model, combined with magneto-rotational and gravitational instability in the outer regions of the disk was proposed by Armitage et al. (2001) and refined by Zhu et al. (2009). In their model a 'dead zone' is present in the inner disk, which is a specific region of the disk where angular momentum transport and magnetic/viscous energy dissipation is not active, the magneto-rotational instability (MRI) occurs in upper disk layers (Gammie 1996) They suggest that gravitational instability drives accretion in the outer disk and material is accumulated at $\sim$ 1–2 AU. This region slowly heats up until temperatures for the thermal activation of the MRI is reached. Then MRI becomes suddenly active and material starts moving in rapidly resulting in high surface densities and high temperatures. The rest of the outburst physics is similar to the case of the thermal instability model. This model is favored to the simple thermal instability models, because they make accretion events possible after the infall from the envelope ceased, and they do not concentrate rapid accretion to very small distances from the center.

(d) *Tidal forces from binary companion* – A further possibility is that at least some of the events may be the result of the interactions of binary or multiple systems where tidal forces perturb the circumstellar disk (Bonnell & Bastien, 1992). This hypothesis relies on the fact that most stars and more importantly several of the eruptive objects are members of binaries or multiple systems. FU Ori itself is a binary with a separation of 225 AU, similar to the separations proposed by the model. However, close passage of a companion necessary for inducing the accretion event may disrupt the disk quickly, and the authors expect to

have outburst events repeated only 3–4 times, contrary to the ~ 10 proposed from statistical arguments (Hartmann, 2009). Note, that contrary to statistics mentioned earlier, where it was proposed that all stars undergo eruptions, here we assume that multiplicity is needed for outburst phenomena to occur.

(e) *Interaction of the magnetic field and the disk at the corotation radius* – D'Angelo & Spruit (2010) recently developed a model, suggesting that eruptions may be caused by matter piling up at the corotation radius, where Kepler-rotation speed and the rotation speed of the star are equal, due to an interaction of the magnetic field and the disk. In their picture, the instability arises as the magnetic field truncates the disk near the corotation radius. In the quiescent phase, the inner edge of the disk is slightly outwards of the corotation radius. As a result, angular momentum is transferred from the star to the disk and accretion stops. Instead of the launch of an outflow, material remains bound to the system and piles up at the inner radius. Consequently, surface densities and gas pressure increase, the inner edge starts moving inward. Accretion suddenly restarts, when the inner edge reaches the corotation radius. As the accumulated mass is removed onto the star, the disk moves outward again and the cycle restarts. The model predicts repeated outbursts and cyclic accretion rates in accordance with EXor observations, and does not require outside replenishment of the disk from an envelope. As the accretion rates drop, the cycle period increases, while the duration of the accreting phase decreases.

Whichever explanation above proves to be valid, the circumstellar environment and especially the regions of the circumstellar disk closest to the star must play an essential role in driving the eruptions.

Chapter 2

Methodology

The most important advance in the past 20–30 years for the study of young stellar objects was the opening up of the infrared sky. Many YSOs, especially at the early stages of the star formation process, remain hidden from view when observed with optical telescopes, because they are covered in dense dusty clouds (Fig. 1.1). Short wavelength radiation, i.e. starlight or accretion-related hot radiation is scattered, absorbed and re-emitted at longer wavelengths by dust grains found in the disk–envelope system. Infrared radiation, however, can pass through dusty environments too, so we rather observe young systems at longer wavelengths, complemented with optical measurements where possible.

In the meantime, improvement of methods for interpreting observational data were also inevitable. Depicting the nature of the sources from the spectra, images, interferometric visibility curves, and polarization maps can be complicated, and simulations are generally used for comparison of observations and recent theoretical models. Sophisticated numerical radiative transfer codes have been developed to serve as a basic tool for this purpose. Due to the increase of computing power and better algorithms, today multidimensional codes treat the radiative transfer problem also for complex configurations, contributing greatly to the rapid progress of the study of YSOs.

During my PhD research I used two of the leading continuum radiative transfer codes called *RADMC* (Dullemond & Dominik, 2004) and *MC3D* (Wolf et al. 1999, Wolf 2002) for simultaneous modelling of continuum measurements at the optical–

far-infrared wavelengths range, and when available mid-infrared interferometric data for delivering a physical picture of the studied sources.

In the following I will review briefly how the environment of a young star is characterized via its SED. I describe the most important instruments used, and the basics of interferometry and radiative transfer, including the most important features of the circumstellar disk implemented in the radiative transfer codes.

2.1 Classification and SED of YSOs

In the dusty circumstellar environment of young stars various temperatures are present, resulting in an emission of thermal radiation in a wide range of wavelengths from the UV to the millimeter-centimeter regime (Fig. 1.5). Close to the center, temperatures tend to be higher than farther from it, though diverse geometry and optical depths modify this picture. By examining the sources in different wavelength ranges, we can gain information on the structure on different spatial scales (Fig. 1.5), and may categorize YSO based on characteristics of their SEDs. Originally, Lada (1987) classified YSOs to three classes (Class I, II and III objects) based on the mid-infrared (MIR) slope defined as $\alpha_{IR} = d \log \nu F_\nu / d \log \nu$ between $2-25\,\mu$m. The classification scheme was also interpreted as an evolutionary sequence. Later it was completed with a class for an earlier phase (Class 0), and the so called 'flat-spectrum sources', placed between the Class I and II YSOs (Andre et al., 1993; Andre & Montmerle, 1994). Typical SEDs and geometries of the various classes are presented schematically in Fig. 2.1. Class 0 sources are very red objects characterized by no optical or near-infrared emission. In this class protostars are surrounded by massive optically thick dusty environments. Class I SEDs also imply high levels of obscuration, the mid-infrared slope is $\gtrsim 0$. The protostar is believed to be more evolved but still embedded with the circumstellar disk in an envelope. Flat-spectrum sources show flat SEDs ($\alpha_{IR} \sim 0$), the disk and the star are embedded in a much thinner and smaller envelope than at earlier phases. In the Class II and Class III stages (with IR slopes $0 \gtrsim \alpha_{IR} \gtrsim -1.6$ and $\alpha_{IR} \gtrsim -1.6$, respectively) the disk dominates the circumstellar environment and the IR spectrum. Young stars with Class II – III SEDs are in the T Tauri stage, and the evolutionary state of the disk determines which

of the two classes the source belongs to. There is a parallel categorization based on the strength of their Hα emission, indicative of accretion characteristics. Class II objects correspond to classical T Tauri stars (CTTS). They have more pronounced infrared excess indicative of a significant circumstellar disk, and are characterized by active accretion. Meanwhile in the case of Class III objects or weak-line T Tauri (WTTS) stars, the pre-main sequence star is surrounded by a disk where dust is dissipated or coagulated and show no signs of accretion. The two types of classification do not necessarily correspond, though in most cases they do (Hartmann, 2009), as described in Sect. 1.1, thus in the following I use the terms interchangeably. Sources evolve from Class II to Class III stages through a "transitional/evolved" disk phase, characterized by SEDs similar to Class III objects at NIR wavelengths and in the short wavelength regime of the MIR, while they resemble Class II SEDs at longer wavelengths.

Attention should be drawn to the fact that investigating only the SEDs of the YSOs can be misleading due to different inclinations of the system. A system observed more edge-on will suffer from more extinction than objects more face-on, and thus might be interpreted as an object having more circumstellar material and being in an earlier evolutionary phase. This effect is illustrated in Fig. 2.1.

It is also important to note that the classification scheme shows the evolutionary trends, however, the degree of disk evolution does not necessarily correlate with age during the first few million years of a star's life. Disk evolution may alter from object to object, and pre-main sequence stars can lose their disks due to effects like binarity, planet formation, etc. already within 1 Myr, while they may also survive as long as 10 Myr. It seems that dust evolution starts early and it is more determined by individual properties of the objects than universal processes happening at a certain time interval. Even systems that formed close to each other and are of roughly the same age are found in different evolutionary states. An evolutionary track from accreting disks through passive disks to diskless stars is likely, however the times for the transitions differ.

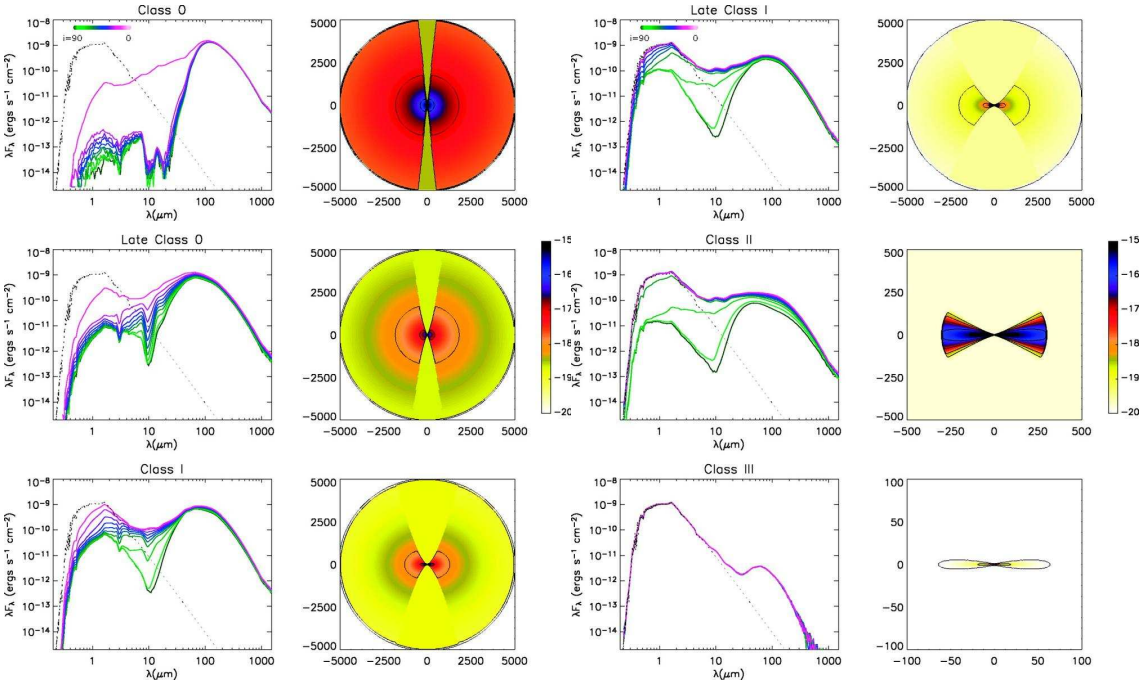

Figure 2.1 – SEDs (left) of YSOs at various evolutionary stages seen under different inclination angles. Inclinations are color-coded, with pink being face-on and green edge-on. Right panels show model density distributions typical of the given evolutionary stage. Densities are shown logarithmically by color, sizes are in AU (Whitney et al., 2003).

2.2 Optical and infrared data

I used both new and archival data obtained by ground-based and space-borne instruments. Optical and NIR observations were mostly carried out at the Piszkéstető Mountain Station of the Konkoly Observatory (Hungary) and at the Teide Observatory (Canary Islands, Spain), observed by several colleagues.

I used infrared data from the first large missions like the Infrared Astronomical Satellite (IRAS) and the Infrared Space Observatory (ISO), and recent front-line instrumentation like the Spitzer Space Telescope and the Mid-Infrared Instrument for the Very Large Telescope Interferometer (VLTI/MIDI). A short description of the infrared space observatories used in this thesis is given below, while the VLTI/MIDI interferometer is discussed in the next section.

The atmosphere of the Earth, especially the water vapor in it absorbs a significant amount of the infrared radiation coming from space. Consequently, ground-based telescopes are mostly installed at dry locations at high altitudes. A much better so-

lution to this problem however, is to observe from above the disturbing atmosphere. After early attempts of measuring infrared radiation on board rockets and balloons, in 1983 IRAS[1], the first infrared space-based mission was launched. It scanned 96% of the sky four times at 12, 25, 60 and 100 μm wavelengths.

ISO[2] (Kessler et al., 1996), started in 1995 was the next infrared space mission that had a great impact on astronomy. The observatory operated for about 2.5 years. It covered a very wide wavelength range between 2.5 and 240 μm for photometric observations and 2.5 to 196.8 μm for spectroscopy. It had a much better sensitivity and resolution than IRAS, ranging from 1.5″ at the shortest wavelengths to 90″ at longer wavelengths. It carried four scientific instruments, an infrared camera (ISOCAM), an imaging photo-polarimeter (ISOPHOT) and two spectrometers (SWS and LWS).

Spitzer Space Telescope[3] (Werner et al., 2004) was launched in August 2003 and is still operational, although after its on-board liquid helium supply was exhausted in May 2009, only instruments measuring at the shortest wavelengths are functional. Spitzer had a unique resolution and sensitivity, that has only very recently been overcome by Herschel Space Observatory (Pilbratt et al., 2010) at 70 and 160 μm. It had three instruments on-board. IRAC (Infrared Array Camera) is an infrared camera which operated simultaneously at four wavelengths (3.6, 4.5, 5.8 and 8 μm), and the two shorter wavelength are still used during the 'Spitzer Warm Mission'. IRS (Infrared Spectrograph) is an infrared spectrometer with four sub-modules which measured at the wavelengths 5.3–14 μm (low resolution), 10–19.5 μm (high resolution), 14–40 μm (low resolution), and 19–37 μm (high resolution). MIPS (Multiband Imaging Photometer for Spitzer) performed imaging and photometry at far-infrared wavelengths with three detectors at 24, 70 and 160 μm, and low-resolution spectroscopy between 55 and 95 microns.

For new observations, data reduction was done mostly using standard procedures, however, data reduction of the used measurements is not discussed in detail in this thesis, as these tasks were carried out by other members of the group.

[1]Further details about the mission and data catalogues are to be found at the homepage of the satellite *http://irsa.ipac.caltech.edu/IRASdocs/iras.html*

[2]For details and archive visit: *http://iso.esac.esa.int/*

[3]For the Spitzer homepage and archive visit: http://www.spitzer.caltech.edu/

2.3 Mid-infrared interferometry

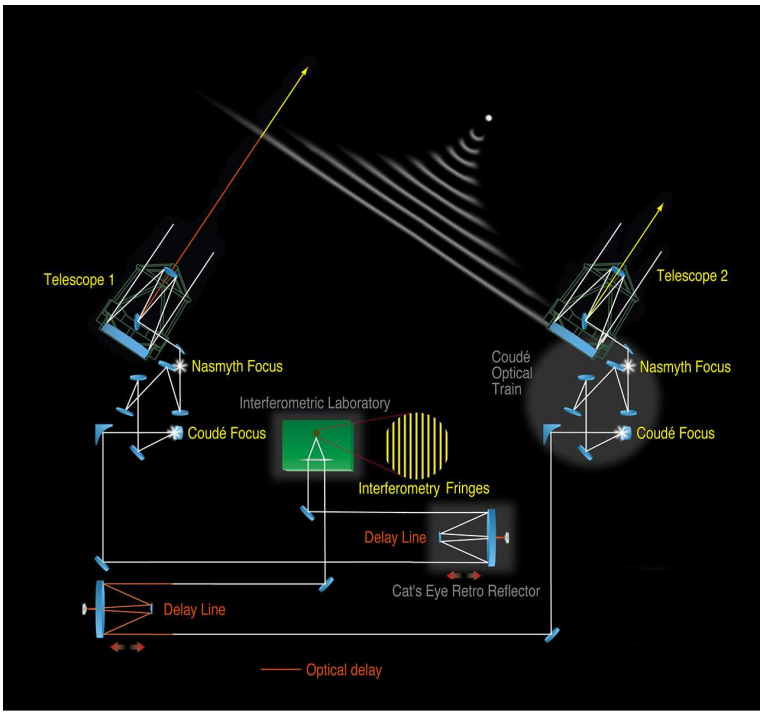

Figure 2.2 – Basic geometry of a two-telescope interferometer (*www.eso.org*)

The closest star formation regions are at a distance of $\sim$ 100–400 pc, and typical disk sizes are in the order of $\sim$ 100–300 AU. With the largest 8–10 m class telescopes available, we are limited to resolving only the region outside of tens of AU in the infrared. If we would like to study the regions of the circumstellar environment closest to the star, we need much higher angular resolution. This is only possible to obtain with the use of stellar interferometers, where beams coming from two or more telescopes are combined. While in the case of a conventional, single-dish telescope the diffraction limited angular resolution at a given wavelength depends on the diameter of the mirror, the resolution of the interferometer will depend on the telescope separation, or more precisely the baseline, which is the projected distance of the telescopes as seen from the observed object.

The VLTI/MIDI interferometer is a European Southern Observatory (ESO) instrument in Paranal, Chile. It operates in the mid-infrared N-band, an atmospheric window between 8–13 μm. MIDI is a stellar interferometer, combining two telescopes which can be either two of the four 8.2 m unit telescopes (UTs), or two of the

1.8 m auxiliary telescopes (ATs) of the Very Large Telescope Interferometer (VLTI). Interferometric data can be measured with several filters in the N-band, and the instrument also has low (R=30) and medium (R=230) resolution spectroscopic capabilities, thus chemical composition of the sources can also be studied at small spatial scales. Basics of the optical–infrared interferometry and applications in the study of star formation and the circumstellar environment is described in detail in a series of proceedings of the VLTI Interferometry Summer Schools (edited by Malbet & Perrin 2007; Wolf & Garcia 2008; Delplancke & Mosoni 2009). Here I sum up the concept used in this thesis briefly, based on the proceedings, in the case of a two-element stellar interferometer.

The schematic geometry of a two-telescope interferometer, such as MIDI is shown in Fig. 2.2. In principle, during a measurement, wavefronts from a distant celestial target enter the pupils of the two elements of the stellar interferometer, usually at different times. The light beams reflect on several mirrors and move along a path to the beam combining device, which produces the interferometric signal. The path-lengths of the different beams is constantly adjusted in a way that the difference of the optical path delays are eliminated. The delays are either due to the geometry of the system (location of the telescopes and the elevation of the target), or atmospheric effects. If the path delay difference is close to zero the beams can be combined and the interference pattern, the so-called fringe, is created. In that case the interferometer measures the spatial coherence function of a given wavefront at different locations (i.e. telescope pupils).

The contrast ($\frac{I_{\max}-I_{\min}}{I_{\max}+I_{\min}}$) of the emerging signal is the visibility. The visibility is the Fourier transform of the brightness distribution of the object (as seen on the sky) at a special *(u,v)* position in the Fourier plane, which corresponds to the length and direction of the telescope baseline (Van Cittert-Zernike theorem, Born & Wolf 1999). A 2-element stellar interferometer increases the angular resolution with the baseline. The Fourier tansform is a complex quantity at each *(u,v)* coordinate, but in many cases, like in that of MIDI, one can only measure the amplitude of the visibility, the phase information is lost. For the interpretation of this one measured point, models are needed, and usually visibilities are measured either at more wavelengths (the case in this thesis), or more position angles or more baselines (Fig. 2.3) in order to

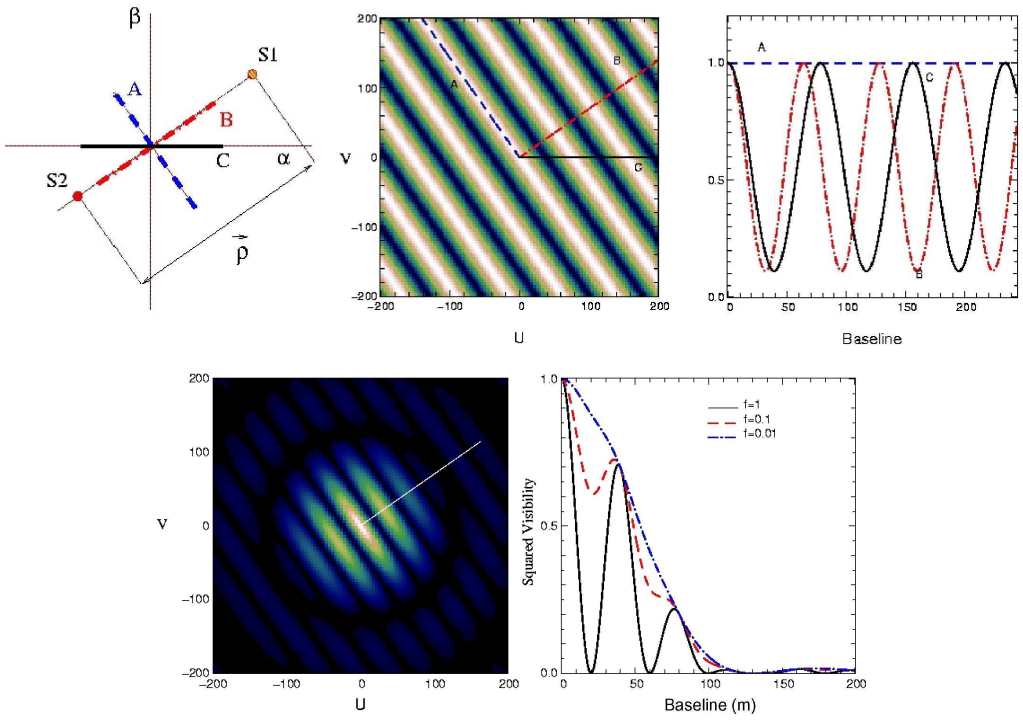

Figure 2.3 – *Upper panels:* On the left an unequal binary with a separation of ρ=5 mas is shown as it could be seen on the sky. The middle panel gives the amplitude of the Fourier transform in the *(u,v)*-plane. Lines show three position angles along which the measurements are taken, one parallel, one perpendicular to the position angle of the binary. On the right, the measured normalized visibility curves are given as a function of baseline length. *Bottom panels:* Squared visibility amplitude map and visibility curves measured for a binary, where both components have a uniform disk. Different visibility curves are shown for different flux ratios (f) of the object, the map refers to the $f = 1$ case (Berger & Segransan, 2007).

have more constraints.

The visibility depends on the relation of the observed source and the baseline of the interferometer. In the case of a point-source, waves interfere only constructively and the amplitude of the signal is maximal (the visibility will be $V = 1$), while for an extended source (relative to the angular resolution) the amplitude of the outcoming signal will be smaller and the visibility will be $V < 1$, as waves coming from different parts of the observed source may interfere destructively. The interpretation of visibilities $V < 1$ is not unique, but combined with other data, e.g. an SED, reasonable amount of constraints will be available for the model-fitting procedure.

2.4 Radiative transfer and models of disks

While radiation from a source reaches the observer, it comes in contact with the medium it passes through, either in its direct environment or outside of the system. Due to the interaction, radiation is modified. The radiative transfer problem investigates this process.

Although dust gives only 1% of the material in the circumstellar environments of young stars, dust grains play an essential role in defining the emerging radiation field. They dominate the opacity in the system, and they define the energy balance in the disk and envelope. Dust grains scatter, absorb, and polarize the starlight and the short wavelength radiation from viscous dissipation of gravitational energy due to accretion. The absorbed energy heats up the dust, resulting in a re-emission of thermal radiation at longer wavelengths. The characteristics of this process is defined by the geometry of the circumstellar environment and the properties of dust. Even though gas also contributes, its effect is much less important than that of dust. Thus the gas temperature is generally assumed to be equal to the dust. During my PhD thesis I worked with the dusty environment of YSOs and concentrated on continuum, dust radiative transfer modelling. For this reason aspects of the gas transfer are not discussed.

Eventually, our goal is the understanding of the structure and evolution of the circumstellar environment of stars being born. By measuring the emitted thermal spectrum of dust (preferentially combined with scattered light images, visibilities, polarization maps, etc.) and knowing how radiation is transported, in principle we can infer the physical properties of the system the radiation emerged from. This is done by solving the radiative transfer problem.

The monochromatic radiative transfer equation gives the change of the specific intensity (I_ν) of the radiation field at each wavelength, for every point and every direction of the geometry over a path s like

$$\frac{\mathrm{d}I_\nu}{\mathrm{d}s} = -\kappa_\nu I_\nu + \epsilon_\nu,$$

where κ_ν is the opacity, and ϵ_ν is the emissivity. The first term on the right side of the equation stands for the energy loss of the radiation, while the second gives the sources of radiation. Analytical solutions for the equation exist only in simple

cases, that are not suitable for investigating the complex structure of real dusty environments. For a numerical solution of the problem, semi-analytic models and sophisticated radiative transfer codes were developed. The models in the codes consist of two main components: the density distributions of the scattering and absorbing medium and the radiative sources.

Before turning to the description of models of different complexity, it needs to be mentioned, that circumstellar disks are generally categorized and implemented in models as being either passive or active. Passive, in this sense means that the heating of the disk is done by reprocessed starlight, while in active disks in the form of accretion. In reality both contribute, though most T Tauri stars may be considered in models as passive, as the emerging radiation from the accretion is only a few percent of that of the star, in case of a sufficiently low accretion rate. During modelling quiescent data of EX Lup in Chapter 3 I used such a passive disk approach. On the other hand, when studying outburst properties of eruptive young stars (like in the case of V1647 Ori discussed in Chapter 5), accretion plays and important role, so disks should be considered in this case as active.

Early treatment of the problem was the use of semi-analytic models, where the density distribution, the radiative sources and the transport of radiation were all much simplified. The first approach for describing active, accreting disks was of Lynden-Bell & Pringle (1974), who showed that for a geometrically thin disk with steady accretion rate, the temperature structure is like Eq. 1.1, which for large radii changes as $T(r) \propto r^{-3/4}$. Adams & Shu (1986) showed that this proportion is also true for passive flat disks. Their reasoning was simple. If we take a geometrically thin but optically thick disk, then the disk will absorb radiation from the star under a certain irradiation angle ($\phi \simeq 0.4R_\star/r$, where $R_\star$ is the stellar radius) and re-emit it as a black body, all other processes are neglected and we assume thermal equilibrium. This yields:

$$\frac{1}{2}\phi\frac{R_\star}{4\pi r^2} = \sigma T^4, \tag{2.1}$$

where σ is the Stefan-Boltzmann constant, and the $T(r) \propto r^{-3/4}$ follows. The disks with the given temperature profile are treated as thin annuli emitting black body radiation of the given temperature, from which the resulting flux (F_ν) could be easily

obtained as

$$F_\nu \propto \int_{R_{in}}^{R_{out}} 2\pi R B_\nu(T) \mathrm{d}R \propto \nu^3, \tag{2.2}$$

where $B_\nu(T)$ is the Planck function of a given temperature T.

However, thin disks cannot account for the large infrared excess observed at many T Tauri stars at the mid- to far-infrared. For explaining the excess, Kenyon and Hartmann (1987) provided a natural explanation by the flared-disk geometry, where the scale height of the disk increases with the radial distance to the star. This way the outer disk receives more illumination ($\phi \simeq 0.4R_\star/r + r\mathrm{d}(hr)/\mathrm{d}r$, h is the vertical distance from the midplane), which increases the emitted flux at longer wavelengths. Assuming a thermal equilibrium again, and supposing that for the pressure scale height (h_p) in the disk $h_p \propto h$, the shape of the disk will be $h \propto r^{9/7}$. The temperature profile for this type of flared disks is typically about $T(r) \propto r^{-1/2}$ (Chiang & Goldreich, 1997).

Although this model-geometry is already more sophisticated than the flat-disk approach, it handles transport of radiation in the same simple way. An improvement is, if we suppose that the emitting radiation depends also on the optical depth in the system and not only the irradiation angle. This means that only the upper surface of the disk is subject to heating from the star, the underlying disk is irradiated by the thermal radiation of the dust grains in the surface. The disk surface is usually warmer than deeper layers. This picture is modified for active disks, when we have an additional heating source at/close to the midplane[4]. Models of various complexity are treating this problem, in the simplest case using only two layers of dust, emitting in a different fashion (a disk atmosphere and an inner disk) e.g., Chiang & Goldreich (1997). The basic ideas described above are illustrated in Fig. 2.4.

Recent numerical codes aim at solving the radiative transfer equation with conservation of energy and thermal equilibrium for various density structures. The literature of radiative transfer problem is vast, explaining in detail both the analytical and various modelling concepts, e.g. Rutten (2003) gives a good summary on the theory. Algorithms, disk/envelope models and various codes used are summarized in e.g., Pascucci et al. (2004), Dullemond et al. (2007), Pinte et al. (2009), Min

[4]Note that there are models of accretion assuming layered accretion not originating from the midplane.

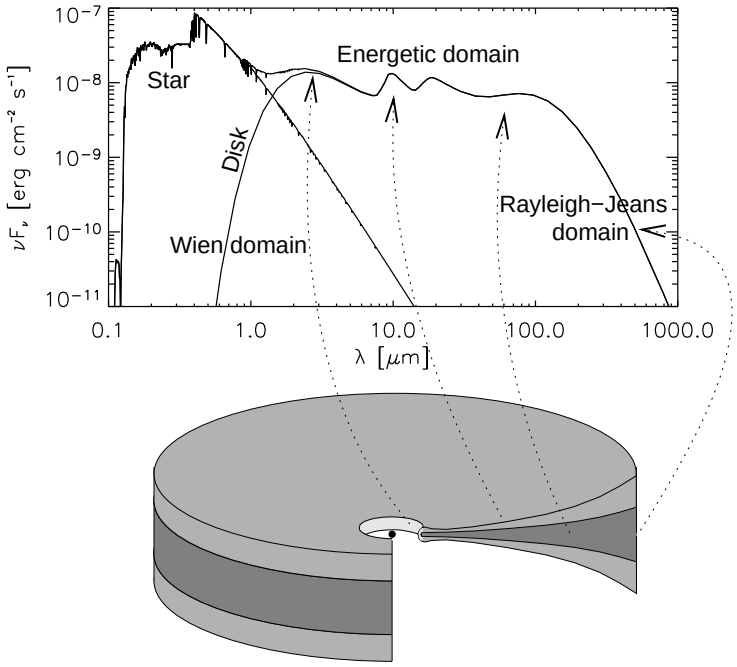

Figure 2.4 – Passive two-layered flared disk and its SED. Flux at the optical wavelength regime is dominated by the star, near-infrared radiation originates from the very inner regions of the circumstellar disk, the geometry of the inner edge of the system determines the shape of the SED here. The infrared SED is emitted by the disk, dust features come from the warm upper layer, the surface of the disk, while the continuum from layers below the surface. While mid-infrared emitting regions are relatively close to the star, the far-infrared comes from the outer regions. Submm and mm continuum emission is from the deepest and outermost parts of the disk. (Dullemond et al., 2007)

et al. (2009) and references therein. Here I turn to multidimensional Monte Carlo radiative transfer codes with arbitrary density distributions. They are considered to be the most sophisticated for dealing with this subject as of today. I summarize only aspects that are important for this thesis.

Radiative transfer codes can be either grid based or based on the Monte Carlo method, and they are able to treat complex geometries in 2/3 dimensions. The codes I have been using, *MC3D* and *RADMC* are both Monte Carlo codes, so I will only describe them in the following. The models in the codes consist of two main components: the density distributions of the scattering and absorbing medium, and the radiative sources. The radiation field in Monte Carlo codes is given in the form of photon or energy packages that are emitted stochastically from the sources of

radiation. Early algorithms were iterative and thus very time consuming. Today we have efficient algorithms resulting in fast(er) and accurate calculations. Both *MC3D* and *RADMC* use the Bjorkman-Wood algorithm (Bjorkman & Wood, 2001) or 'immediate-reemission' concept including the steps given below.

1. The photon packets are released stochastically from the radiation sources.

2. Photon packets are moved to a random location determined by the optical depth in the dusty environment, where they are either scattered or absorbed with a probability determined by the albedo.

3. (a) If the photon packet was scattered, a random scattering angle is obtained from the scattering phase function (differential cross section);

   (b) If the photon packet was absorbed, its energy is added to its environment, which leads to an increase in the local temperature. The packet is re-emitted immediately at a new frequency determined by the increased temperature.

4. The photon packet continues to a new interaction location.

5. The process is repeated until all packets leave the dusty environment.

6. Along with the temperature structure, the direction and frequency of emergent photons provide the SED.

A great advantage of this algorithm is that it inherently includes energy conservation, as all photons put in the system finally escape. However, especially in optically very thick environments, photon packets might be stuck, which increases computation time. This problem is solved by photons being removed after going through the above listed steps a fixed number of times. This might lead to the simulation not conserving the energy, and also cause that high density regions are not visited by a sufficient number of photons. To avoid the latter, in *RADMC* a diffusion approximation is used (Dullemond & Dominik, 2004).

The exact definition of the circumstellar environments and the nature of the radiation sources are given in each chapter separately, as they slightly differ from each other.

Chapter 3

EX Lupi in quiescence

In quiescence the optical and near-infrared properties of EX Lup cannot be distinguished from those of normal T Tauri stars. Here I investigate whether it is the circumstellar disk structure that makes EX Lup an atypical Class II object. During an outburst the disk might undergo structural changes. My characterization of the quiescent disk is also intended to serve as a reference for studying the physical changes related to one of EX Lupi's strongest known eruptions in 2008 Jan–Sep, discussed in Chapter 4. We searched the literature for photometric and spectroscopic observations including ground-based, IRAS, ISO, and Spitzer data. After constructing the optical–infrared spectral energy distribution, I compared it with the typical SEDs of other young stellar objects and modeled the circumstellar environment using the Monte Carlo radiative transfer code *RADMC*. My results were published in Sipos et al. (2009)

3.1 Introduction

As described in Sect. 1.2, according to the current paradigm, eruptive phenomena in pre-main sequence stars are caused by enhanced accretion from the protoplanetary disk onto the central star. In this picture, circumstellar matter must play a crucial role in the eruption mechanism. Still, prior to this study, surprisingly little was known about the circumstellar environment of EXors, including the prototype of the class, EX Lup. While its infrared excess emission detected by IRAS and ISO was

attributed to a circumstellar disk (Gras-Velázquez & Ray, 2005), no detailed analysis or modelling of the disk structure has been performed so far. Such an analysis could contribute to clarifying the eruption mechanism and also answering the long-standing open question of what distinguishes EXors from normal T Tauri stars. This question has already been addressed by Herbig (2008) from a spectroscopic point of view. He found no optical spectroscopic features that would uniquely define EXors. He also concluded that their location in the $(J-H)$ vs. $(H-K_s)$ color–color diagram coincides with the domain occupied by T Tauri stars. If quiescent EXors and FUors show distinctive features that can be related to their eruptive nature, then these young stars form a small special group among T Tauri stars that evolve in a different fashion from the majority of objects. However, if we find that EXors are indistinguishable from normal young stars except for their brightenings, then we may suppose that most stars go through eruptive phases during their youth. This means that eruptive periods influence the life of all stellar systems: about 10% of the stellar mass may be built-up during these phases (Hartmann, 2009), restructuring in the circumstellar environment may occur, and chemical changes are induced.

In this work we aimed at settling this important question, and investigated if it is the circumstellar environment that makes EX Lup an atypical Class II object. We searched the literature and constructed a complete optical–infrared SED of the source that is representative of the quiescent phase. The SED was modeled using a radiative transfer code and was compared with typical SEDs of T Tauri stars, in order to reveal differences possibly defining the EXor class. The project was carried out as a result of the joint efforts of several colleagues. Data reduction of mostly archival data was done by members of our group (for details see Sipos et al. 2009). My main contribution to the research was the radiative transfer modelling of the circumstellar environment, the comparison with other young sources and the analysis of the results. I also took part in collecting data from the literature. In this chapter I present mainly these aspects of our work.

EX Lupi is the prototype of the EXor class of pre-main sequence eruptive variables. Its eruptive nature was first recognized in 1944 (McLaughlin, 1946) and its behavior was examined on archival photographic plates of the Harvard Observatory taken between 1893 and 1941. The object underwent a number of eruptions of 1-3

magnitudes during this period, separated by longer low-phases. In the past decades it continued showing unpredictable variations in its brightness (Fig. 1.7). Typical outburst magnitudes were between 2-3 mag but on two occasions as high as 5 mag. The object usually spent a period of several months (Herbig, 1977; Herbig et al., 2001; Herbig, 2007) in high state, and then remained inactive sometimes for years. The quiescent phase brightness of EX Lup is V $\approx$ 13 mag, and it is an M0 V star in the Lupus 3 star-forming region.

3.2 Optical / infrared data

We searched the literature and collected all available optical and near-infrared photometric observations of EX Lup obtained during its quiescent phases. We defined quiescence periods as, when the source was fainter than 12.5 mag according to the visual estimates and V-band magnitudes in the AAVSO International Database. A visual inspection of the DSS and the 2MASS images revealed no nebulosity surrounding the star, so we concluded that measurements with different apertures can be safely compared. The query results are shown in Table 3.1 and plotted in Fig. 3.1.

Besides the optical – near-infrared photometry, we found archival spectroscopic measurements and mid-infrared data. Members of our group reduced the data used for the analysis. The color-corrected fluxes and flux uncertainties can be seen in Table 3.2. The observations used are listed below.

ESO 2.2/FEROS optical spectroscopy — Three spectra of EX Lup in quiescent phase were taken in 2007 July with FEROS at the 2.2 m MPG/ESO telescope in ESO La Silla, Chile. FEROS has a spectral resolution of 48000 and a wavelength coverage from 360 to 920 nm (Kaufer et al., 1999).

NTT/SOFI near-infrared spectroscopy — We found near-IR spectra in the ESO Data Archive, obtained on 2001 May 4 using SOFI at the ESO 3.5 m NTT telescope, under the program 67.C-0221(A) (PI: D. Folha). Two spectra were taken using the blue and red grisms (R $\sim$ 1000), which cover the ranges 0.95–1.64 and 1.53–2.52 μm, respectively. In both cases, the total exposure time was 500 s.

IRAS — EX Lup is included in the IRAS Point Source Catalog with detections at 12, 25 and 60 μm, and with an upper limit at 100 μm. The measurements took place during a quiescent phase of EX Lup. In order to refine these data and also try to obtain a 100 μm flux density value, we analyzed the IRAS raw scans again.

ISO — EX Lup was observed on 5 dates with ISOPHOT, the photometer onboard ISO (Lemke et al., 1996). Four measurements belong to a small monitoring program that adopted similar instrumental setups at each epoch (PI: T. Prusti). The fifth photometric dataset was published by Gras-Velázquez & Ray (2005), but these data were not used in our analysis due to their presumably higher uncertainties. At the four epochs of the monitoring program low-resolution spectrophotometry was also performed with the ISOPHOT-S sub-instrument in the 2.5–11.6 μm wavelength range. These observations were also reduced.

Spitzer Space Telescope/IRAC and IRS — EX Lup was observed with IRAC at 3.6, 4.5, 5.8, and 8.0 μm on 2005 March 29 (PID: 3716, PI: G. Stringfellow), in the subarray mode. Observations with the IRS were carried out on 2004 Aug 30 (PID: 172, PI: N. Evans) and on 2005 March 18 (PID:3716, PI: G. Stringfellow). On the first date, the target was measured using Short Low (5.2–14.5 μm), Long Low (14.0–38 μm), Short High (9.9–19.5 μm), and Long High (18.7–37.2 μm) modules. The integration time was 14 s for the low-resolution, and 30 s and 60 s for the Short High and Long High modules, respectively. At the second epoch only the Short Low, Short High, and Long High modules were used and a PCRS peak-up was executed prior to the spectroscopic observation to acquire the target in the spectrograph slit. The integration times were 14 s for the Short Low module with 4 observing cycles for redundancy, and 120 s and 60 s for the Short High and Long High modules, respectively, both with 2 observing cycles. The two spectra obtained agree within an uncertainty of $\leq 11\%$ and are shown in Fig. 3.1.

Table 3.1 Optical and infrared observations of EX Lup collected from the literature, obtained in its quiescent periods.

λ [μm]	Julian Date	Magnitude	Reference
0.36 (U)	2443349.545	14.21	1
	2443349.572	14.2	1
	2443349.681	14.23	1
	2443349.717	14.25	1
	2443349.728	14.28	1
	2443350.653	14.22	1
	2443353.659	14.13	1
	2443895.85	14.52	2
0.44 (B)	2443349.545	14.33	1
	2443349.572	14.36	1
	2443349.681	14.24	1
	2443349.717	14.36	1
	2443349.728	14.33	1
	2443350.653	14.20	1
	2443353.659	14.07	1
	2443894.85	14.52	2
	2443895.85	14.42	2
	2448896	14.21	3
0.55 (V)	2443349.545	13.13	1
	2443349.572	13.19	1
	2443349.681	13.27	1
	2443349.717	13.27	1
	2443349.728	13.21	1
	2443350.653	13.14	1
	2443353.659	13.22	1
	2443894.85	13.20	2
	2443895.85	13.22	2
	2448896	13.03	3
0.64 (R)	2448896	12.15	3
0.79 (I)	2451295.81	11.109	4
1.25 (J)	2441474	9.76	5
1.25 (J)	2445075	9.92	6
1.235(J)	2451314.781	9.728	7
1.221(J)	2451295.81	9.92	4
1.65 (H)	2441474	9.04	5
1.65 (H)	2445075	9.11	6
1.662(H)	2451314.781	8.958	7
2.2 (K)	2441474	8.82	5
2.2 (K)	2445075	8.78	6
2.159 (K_s)	2451314.781	8.496	7
2.144 (K_s)	2451295.81	8.82	4
3.4 (L)	2441474	≥ 8.7	5
3.4 (L)	2445075	8.05	6
4.8 (M)	2445075	7.54	6

References: (1) Bastian & Mundt (1979); (2) Mundt & Bastian (1980); (3) Herbig et al. (1992); (4) The DENIS database – DENIS Consortium (2005); (5) Glass & Penston (1974); (6) Hughes et al. (1994); (7) 2MASS All-Sky Catalog of Point Sources – Cutri et al. (2003)

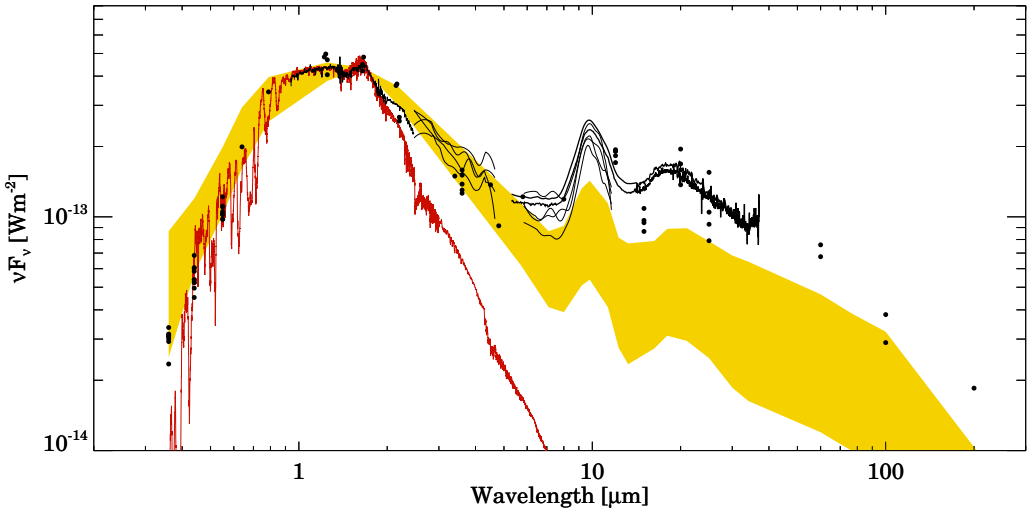

Figure 3.1 – Spectral energy distribution of EX Lup, showing all data points from Tables 3.1 and 3.2 and the smoothed spectra obtained with NTT/SOFI, ISOPHOT-S, and Spitzer/IRS. The yellow band marks the median SED of T Tauri objects from the Taurus – Auriga star-forming region. The $5 - 36$ μm section of the median SED was constructed by Furlan et al. (2006) based on Spitzer IRS data of 55 Class II objects with spectral types between K5 and M2, while the remaining part of our median SED was taken from D'Alessio et al. (1999) who computed their SED from 39 T Tauri stars. The red line overplots the stellar photosphere used in the models (Sect. 3.4.3).

Table 3.2 – Color-corrected fluxes of EX Lupi*

$\lambda[\mu m]$	1983 IRAS	1997 Feb 5 ISOPHOT	1997 Mar 18 ISOPHOT	1997 Aug 24 ISOPHOT	1997 Sept 19 ISOPHOT	2005 Mar 29 Spitzer/IRAC
3.6		0.17 ± 0.03	0.18 ± 0.03	0.15 ± 0.02	0.16 ± 0.03	0.190 ± 0.004
4.5						0.206 ± 0.004
5.8						0.236 ± 0.005
8.0						0.317 ± 0.007
12	0.76 ± 0.1	0.73 ± 0.11	0.78 ± 0.12	0.76 ± 0.12	0.68 ± 0.11	
15		0.54 ± 0.08	0.43 ± 0.07	0.47 ± 0.07	0.48 ± 0.07	
20		1.06 ± 0.15	1.30 ± 0.18	0.91 ± 0.13	1.12 ± 0.16	
25	1.04 ± 0.1	0.78 ± 0.12	0.87 ± 0.14	0.66 ± 0.11	1.29 ± 0.21	
60	1.35 ± 0.4	1.52 ± 0.32				
100	0.97 ± 0.5		1.27 ± 0.17			
200				1.23 ± 0.35		

*For the ISOPHOT data we adopted a conservative formal uncertainty of 15%.

3.3 Results

3.3.1 Variability in the quiescent phase

The observations of EX Lup are sporadic, so no complete SED could be constructed for any given epoch. We decided to merge all quiescent data regardless of their dates. In Fig. 3.1 we plotted all fluxes listed in Tables 3.1 and 3.2. At most wavelengths, the scatter of data points is on the order of 25%, though at optical and a few mid-infrared wavelengths, the difference between the lowest and highest values can be considerably larger. The ISOPHOT-S and Spitzer spectra shown in Fig. 3.1 also exhibit differences at similar levels. Although part of this scatter is related to instrumental and calibration effects, the individual error bars are typically much smaller than the scatter of the data points, strongly suggesting the existence of an intrinsic variability. However, in the case of the 60 and 100 μm data points, the uncertainty of the measurements is much higher than at shorter wavelengths, so here the difference between the fluxes is within the error bars. We consider the 25% peak-to-peak variation as an upper limit for the variability of EX Lup in quiescence. According to Fig. 3.1, the variability might be somewhat greater at optical wavelengths, but the low number of data points prevents us from claiming a wavelength dependence.

3.3.2 The optical–infrared SED

The measured SED of EX Lup is presented in Fig. 3.1. The optical part is clearly dominated by the stellar photosphere. The optical and near-infrared colors, however differ slightly from the standard colors of an M0 V star. This fact has already been mentioned by Gras-Velázquez & Ray (2005), who could not derive a positive extinction value from the $E_{\mathrm{B-V}}$ and $E_{\mathrm{R-I}}$ colors. Similarly, Herbig et al. (2001) claim it is unknown as well. An infrared excess above the photosphere is detectable longwards of the K-band. The 3–8 μm range is smooth and devoid of any broad spectral features, indicating that EX Lup is neither deeply embedded to exhibit ices nor hot enough to excite polycyclic aromatic hydrocarbons (PAHs). A strong silicate emission appears at 10 μm, and a corresponding – though broader and shallower – silicate band can be seen around 20 μm. At longer wavelengths, the continuum

emission decreases following a power law with a spectral index of about $-4/3$. The lack of any sub-mm or mm measurement means that the SED cannot be followed longwards of 200 μm.

3.3.3 Spectroscopy and accretion rates

The high-resolution optical spectrum of EX Lupi, obtained on 2007 July 30, shows several emission lines in addition to the photospheric absorption features characteristic of the young late-type star. The shape of the near-infrared spectrum is similar to that of an unreddened M-type star without near-infrared excess (Greene & Lada 1996). The spectroscopic line identification and most of its analysis was done by Dr. Mária Kun, details of this analysis is given in Sipos et al. (2009). I only inculde here the determination of the accretion rate, which is important for the discussion in the following.

The Hα line of the optical spectrum can be used to measure accretion. According to the most widely accepted magnetospheric accretion model for young stars, the disk is truncated by the magnetosphere of the star at a few stellar radii. From this point, the gas moves along the magnetic field lines and reaches the stellar surface at an accretion shock (Hartmann, 2009). This shock produces emission in the lines of the Balmer and Paschen series, which thus serve as accretion tracers.

The shape of the Hα line in the spectrum of EX Lupi is nearly symmetric. Its equivalent width, W(Hα) = -35.9 Å, is significantly larger than the upper limit of the chromospheric Hα emission of M0 type stars (~ 6 Å, Barrado y Navascués & Martín 2003), indicating active accretion during the quiescent phase. The velocity width of the Hα line 10% above the continuum level is 362 km s^{-1}, larger than the lower limit of 270 km s^{-1}, set by White & Basri (2003) for accreting T Tauri stars. The empirical relationship between the 10% width above the continuum level of the Hα line and the accretion rate $\dot{M}_{\rm acc}$, found by Natta et al. (2004), allowed us to derive $\dot{M}_{\rm acc} = 4.2^{+8.1}_{-2.3} \times 10^{-10}\,{\rm M}_{\odot}/{\rm yr}$.

The Paβ emission line is also a useful accretion tracer, its luminosity correlates well with the accretion luminosity (e.g., Muzerolle et al. 1998; Dahm 2008). We used the relationship established by Muzerolle et al. (1998) to derive the accretion luminosity of EX Lup during quiescence from the measured flux F(Paβ)=1.7 $\times$

$10^{-17}\,\mathrm{W\,m^{-2}}$. The resulting $L_{\rm acc} = 3.7 \times 10^{-3} L_{\odot}$ allowed us to determine the mass accretion rate $\dot{M}_{\rm acc}$, taking the mass and the radius of the star from Table 3.4. The accretion was assumed to proceed through a gaseous disk; for its inner radius we adopted $R_{in} \approx 5\,R_{*}$ (Gullbring et al., 1998). The result is $\dot{M}_{\rm acc} \approx 4.0 \times 10^{-10}\,\mathrm{M_{\odot}/yr}$, in agreement with $\dot{M}_{\rm acc}$ obtained from the velocity width of the Hα line. A flux calibration uncertainty of 20% and the uncertainty of the empirical relationship sets the lower and upper limits for mass accretion rates at $1.3 \times 10^{-10}\,\mathrm{M_{\odot}/yr}$ and $1.1 \times 10^{-9}\,\mathrm{M_{\odot}/yr}$, respectively.

3.4 Discussion

3.4.1 Comparison with young stellar objects

Infrared SEDs of eruptive young stars (EXors and/or FUors) were examined by Green et al. (2006), Quanz et al. (2007) and Sipos & Kóspál (2012). Some of these stars (eg. UZ Tau, VY Tau, DR Tau, FU Ori, Bran 76) resemble EX Lupi. Their SEDs decrease towards longer wavelengths and show a silicate feature in emission. The SEDs of the other group of FU Ori-type or EXor-like variables (e.g. V1057 Cyg, V1647 Ori, PV Cep, OO Ser) exhibit flat or increasing SEDs in the $20-100\,\mu$m wavelength range (Ábrahám et al., 2004a; Kóspál et al., 2007), which is clearly different from the shape of EX Lupi's spectral energy distribution. Green et al. (2006) and Quanz et al. (2007) suggest, that the diversity in the shape of the SEDs is related to the evolution of the system. Younger objects, still embedded in a large envelope exhibit flat SEDs, while more evolved objects, emitting T Tauri-like SEDs have already lost their envelopes and only have circumstellar disks. According to this categorization we conclude that EX Lupi is relatively evolved among eruptive stars, and expect that its circumstellar environment only consists of a disk without an envelope.

To compare EX Lup with other – not eruptive – young stars, in Fig. 3.1 we overplotted a yellow stripe marking the median SED of T Tauri objects from the Taurus-Auriga star-forming region (D'Alessio et al., 1999; Furlan et al., 2006). The SED of EX Lupi follows the Taurus median at shorter wavelengths. Longwards of approximately $7\,\mu$m, however, its absolute level becomes higher than the median by

a factor of ∼2.5. Nevertheless, even in this longer wavelength range its shape still resembles the Taurus slope.

Another comparison of EX Lupi with other pre-main sequence stars can be based on the mid-infrared spectrum. Furlan et al. (2006) present a large sample of Spitzer IRS spectra of young stars and group them into several categories by measuring the slope of the SEDs and the strength of the 10 and 20 μm silicate features. A visual classification places EX Lup in their scheme in group A or in group B, defined by a relatively strong silicate feature and a flat or somewhat decreasing SED over 20 μm. Furlan et al. (2006) suggest that only limited dust-growth and settling has taken place in these groups. Nonetheless, we find that EX Lup is not a typical member of these groups, since shortwards of 8 μm the steep decrease of excess emission characteristic of their objects is missing in the case of EX Lupi. These qualitative conclusions can be verified by calculating color indices for EX Lup (Fig. 3.2). The strength of its silicate feature $(F_{10} - F_{\rm cont})/F_{\rm cont} = 0.58$ is an intermediate value between group A and group B objects. However, the n_{6-25} spectral index is typically negative for all objects in the sequence while positive (0.03) in the case of EX Lupi, making it an "outlier" in the scheme. Also, the correlation between the n_{6-13} and n_{13-25} indices found by Furlan et al. (2006) does not seem to hold for EX Lup. The colors of IRAS 04385+2550, a star exhibiting IRS spectrum very similar to that of EX Lup, were interpreted by Furlan et al. (2006) as indicating for the opening of an inner gap in the disk. This might also give an explanation in case of EX Lup for the lower 6 μm flux compared to that at longer wavelengths. Other sources from their sample that resemble EX Lup are UY Aur, CZ Tau, and HP Tau. It is interesting to note that all four objects are binary systems with different separations (Fig. 3.2).

Finally we calculated the $T_{\rm bol}$ bolometric temperature and $L_{\rm bol}$ bolometric luminosity of EX Lup following the method of Chen et al. (1995). They studied the Taurus and Ophiuchus star-forming regions, and analyzed the distribution of young stars of different evolutionary stages in the $L_{\rm bol}$ vs. $T_{\rm bol}$ diagram. In a later paper (Chen et al. 1997), they repeated the study for the objects of the Lupus cloud as well, including EX Lup. They found $T_{\rm bol} = 2365\,{\rm K}$ and $L_{\rm bol} = 0.7\,{\rm L}_\odot$ based on IRAS data. Using our newly constructed SED, we recalculated these two values. Assuming $A_V = 0\,{\rm mag}$, our result is $T_{\rm bol} = 1982\,{\rm K}$ and $L_{\rm bol} = 0.73\,{\rm L}_\odot$. According to

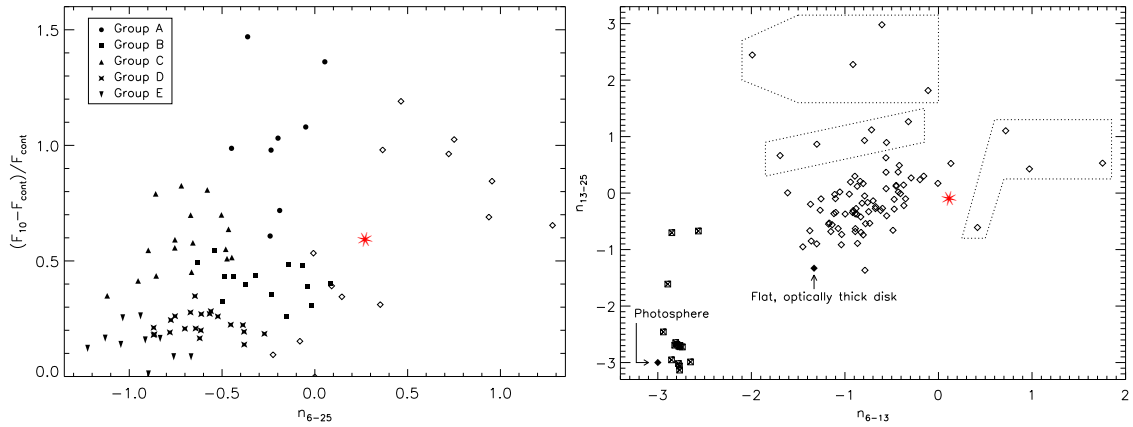

Figure 3.2 – Figures taken from Furlan et al. (2006) with EX Lup overplotted with a red symbol. *Left:* Strength of the continuum-subtracted 10-μm feature, normalized to the continuum, vs. the spectral index between 6 and 25 μm, n_{6-25}. The data points belonging to the groups defined in their morphological sequence of Taurus objects are identified by different filled plotting symbols. The open diamonds identify the "outliers" of the morphological sequence. *Right:* Spectral indices n_{6-13} vs. n_{13-25} for a sample of Class II (*open diamonds*) and Class III (*crossed squares*) objects in Taurus, together with values for a stellar photosphere in the Rayleigh-Jeans limit and for a geometrically thin, optically thick disk. The dotted regions delinate outliers.

these parameters, EX Lup seems to be a typical classical T Tauri star. The location of EX Lup on the $L_{\rm bol}$ vs. $T_{\rm bol}$ diagram implies that it is a Class II object, and its age is $3.8^{+9.2}_{-2.7} \times 10^6$ yr.

3.4.2 Mineralogy

In the following we assume that circumstellar matter around EX Lup is distributed in a disk. To derive the dust composition, an important input parameter for the radiative transfer modelling, in the surface layer of the disk, we fitted the Spitzer IRS spectrum using the Two-Layer Temperature Distribution (TLTD) method (Juhász et al., 2009). Fitting of the dust composition was carried out by another member of our group, Attila Juhász. I present here only the results.

In Table 3.3 we list the used dust species. For each component we specify itsshape and reference to the laboratory measurements of the optical constants. For the homogeneous spheres we used Mie theory to calculate the mass absorption/scattering coefficients. For the inhomogeneous spheres, we used the distribution of hollow spheres (Min et al., 2005), to simulate grain shape deviating from perfect symmetry.

Table 3.3 – Overview of dust species used in fitting the 5–17 μm Spitzer IRS spectrum* and fitted dust composition, with mass fractions larger than 0.1 %.

Dust species	Shape	Ref	Mass fraction [%]		
			0.1 μm	1.5 μm	6.0 μm
Amorphous silicate (olivine stoichiometry)	Homogeneous sphere	(1)	65.6 ± 0.5	–	–
Amorphous silicate (pyroxene stoichiometry)	Homogeneous sphere	(1)	–	32.80 ± 0.5	–
Forsterite	Hollow sphere	(2)	0.7 ± 0.08	–	–
Clino Enstatite	Hollow sphere	(3)	–	0.5 ± 0.3	0.4 ± 0.4
Silica	Hollow sphere	(4)	–	–	–

* References: (1) Dorschner et al. (1995), (2) Servoin & Piriou (1973), (3) Jaeger et al. (1998), (4) Henning & Mutschke (1997)

In Fig. 3.3 we present the fit to the 5–17 μm region of the Spitzer IRS spectrum. The derived dust mass fractions are given in Table 3.3. The spectral decomposition shows that the main contributors to the optically thin 10 μm silicate emission complex are the amorphous silicates (98.4 ± 1.0% in terms of mass). The mass fraction of crystalline silicates is below 2 %, which agrees with the value for the diffuse ISM (Kemper et al., 2005). It is interesting to note that the mass-weighted average grain size of the amorphous silicates (0.57 μm) in our fit is somewhat larger than typically found in the ISM.

Although the reduced χ^2 of the fit is 14.5, which is far higher than unity, as expected for a good fit, the average deviation from the observed spectrum is about 1%. The reason for the high χ^2 can be found in the relatively high signal-to-noise ratio of the Spitzer IRS spectrum (>300 in the fitted wavelength range) and in the deficiencies of the applied dust model (optical constants and grain-shape model). The latter is probably responsible for the differences between the 2D radiative transfer model (see next section) and the observed IRS spectrum between 14 and 21 μm.

Given that EX Lup is a young eruptive star, one would expect to observe an increased value for crystallinity in the mid-infrared features, compared to "normal" T Tauri stars. Since the only requirement of the crystallization is the high temperature, the enhanced irradiation luminosity and viscous heating during the outbursts should lead to rapid crystallization in the disk. In accordance with our results, Quanz

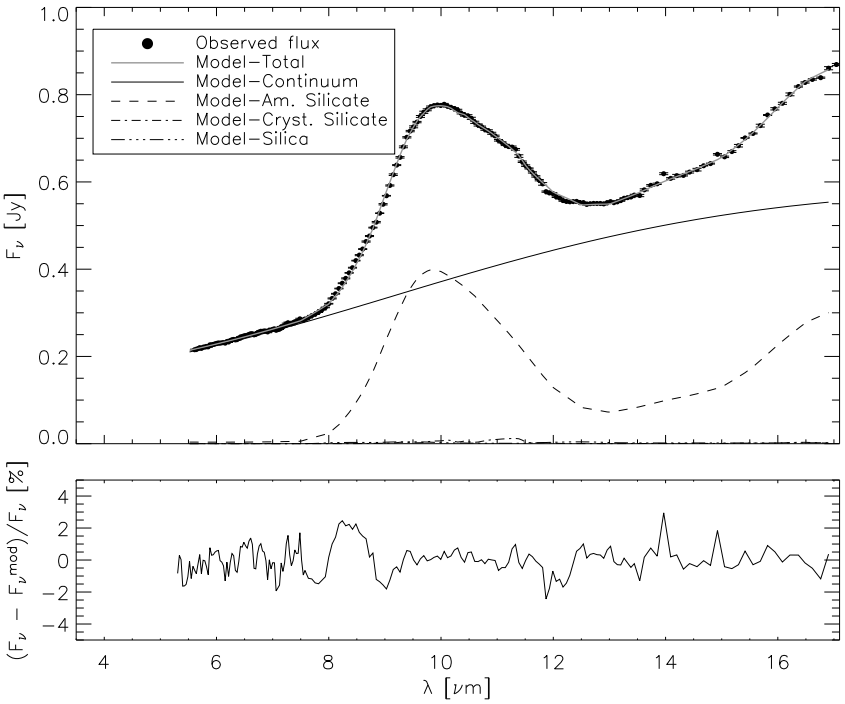

Figure 3.3 – Fit of the observed spectrum. The spectral decomposition shows that the mid-infrared spectrum of EX Lup can be reproduced by a mixture of amorphous silicates with olivine and pyroxene stoichiometry. The contribution of crystalline silicates derived from the spectral decomposition is below 2%.

et al. (2007) report the lack of crystalline emission and the presence of emission from larger grains ($a > 0.1\,\mu$m) in the mid-infrared spectra of FU Orionis objects. They hypothesize that the reason for the lack of crystals can be twofold. One can be the replenishment of the dust content of the disk atmosphere (where the mid-infrared features originate) by pristine dust from an infalling envelope of the FU Ori object. Another possible explanation is strong vertical mixing in the disk that transports the crystals into deeper layers of the disk where they cannot be detected any longer by mid-infrared spectroscopy. Out of these two speculative scenarios, the latter is favorable for EX Lup, since to our knowledge, there is no infalling envelope around the source.

3.4.3 Modelling

In this section we perform a detailed modelling of the EX Lup system, to derive the geometry of its circumstellar environment. We fit the data points presented in

Fig. 3.1, except the mid-infrared domain where, due to the intrinsic variability and the different quality of the data, we considered only the Spitzer measurements: the IRAC and IRS observations form a quasi-simultaneous high quality data set covering the 3.6–38 μm wavelength range.

For the stellar parameters (radius R_*, effective temperature T_*, and mass M_*) we adopted the values used by Gras-Velázquez & Ray (2005). These parameters were fixed during the modelling. (Table 3.4 lists all input parameters marking differently the fixed and the optimized ones.) For the distance of the star we adopted 155 pc, the mean distance of the Lupus Complex as measured by the Hipparcos (Lombardi et al., 2008). The unknown location of EX Lup within the complex introduces an additional uncertainty of about 30 pc. For the value of extinction we assumed $A_V = 0$ mag (Sect. 3.3.2).

We used the Monte Carlo radiative transfer code *RADMC* (Dullemond & Dominik, 2004) combined with *RAYTRACE*[1]. The circumstellar environment is supposed to be axially symmetric, so we used a two-dimensional geometry in polar coordinates (r, θ). As mentioned in Sects. 3.1 and 3.4.1, we had no indication of an envelope around EX Lupi, thus our system only consists of a central star and a dusty disk. For the structure of the disk we assume the density profile as

$$\rho_{\rm disk}(r,z) = \frac{\Sigma(r)}{h(r)\sqrt{2\pi}} \exp\left\{-\frac{1}{2}\left[\frac{z}{h(r)}\right]^2\right\},$$

where r and z are the radial and vertical coordinates, respectively, and $\Sigma(r) = \Sigma_{\rm disk}\left(\frac{r}{r_{\rm disk}}\right)^{-p}$ is the surface density. The 'disk' subscript denotes values of the given parameter at the outer radius. The scale height $h(r)$ increases with radius as

$$\frac{h(r)}{r} = \frac{h_{\rm disk}}{r_{\rm disk}}\left(\frac{r}{r_{\rm disk}}\right)^{\alpha_{\rm fl}},$$

where $\alpha_{\rm fl}$ is the flaring index. A schematic picture of the geometry is presented in Fig. 3.4.

The temperature distribution is determined by the heating sources: the central star, for which we used a Kurucz model atmosphere (Castelli & Kurucz, 2003), and the heated dust grains emitting black body radiation. We used a passive disk and did not consider accretion, due to the low accretion rate in quiescence (Sect. 3.3.3).

[1]for details see: http://www.mpia.de/homes/dullemon/radtrans/radmc/

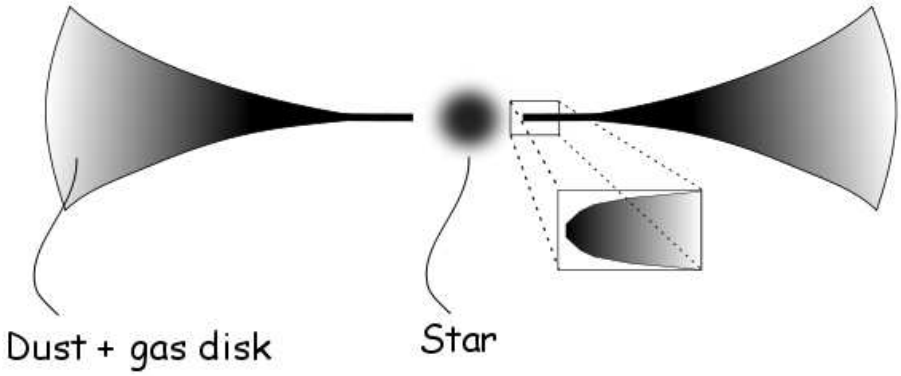

Figure 3.4 – Schematic picture of the geometrical structure of the model of EX Lup. The figure is not to scale.

The accretion luminosity is $< 1\%$ of the stellar luminosity, thus its contribution is negligible compared to direct irradiation coming from the central star. After the calculation of the temperature distribution, the SED of the system is produced at an inclination angle ϑ with the ray-tracer.

We used the dust composition derived from the fitting of the Spitzer IRS spectrum (Sect. 3.4.2), but excluded dust species whose contribution to the total mass is $\leq 1\%$. This way, the dust model used in *RADMC* contained only amorphous silicates of olivine and of pyroxene types with a mass ratio of 2:1. The size of the dust grains were 0.1 μm and 1.5 μm for olivine and pyroxene stoichiometry, respectively. Besides these, we added 20 % amorphous carbon with a grain size of 0.1 μm. The mass absorption coefficients of amorphous carbon were calculated using Mie theory from the optical constants of Preibisch et al. (1993).

We could reasonably fit most of the measured data points by adopting the geometry described above. In the best model of this type we had to move the inner radius of the dusty disk out to 0.5 AU, significantly exceeding the dust sublimation radius (at T=1500 K) of less than 0.1 AU. However, in the 3–8 μm wavelength range this model underestimated the measured points (Fig. 3.5, dotted line). Using smaller values for the inner radius, we could improve the fit of the 3–5 μm range, but then it was not possible to reproduce the measured fluxes at longer wavelengths (Fig. 3.5, dashed line). Reducing the inner radius below 0.2 AU the model fluxes even in the near-infrared wavelength range became too high. To solve this problem, we introduced a rounded inner rim to the disk (see inset in Fig. 3.4); thus instead of having a

Table 3.4 – Parameters used in the best-fit model, where those in italics were adopted from the literature and kept fixed during the modelling.

Parameters	Fitted value
System Parameters	
Distance (d)	155 pc
Inclination (ϑ)	20 °
Stellar Parameters	
Temperature ($T_{\rm star}$)	3800 K
Mass ($M_{\rm star}$)	0.6 $M_\odot$
Radius ($R_{\rm star}$)	1.6 $R_\odot$
Visual extinction ($A_{\rm V}$)	0 mag
Circumstellar Disk Parameters	
Inner radius of dusty disk ($r_{\rm in,disk}$)	0.2 AU
Outer radius of dusty disk ($r_{\rm disk}$)	150 AU
Scale height ($\frac{h_{disk}}{r_{\rm disk}}$)	0.12
Flaring index ($\alpha_{\rm fl}$)	0.09
Exponent of radial density profile (p)	−1.0
Total mass (M)	0.025 $M_\odot$

sharp inner edge with a high wall, we decreased the disk height to $\frac{h_{\rm disk}}{r_{\rm disk}} = 0.05$ at the inner edge of the disk and at the same time moved the inner radius inward. Behind 0.6 AU we left the structure of the disk unchanged. With this modification we could obtain a fit that is in good agreement with all infrared observations. Nevertheless, the inner radius of 0.2 AU used in the best model is still beyond the sublimation radius.

Our best-fit model is presented in Fig. 3.5 with a solid line, and the corresponding parameters are listed in Table 3.4. In the literature we could not find any constraints for the inclination of the system, and its value is not defined well by the model either. The disk is definitely seen closer to face-on than edge-on, and we obtained our best fit using a value of 20°, though fits for inclinations between 0° (face on) and 40° are very similar. The outer radius of the circumstellar disk is typical of young systems, while the disk is massive among T Tauri disks. For the value of the flaring index $\alpha_{\rm fl} = 0.09$ gave the best result, which means that the disk only flares very modestly. The scale height is $h = 12$ AU at the outer radius of the disk, which is slightly higher than the typical value for T Tauri disks. The exponent of the radial surface

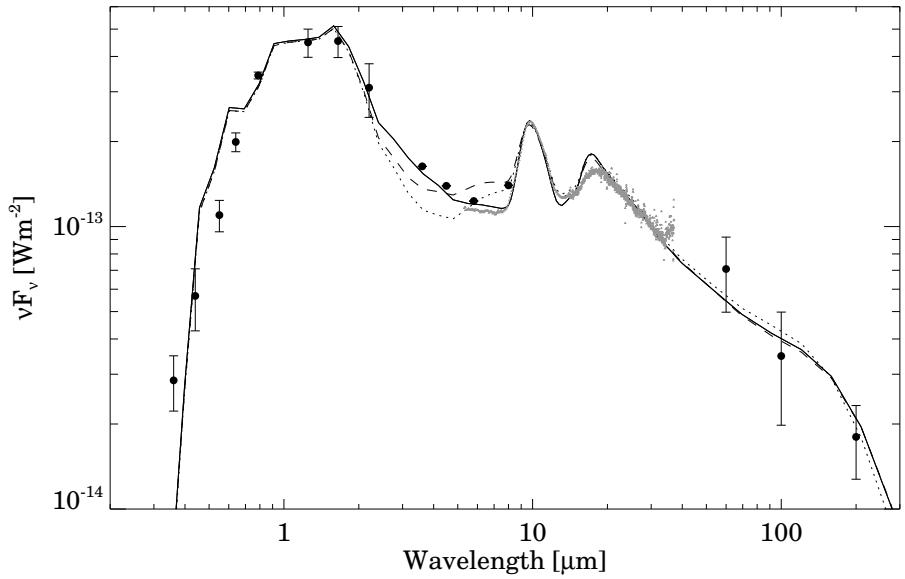

Figure 3.5 – Spectral energy distribution of EX Lup. The solid line shows our best fit model with the rounded inner wall, while the dashed and dotted lines correspond to the best models using a sharp inner edge. The plotted error bars mark the range of observed fluxes at different epochs, also taking the individual measurement uncertainties into account (filled dots correspond to the middle of the range). Error bars on the IRAC points are smaller than the size of the symbols.

density profile is $p = -1.0$.

3.5 Summary and conclusions

We characterized the quiescent disk of EX Lupi and investigated whether it is the structure of the circumstellar environment that makes it an atypical, eruptive young stellar object. Our main findings are the following:

- During quiescent phase there is an indication of an intrinsic variability of less than 25% in the optical–mid-infrared wavelength regime.
- Our new spectra are consistent with the classification of EX Lup as an M type star. Based on the Hα and Paβ spectral lines, we derived a very low quiescent accretion rate of $\sim 4 \times 10^{-10}\,\mathrm{M}_\odot/\mathrm{yr}$.
- EX Lupi is relatively evolved among eruptive stars, and based on its SED its circumstellar environment only consists of a disk without an envelope.

- In general the shape of the SED is similar to those of typical T Tau stars, but above 7 μm EX Lup is brighter than the Taurus median by a factor of $\sim$2.5. The relative flux contribution from shorter and longer wavelengths is a parameter that may distinguish EX Lup from the majority of classical T Tau stars.

- The 10 μm silicate feature of EX Lup can be reproduced well by amorphous silicates with olivine and pyroxene stoichiometry, but no crystalline silicates were found.

- A modestly flaring disk model with a total mass of 0.025 $M_\odot$ and with inner and outer radii of 0.2 and 150 AU, respectively, is able to reproduce the observed SED. The radius of the inner hole is larger by a factor of $\sim$3.5 than the dust sublimation radius.

The existence of this dust-free inner hole points to a clearing mechanism, for which several explanations can be invoked:

(a) Eisner et al. (2007) claim that low-mass young stars with low accretion luminosities tend to have inner disk radii larger than the sublimation radius, probably due to magnetic field effects. Using the relationship in Eisner et al. (2007) and taking 0.2 AU as the magnetospheric inner radius and an accretion rate of 4×10^{-10} $M_\odot$/yr, EX Lupi should have a magnetic field strength of 2.3 kG, which is typical of T Tauri stars (Johns-Krull, 2007).

(b) Binarity might also be responsible for clearing up regions of the disk. In the case of EX Lup the possible binarity has been studied by several authors. Ghez et al. (1997) used high angular resolution techniques to find wide components, and detected no companion of EX Lup between 150–1800 AU separation. Bailey (1998) detected no companion between 1–10 AU. Melo (2003) claims that EX Lup is not a spectroscopic binary, and similarly Herbig (2007) concludes the same based on spectroscopic data measured by the Keck telescope. Guenther et al. (2007) performed an eight-year long radial velocity monitoring program, but they could not detect binarity in the case of EX Lupi either, although they

only had 3 spectra. Nevertheless, we note that, if the inclination of EX Lupi is indeed close to a face-on geometry, that makes it difficult to detect a binarity.

(c) Inner gaps are characteristic of disks in the transitional phase between the Class II and Class III stages. These 'evolved' or 'transitional' disks, exhibit little or no excess over the photosphere in the near-infrared wavelength range (e.g., Luhman et al. 2010). Furlan et al. (2006) suggest that IRAS 04385+2550, an object whose SED is similar to that of EX Lup, could be in a state preceding the transition. This explanation would mean that EX Lup might also be in a pre-transitional state. Recently mostly based on Spitzer observations of large samples of T Tauri stars in various star forming regions, it became evident that signs of being in a later stage of disk evolution among low mass stars is not exceptional. This strengthens the non-exceptional status of EX Lupi among young stars.

(d) Alternatively, with such a low quiescent accretion rate, photoevaporation by EUV radiation may also contribute to the clearing of this innermost region (Gorti & Hollenbach (2009) and Sect. 1.1), similarly to other objects in the transitional phase.

(e) It cannot be excluded that the large inner hole is a phenomenon connected with the eruptive behavior, although details of this connection are unclear yet.

Our detailed modelling of the quiescent disk structure of EX Lup (Sect. 3.4.3) may be a good basis for studying the physical changes related to the 2008 eruption (Chapter 4). Assuming that the outburst stems from temporarily increased accretion, one could scale up the accretion rate in our quiescent model and check whether this new model would reproduce the outburst SED. If this strategy fails to provide a good enough fit to the outburst data, it may be a hint of geometrical restructuring of the circumstellar environment during the outburst.

Our main goals in the present work were to identify atypical features in the circumstellar structure of EX Lup, which may explain its eruptive nature. The

inner-disk hole revealed by our modelling is an unexpected result in this sense, but apart from that, no other observational difference has been found which would distinguish EX Lup from other T Tauri stars. Comparison of EX Lup with other EXors at infrared wavelengths would be important. It may answer the question of whether an inner gap in the dusty disk is characteristic of the EXor phenomenon connecting the hole to the eruption mechanism, and we could learn to what extent EX Lup is a good representative of eruptive stars.

Chapter 4

EX Lupi in outburst

In 2008 January the amateur astronomer Albert Jones announced that EX Lupi had brightened dramatically (Jones, 2008). The object entered its largest known outburst, becoming by about 5 magnitudes more luminous in visual light. The 2008 outburst of EX Lup belongs to the strongest ones ever observed among EXors. A flare-up like this, represents a natural cosmic laboratory to study high temperature energetic phenomena and solid state chemical processes in a protoplanetary disk, that cannot be studied elsewhere. The extreme outburst of EX Lup provided a unique opportunity to collect more information on and understand better the EXor phenomenon and its effects on the circumstellar environment. Our group made use of this opportunity in the framework of a broad observing campaign, that revealed interesting new results in several aspects of the eruption. In this chapter, I will focus on my contribution to the project, connected to the changes induced by the outburst in the dusty environment of the young star.

4.1 Introduction

Upon the news, that EX Lupi was unusually bright, and apparently entered a new outburst period , our group, in collaboration with the star formation group of the Max-Planck Institut für Astronomie (Heidelberg), initiated a large scale observing campaign and submitted several observing proposals to various ground- and space-based telescopes/instruments, with the main goal to be able to examine the outburst

of EX Lup in detail from different perspectives.

Due to the greatly (up to 100-fold) increased luminosity of the central object during an outburst, the disk might undergo structural changes, and the SED becomes radically different. Thus one of our goals was the comparison of the quiescent and outburst SED, that we expected to reveal changes in the temperature/density structure related to the EXor eruption. We gathered data from a wide wavelength range in order to obtain a complete optical-to-submm outburst SED. We analysed the wavelength-dependence of the flux increase, and interpreted the results in terms of disk structure and outburst physics (Juhász et al., 2012). Besides that, we aimed at proving whether crystalline silicates are formed during the outburst (Sect. 4.3). We proposed MIR spectroscopic measurements in order to study changes in the dust composition of the disk due to the outburst heat (Ábrahám et al., 2009; Juhász et al., 2012). NIR-MIR spectroscopic observations (VLT/SINFONI, VLT/CRIRES) were also performed in order to study the dynamics of the very inner, outbursting region of the gas disk and look for probable companions causing variation of the radial velocity (Kóspál et al., 2011; Goto et al., 2011).

In the project I contributed to research related to the dusty environment during the high-state of EX Lup, where the modification of the dust composition is investigated. The dust in stellar systems, including our Solar System has its origins in amorphous silicate grains that can be found in the interstellar medium (Kemper et al., 2004; Li et al., 2007). However, composition of the most ancient bodies in our Solar System, like e.g., comets, contain crystalline silicates (Hanner et al., 1994). These crystals must have formed from amorphous grains by some unknown crystallization process in the protosolar nebula. We reported the first direct observation of on-going silicate crystal formation in the surroundings of a young star, during the 2008 outburst of EX Lup. Our measurements showed new mid-infrared crystalline forsterite features in the outburst spectrum which were not present in quiescence. The observing campaign was coordinated within the group by Péter Ábrahám, research concentrating on the dust composition and outburst physics was lead by Attila Juhász. Our results are published in Ábrahám et al. (2009) and Juhász et al. (2012). I took an active part in proposal writing and preparation and the interpretation of the results. I set up the first model of the outburst and exam-

ined the temperature distribution of the disk, heated by the accretion energy. This gave constraints on the size of the crystal-forming region of the disk both during the 2008 flare-up of EX Lup and in quiescence. It also showed the temperature range where crystallization could be active. The crystals were produced through thermal annealing in the surface layer of the inner disk due to the outburst heat. Our results point to the importance of episodic outbursts in the crystal forming process and thus episodic crystallization.

4.2 Observations

Our proposals were approved and were allocated time within 24 hours on 2008 April 20/21, shortly after the outburst-peak (Fig. 4.1). We attempted to perform the observations as simultaneously as possible to build the SED of EX Lup in the outburst, as previous research on the eruption of another source, V1647 Ori, has shown, that changes in the circumstellar environment of EXors/FUors may happen on daily timescales (Chapter 5). In our observation campaign we used a variety of ground- and space-based instruments. A red line shows the epoch of our measurements in Fig. 4.1. The observation log is given in Table 4.1. Details of data reduction are presented in Ábrahám et al. (2009); Juhász et al. (2012), here I only summarize our observations. The optical brightness variations during the course of the outburst were monitored by amateur and professional astronomers. We collected V-band CCD observations from the ASAS-3 database (Pojmanski, 2002), visual brightness estimations from the AAVSO[1] database and from Albert Jones, a remarkably active amateur astronomer, who has been following the brightness variations of EX Lupi since World War II until today. For the visual magnitude estimation we used an uncertainty of 0.3 mag, which was the average difference between EX Lup and the comparison stars. From the ASAS-3 database we used only the highest quality measurements (quality flag 'A'), for which the uncertainty of the measured V-band magnitude was less than 0.1 mag. The optical light curve is presented in Fig. 4.1.

GROND — We observed EX Lup with the Gamma-Ray Burst Optical and Near Infrared Detector (GROND), which is a 7-channel simultaneous optical-infrared

[1] www.aavso.org

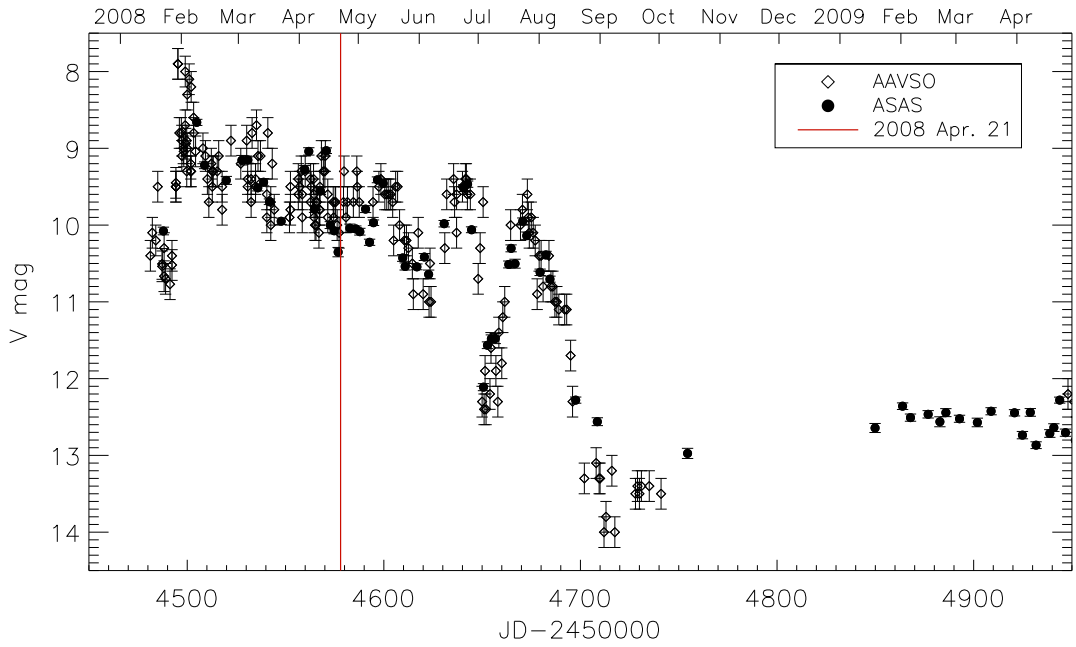

Figure 4.1 – Optical light curve of the 2008 outburst of EX Lupi. The beginning of the outburst was not observed, the last optical measurement (ASAS) in the quiescent phase was on 2007 October 10 (∼110 days before the peak brightness), when the brightness of the source was V=12.7 mag. The maximum brightness of the source was $V \approx 8$ mag. The total length of the outburst was estimated to be about 10 months. The red line shows the epoch of our measurements (Juhász et al., 2012).

imager at the ESO 2.2 m telescope, on 2008 April 20. Optical images, covering a field of view of $5.4' \times 5.4'$, were obtained in the g', r', i', z' bands. At near-infrared wavelengths (JHK_S) images were obtained with a field-of view of $10' \times 10'$.

WFI — EX Lup was observed with the Wide Field Imager (WFI) on the 2.2m telescope in La Silla on 2008 April 20, with about one hour difference with respect to the GROND observations. The field of view of WFI spans $33' \times 34'$ with small holes between the 8 CCD detectors. EX Lup was observed using standard Johnson UBV filters.

NTT SOFI — Observations of EX Lup was carried out on 2008 April 20 using SOFI at the ESO 3.5 m New Technology Telescope (NTT). We obtained near infrared images using the narrow band filters NB1.215, NB1.71 and NB2.195. In addition, SOFI was used to obtain a spectrum using the high resolution grism covering the K band with a slit width of 1".

Table 4.1 Log of observations of EX Lup in our campaign, supplemented with a pre-outburst Spitzer IRS spectrum presented in Chapter 3. For photometric observations F_ν is the derived photometric flux density for a given filter/wavelength, while $F_{\nu,corr}$ is the corrected value for the emission lines (optical photometries only).

Instrument	Date	λ [μm]	F_ν [mJy]	$F_{\nu,corr}$ [mJy]
Spitzer/IRS	18 Mar 2005	5.5–38.0	-	-
WFI	20 Apr 2008	0.36 (U)	159±1.46	159±1.46
GROND	20 Apr 2008	0.45 (g)	450±62	293±62
WFI	20 Apr 2008	0.46 (B)	486±5	319±5
WFI	20 Apr 2008	0.54 (V)	554±5	419±5
GROND	20 Apr 2008	0.61 (r)	675±93	557±93
GROND	20 Apr 2008	0.77 (i)	825±114	754±114
GROND	20 Apr 2008	0.89 (z)	1025±141	721±141
SOFI	20 Apr 2008	1.21	462±13	-
GROND	20 Apr 2008	1.25 (J)	400±9	-
GROND	20 Apr 2008	1.65 (H)	529±13	-
SOFI	20 Apr 2008	1.71	586±16	-
GROND	20 Apr 2008	2.15 (K)	670±31	-
SOFI	20 Apr 2008	2.19	643±18	-
Spitzer/IRS	21 Apr 2008	5.5–38.0	-	-
Spitzer/MIPS	21 Apr 2008	71.42	3130±220	-
LABOCA	21 Apr 2008	870	41±10	-

Spitzer/IRS and MIPS— We obtained spectra of EX Lupi with the Spitzer/IRS instrument on 2008 April 21. We used both the low-resolution modules ($R = 60 - 120$) in the 5.2–14.5 μm wavelength range, and the high-resolution modules ($R = 600$) between 9.9–37.2 μm. We obtained photometry at 70 μm and a low resolution spectrum of EX Lup, using the Spitzer/MIPS instrument. The 70 μm imaging was performed in photometry mode. The low-resolution far-infrared (55–95μm; R$\sim$ 15–25) spectrum of EX Lup was obtained in the SED mode of MIPS.

APEX LABOCA — The source was observed at 870μm using the 295-element LABOCA (Large Apex Bolometer Camera, Siringo et al. 2009) on the 12-m APEX radio telescope (Atacama Pathfinder Experiment, Güsten et al. 2006). The observation was performed on 2008 April 21 in continuous integration mode using a spiral pattern. This observing mode provides a fully sampled map of the total field-of-view of LABOCA.

4.3 Silicate crystals in formation

4.3.1 Observational results

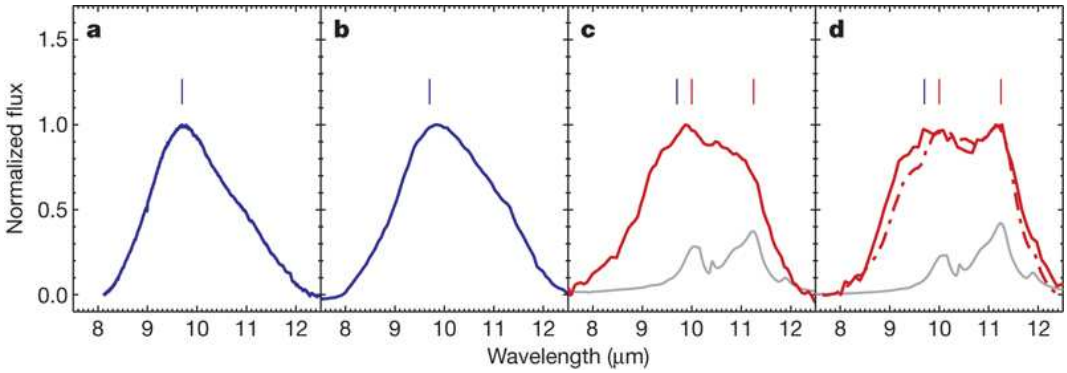

Figure 4.2 – Silicate emission in the 8–12 μm range. (*a*) Spectrum of interstellar grains measured in the direction of the Galactic Centre (Kemper et al., 2004). (*b*) Spitzer Infrared Spectrograph spectrum of EX Lupi, obtained on 2005 March 18, in quiescent phase. (*c*) Our Spitzer spectrum of EX Lupi, obtained on 2008 April 21. (*d*) Red line, ground-based spectrum of Comet 1P/Halley (Hanner et al., 1994); dash–dot line, Spitzer spectrum of the ejecta from Comet 9P/Tempel 1 during the Deep Impact experiment (Lisse et al., 2006). The vertical blue dash at 9.7 μm (repeated in all panels) corresponds to the peak wavelength of the amorphous silicate profile as measured in the laboratory (Dorschner et al., 1995). Peak wavelengths of forsterite at 10.0 and 11.2 μm, as measured in laboratory experiments (Jaeger et al., 1998; Koike et al., 2003), are marked by red dashes. The grey curves in (*c*) and (*d*) display the emissivity curve of pure forsterite (Koike et al., 2003), assuming representative silicate grain temperatures of 1250 K and 300 K, respectively.

MIR spectra — We compared our new Spitzer/IRS spectra of EX Lupi with a pre-outburst measurement from 2005 (Chapter 3), and we observed a significant change (the spectral analysis was done by Attila Juhász). The silicate feature in the 8–12 μm wavelength range (Fig. 4.2) had a triangular shape in quiescence, similar to that of the amorphous interstellar silicate grains (Dorschner et al. 1995; Kemper et al. 2004, Fig. 4.2 a, b). On the other hand, in the spectra measured in 2008, during the outburst, several new, narrow crystalline silicate features are visible (Fig. 4.2 c) on top of the amorphous silicate profile. The new peaks at 10.0 and 11.2 μm correspond to laboratory values of forsterite silicate peaks (Fig. 4.2 c, d), also present in cometary spectra, and in a number of protoplanetary disks (Bouwman et al., 2001; van Boekel et al., 2004). The appearance of a weaker peak at 16 μm supports our

result. At longer wavelengths of the spectrum, no other crystalline features are present. The appearance of crystalline features in the EX Lupi outburst strongly suggests that we witnessed on-going crystal formation. The relative strengths of the 10 μm and 11.3 μm crystal-line features, and the lack of spectral features beyond 16 μm, imply that the new crystals are hot and were formed in a high-temperature process.

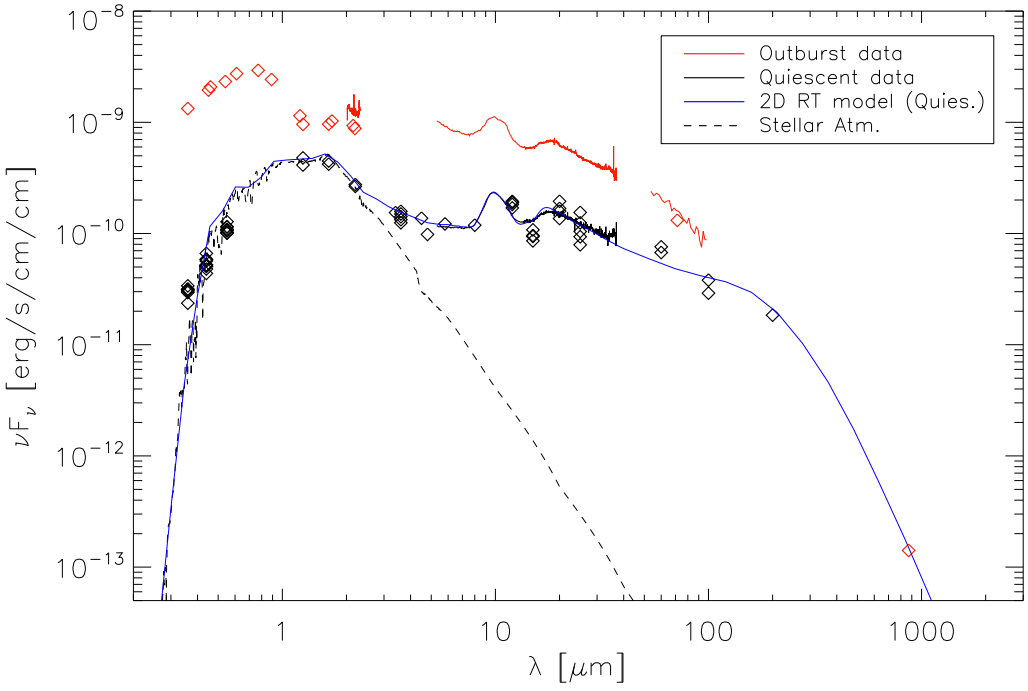

Figure 4.3 – Comparison of quiescent and outburst SED of EX Lup. Black symbols show quiescent data, while the overplotted blue line gives the best fit quiescent model (Chapter 3). Red symbols present our outburst measurements from 2008 April 20/21. The stellar photosphere of an M0 star (T=3800 K), used in the models is shown with a black dashed line.

The outburst SED — The SED of EX Lupi as measured in outburst on 2008 April 20/21 is compared with the quiescent one in Fig. 4.3. At the time of the observations, EX Lupi was already slowly fading after reaching its peak brightness in 2008 February, but was still a factor of 30 brighter in visual light than in quiescence (Fig. 4.1). The outburst-to-quiescent flux ratio was the highest in the U-band and it decreased gradually, though not constantly with wavelength. The shape of the SED in the optical domain is consistent with a black body emission of ∼6500 K, which is far higher than the effective temperature of the star in quiescent phase (3800 K,

Gras-Velázquez & Ray 2005). In the near-infrared domain the flux increased only by a factor of about 2.5 during the outburst compared to the quiescent phase. Moving to longer wavelengths the ratio of the outburst-to-quiescent fluxes increased again to about an order of magnitude at 5.5 μm, which is the shortest wavelength of the Spitzer IRS spectra. Longwards of 5.5 μm the ratio of outburst-to-quiescent fluxes decreased with wavelength.

4.3.2 The temperature structure of the disk and discussion

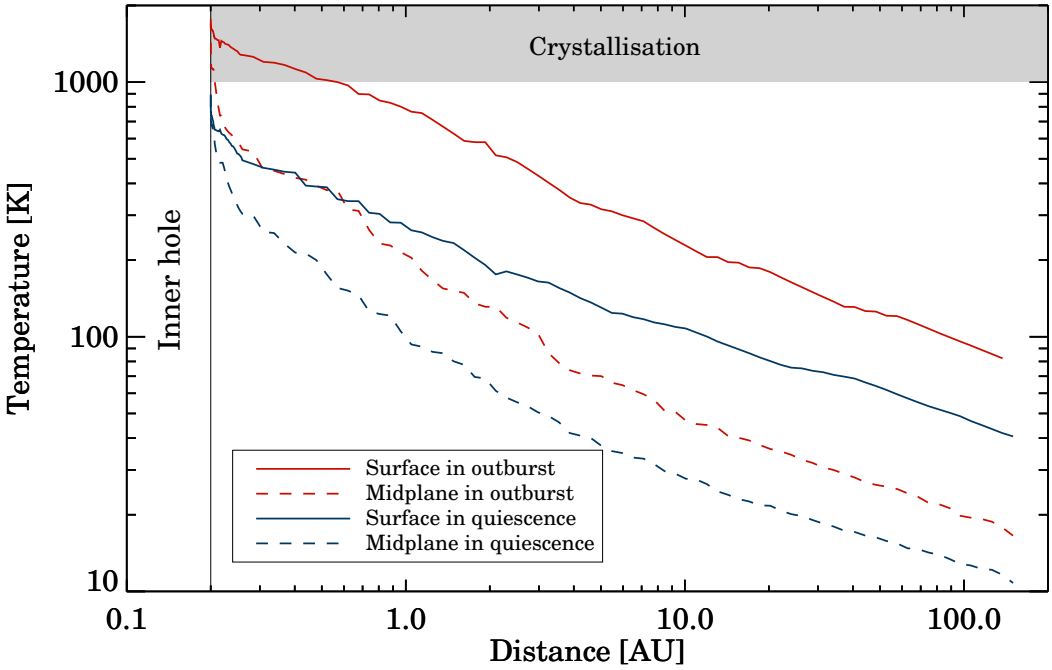

Figure 4.4 – Radial temperature profile of the disk surface (continuous line) and the disk mid-plane (dashed line) in quiescent phase (blue) and in outburst (red). The radius of the inner dust-free hole and the temperature range where crystal formation may take place ($T > 1000$ K) are marked.

I estimated a temperature range for the process of crystal-formation based on the radiative-transfer modelling of EX Lupi in quiescence described in detail in Chapter 3. There, I assumed a circumstellar disk geometry encircling an inner dust-free hole with a radius of 0.2 AU. Owing to this hole, the temperature in the quiescent dusty disk was almost everywhere below 900 K, and outside of a narrow ring located at the inner edge of the disk ($0.2 < r < 0.21$ AU) it decreased to $T \lesssim 700$ K (Fig. 4.4).

The quiescent MIR spectrum indicates that no noticeable crystal formation has occurred at these low temperatures.

For simulating the disk temperature in outburst, I increased the luminosity of the central source compared to the quiescent model by a factor of ten. This was estimated from the flux increase of about an order of magnitude at the highest-frequency part of the Spitzer spectra ($\sim$5 μm, Fig. 4.3). An assumed black body spectrum of 6800 K, typical of outbursting stars (Hartmann & Kenyon, 1996), accounted for the higher temperature of the source during eruption. This value is also close to the black body emission of $\sim$6500 K, consistent with the optical domain of the outburst SED. A comparison of the radial temperature profiles of the disk in quiescence and in outburst are shown in Fig. 4.4. The modelling revealed that, as expected, in outburst the disk temperature became higher both in the midplane and at the disk surface. A significant disk area became hotter than the quiescent value of 700 K, and the inner 0.5 AU area was heated above 1000 K, making crystal formation possible. The temperature in this simple model, was almost everywhere below 1500 K, the approximate vaporization threshold of silicate particles. It only exceeded the sublimation temperature at the inner edge of the disk where it reached a peak temperature of 1700 K. The midplane remained below the crystallization temperature both in quiescence and outburst. Our observations point to a crystallization mechanism that works efficiently between 700 and 1500 K in the protoplanetary environment.

Laboratory experiments suggest that the crystallization mechanism active in this temperature range, is thermal annealing (Hallenbeck et al., 1998; Colangeli et al., 2003). According to laboratory measurements, above 1000 K annealing occurs on very short timescales of seconds to hours (Hallenbeck et al., 1998), in accordance with the observed timescale of the EX Lupi outburst. The radius of this crystal formation zone, 0.5 AU (Fig. 4.3), is comparable to that of the terrestrial-planet region in the Solar System. The high temperature of the crystals excludes their formation in shock fronts at radii of several astronomical units (Harker & Desch, 2002), because grains behind the shock would quickly cool down and produce observable spectral features at wavelengths longer than 20 μm. The low temperatures in the quiescence disk exclude the possibility of crystal formation in a low-state, and also points to

the fact that the crystlas are formed close to the surface due to the outburst, and not in the midplane.

Our observations also indicate that crystals disappear from the surface layers of the disk. Besides smaller scale flarings by factors < 10, EX Lupi underwent a major eruption very similar to the one discussed here in 1955–56 (Fig. 1.7), with a peak visual brightness of 8.5 magnitude (Herbig, 1977). The similar maximum lumiosities of the two eruptions let us suppose that the heating of the disk happened also similarly, thus a region of similar size must have been present where temperatures exceeded the crystallization threshold of 1000 K. Consequently, we may suppose that in the 1955–56 years ago a similar amount of crystalline forsterite was produced, which disappeared from the disk surface by 2005, the epoch of the quiescent spectra.

4.4 Conclusions

Our study demonstrated that crystalline silicates may form in and disappear from the surface layer of the disk within months to decades. This leads us to the assumption, that the observed crystallinity fluctuates, and it depends on the level of the activity of the star and the time elapsed since its last major outburst, and not the dust composition in the deeper layers of the disk. Similar conclusions may hold for many other young stars. Pre-main sequence evolution is generally accompanied by optical–infrared variability (Herbst et al., 2004; Sicilia-Aguilar et al., 2008), and a large fraction of young stars frequently change their luminosity by factors of < 10, resulting in changes of temperatures in the disk. Photometric monitoring of large samples of CTTS over years/decades (Herbst et al., 2004; Grankin et al., 2007) revealed that more than 50% of the CTTS with ages 1–3 Myr exhibit variations over 1 magnitude in the V band, and 10% of them experience even larger variations ($\Delta V \leq$ 1.5–2 mag). Thus, the observed crystallinity may vary considerably, and randomly, among stars of similar mass and age, and correlation of its value with the stellar parameters may be weaker and less informative than previously expected.

The observed new mechanism of crystal formation in protoplanetary disks, episodic surface crystallization, acts in the inner disk region, during accretion-bursts. Such crystallization events may occur in the life of most young stars. With an average

interval of 50 years, EX Lupi may still undergo several thousand such eruptions before the end of its early evolution. The current picture confines crystallization to the very early phases of pre-main sequence evolution (Gail, 2001). Our findings show that crystallization episodes can also continue in later phases, when accretion has significantly dropped (apart from the episodic outbursts), covering a significant part of the pre-main sequence evolution. Moreover, this explanation may work even in disks with large inner holes (such as EX Lupi), where the midplane temperature will never be high enough for crystallization. Although in a single outburst only the thin surface layer of the disk is crystallized, in the case of EX Lupi we saw that subsequent major outbursts can transform a new layer of amorphous grains into crystals, potentially enriching the disk interior through vertical mixing.

Chapter 5

Dynamics during outburst

VLTI observations of the young eruptive star V1647 Ori

By means of our interferometry observing campaign, supplemented by photometric and MIR spectroscopic observations, we investigate the temporal evolution of the inner circumstellar structure of V1647 Ori during its 2003–2006 eruption. We also study the role of the changing extinction in the brightening of the object, and separate it from the accretional brightening. The nature of the changes of the circumstellar environment is studied via detailed radiative transfer modelling at five different epochs, using the radiative transfer code *MC3D*. Variations of the model parameters, together with their timescales, give a direct insight into the dynamics of a pre-main sequence outburst. Probably most, if not all T Tauri stars go through an eruptive phase during their evolution, thus studies of these objects provide information about young low-mass stars in general. Still, until recently, little was known about the circumstellar environment of eruptive stars in outburst. Results of this investigation are presented in Mosoni et al. (2012)

5.1 McNeil's Nebula, a "new" outbursting star

The amateur astronomer, Jay McNeil discovered a new conical reflection nebulosity towards the Orion B molecular cloud, close to the diffuse nebulosity Messier 78 on 2004 Jan 23 (Fig. 5.1, McNeil et al. 2004). The nebulosity, named after the discoverer the McNeil's Nebula, was enlightened by the brightening of V1647 Ori, a low-mass central object, deeply embedded in the dark cloud LDN 1630. The star

Figure 5.1 – LRGB composite image of McNeil's Nebula photographed by Jay McNeil, discoverer of the 'new' nebulosity on 2004 February 15. The cone shaped nebulosity can be seen in the lower right part of the photo, shown by the arrow. The inset shows the object in outburst in a photograph taken in 1966 for the book "The Messier Album" (Mallas & Kreimer 1978)

brightened by ∼4.5 mag in I_C in 3 months (Briceño et al., 2004), until it reached a peak brightness in early 2004.

After its discovery, the source was searched for in various images taken of its surroundings prior to its outburst. A series of observations carried out as part of a

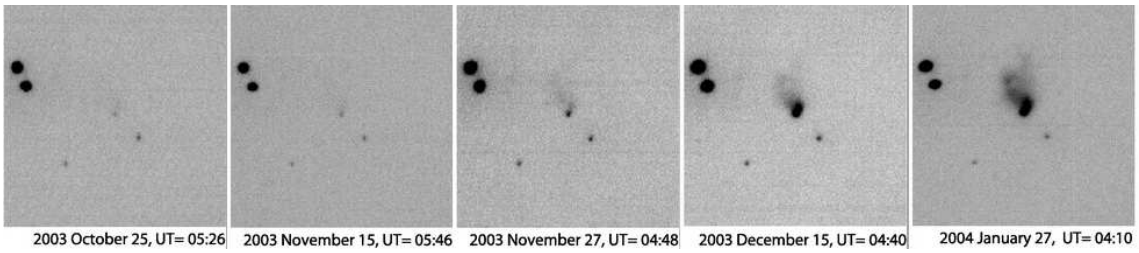

Figure 5.2 – Images of the brightening of McNeil's Nebula (Briceño et al., 2004)

large scale photometric variability study of the Orion OB1 association revealed its brightening, that started in 2003 November (Fig. 5.2, Briceño et al. 2004). Earlier the source was mostly invisible. The object was not present on images of the Palomar Surveys taken in 1951 and 1990, and in the images of the Sloan Digital Sky Survey from 1998 and 2002 the source is very faint. However, in a photograph taken in 1966 for the book "The Messier Album" (Mallas & Kreimer 1978) a bright nebulosity very similar to the one of today appears (see Fig. 5.1, Ábrahám et al. 2004). Also in the very deep [SII] image of Eisloffel & Mundt (1997), taken in October 1995, parts of the nebula are clearly visible, though fainter than in 1966. The object is found in a star forming region, in the vicinity of the Herbig-Haro objects HH22 and HH23. This fact, and the alternation of active and quiescent periods suggested by these earlier observations, indicated that the event is the eruption of a pre-main sequence star. Its behavior is similar to the well-known EXor or FUor outbursts, the reappearance indicating an EXor-type, while the amplitude of the burst rather a FUor-type nature.

The discovery was followed by intense attention of the astronomy community and the 2003–2006 outburst of V1647 Ori became one of the best documented and studied outbursts in the history of eruptive stars (see the references collected by Aspin & Reipurth 2009). Our group also contributed to the investigation of the object, and published their result in several papers (Ábrahám et al., 2004; Ábrahám et al., 2006; Acosta-Pulido et al., 2007). I joined the research related to this outburst of the object in early 2007, shortly after I started working in the group, with two major goals. One of them was to be able to characterize the circumstellar environment of the source quantitatively, the other was to check if the variations of the system during the eruption are restricted to accretion-related changes or obscuration also

plays a role.

The source, after reaching a peak brightness in 2004 March faded slowly for about 20 months. Between 2005 September/October and early 2006 the object faded back rapidly to its quiescent brightness (Acosta-Pulido et al. 2007). Variations of the near-infrared colours along the reddening path suggests that the brightening was partly due to a temporal removal of an extinction slab (e.g., Reipurth & Aspin 2004). Optical and near-infrared spectroscopic observations (e.g., Reipurth & Aspin 2004) showed characteristic spectral features attributed to accretion (Brγ emission) and significant mass-loss (strong Hα emission with P Cyg profile). Measurements also showed the change of the accretion rate over the outburst period (Acosta-Pulido et al. 2007).

Despite the numerous studies (see references in Aspin & Reipurth 2009), the circumstellar structure of V1647 Ori, and its possible variations, have not been investigated in detail yet. The study of Muzerolle et al. (2005) was confined to utilize simple accretion disk/remnant envelope models for data at a single epoch. With the aim at studying the circumstellar disk and envelope of V1647 Ori and the dynamical processes during an eruption, I fitted the SED of the source at several epochs. In order to achieve a better characterization of the inner regions of the source, and obtain more constraints for the modelling, multi-epoch observations with the VLTI/MIDI mid-infrared interferometer were initiated. Spatial information on high angular scales was collected on two epochs. The first dataset from 2005 March was published in a paper by Ábrahám et al. (2006). These data were analysed together with the interferometric data from 2005 September, complemented with SEDs at different phases of the outburst.

The detailed modelling of the circumstellar environment at each epoch helps to decide whether the observed temporal changes are related to the varying illumination of the disk by its central region, or due to a change of the structure of the disk. The results can be directly compared with those on another young eruptive star, PV Cep (Kun et al., 2011), where the observed flux variations are partly explained by variable extinction in the innermost part of the system, due to the evaporation and recondensation of dust grains in the heat of the outburst. Variations of the model parameters, together with their timescales, give insight into the dynamics of

an outburst of the low-mass pre-main sequence star V1647 Ori.

5.2 Observations

5.2.1 VLTI/MIDI

During the 2003–2006 outburst, V1647 Ori was successfully observed twice with MIDI on the VLTI (Leinert et al., 2003): on 2005 March 2 and 2005 September 19. The projected baseline lengths were 56 and 62 m with position angles of 111° and 108°, respectively. Both observing runs were carried out on the UT3–UT4 baseline of the VLTI, and HD 37160 was observed as a calibrator. Due to the optical faintness of the object and the lack of an adequate guide star, MACAO (adaptive optics system of the VLTI for the Unit Telescopes) could not support the observations.

The obtained sets of data consist of acquisition images with the N8.7 filter, 8–13 μm low resolution ($R = 30$) spectra, and interferometric measurements. Data reduction steps, carried out by László Mosoni, are given in the appendix of Mosoni et al. (2012).

Table 5.1 – Log of our VLTI, TCS and RCC observations, and archival Spitzer data of V1647 Ori. The JHK_S photometric errors are in the range of 0.04-0.06 mag, except for the H brightness on 2007 Oct. 22 (0.12 mag) and the I_C brightness on 2007 Oct. 28 (0.10 mag). Notes give the AOR number for Spitzer observations; baseline, projected baseline length and position angle for VLTI observations. Synthetic 8.0, 24 and 70 μm photometry, marked with asterisk, were derived from the Spitzer IRS and MIPS SED spectroscopic data. The mid-infrared MIDI and Spitzer spectra are presented in Sect. 5.3.1

Date	Instrument	Band/Wavelength	Magnitude/flux [Jy]	Notes
2007 Jan. 20	IAC-80	I_J	19.24 mag	
2007 Oct. 28	IAC-80	I_J	19.26 mag	
2008 Feb. 6	RCC	I_C	19.54 mag	
2007 Jan. 20	TCS	J	14.60 mag	
2007 Oct. 22	TCS	J	14.58 mag	
2007 Oct. 28	TCS	J	14.44 mag	
2007 Jan. 20	TCS	H	11.89 mag	
2007 Oct. 22	TCS	H	11.96 mag	
2007 Oct. 28	TCS	H	11.70 mag	
2007 Jan. 20	TCS	K_S	10.01 mag	
2007 Oct. 22	TCS	K_S	9.86 mag	
2007 Oct. 28	TCS	K_S	9.77 mag	

continued on next page

Date	Instrument	Band/Wavelength	Magnitude/flux [Jy]	Notes
2004 Mar. 28	Spitzer/IRAC	3.6 μm	1.883±0.058	9463808
2004 Oct. 27	Spitzer/IRAC	3.6 μm	0.914±0.029	12260864
2005 Feb. 25	Spitzer/IRAC	3.6 μm	0.945±0.034	11570176
2005 Mar. 25	Spitzer/IRAC	3.6 μm	1.117±0.029	11576320
2004 Mar. 28	Spitzer/IRAC	4.5 μm	2.864±0.087	9463808
2004 Oct. 27	Spitzer/IRAC	4.5 μm	1.353±0.044	12260864
2005 Feb. 25	Spitzer/IRAC	4.5 μm	1.443±0.051	11570176
2005 Mar. 25	Spitzer/IRAC	4.5 μm	1.667±0.042	11576320
2004 Mar. 28	Spitzer/IRAC	5.8 μm	3.713±0.111	9463808
2004 Oct. 27	Spitzer/IRAC	5.8 μm	1.716±0.055	12260864
2005 Feb. 25	Spitzer/IRAC	5.8 μm	1.839±0.062	11570176
2005 Mar. 25	Spitzer/IRAC	5.8 μm	2.062±0.052	11576320
2004 Mar. 28	Spitzer/IRAC	8.0 μm	5.721±0.172	9463808
2004 Oct. 21	Spitzer/IRS ($\star$)	8.0 μm	3.71±0.19	12261120
2004 Oct. 27	Spitzer/IRAC	8.0 μm	2.745±0.090	12260864
2005 Feb. 25	Spitzer/IRAC	8.0 μm	3.008±0.097	11570176
2005 Mar. 2	VLTI/MIDI	8.7 μm	3.5±0.5	
2005 Mar. 11	Spitzer/IRS ($\star$)	8.0 μm	2.32±0.12	11569920
2005 Mar. 24	Spitzer/IRS ($\star$)	8.0 μm	2.86±0.14	12644096
2005 Mar. 25	Spitzer/IRAC	8.0 μm	3.217±0.083	11576320
2005 Sep. 19	VLTI/MIDI	8.7 μm	2.0±0.5	
2004 Oct. 21	Spitzer/IRS	4 − 34 μm		12261120
2005 Mar. 2	VLTI/MIDI	8 − 13 μm		56 m / 111°
2005 Mar. 11	Spitzer/IRS	4 − 34 μm		11569920
2005 Mar. 24	Spitzer/IRS	4 − 34 μm		12644096
2005 Sep. 19	VLTI/MIDI	8 − 13 μm		62 m / 108°
2004 Mar. 15	Spitzer/MIPS	24 μm	18.2±2.8	4320256
2004 Oct. 14	Spitzer/MIPS	24 μm	16.5±2.5	12260352
2004 Oct. 21	Spitzer/IRS ($\star$)	24 μm	13.68±0.71	12261120
2005 Mar. 11	Spitzer/IRS ($\star$)	24 μm	8.65±0.45	11569920
2005 Mar. 24	Spitzer/IRS ($\star$)	24 μm	9.95±0.52	12644096
2004 Mar. 15	Spitzer/MIPS	70 μm	25.7±1.7	4320256
2004 Oct. 14	Spitzer/MIPS	70 μm	30.7±1.9	12260352
2004 Oct. 15	Spitzer/MIPS ($\star$)	70 μm	36.6±3.7	12260608
2005 Mar. 1	Spitzer/MIPS ($\star$)	70 μm	30.6±3.1	11570432
2005 Mar. 4	Spitzer/MIPS ($\star$)	70 μm	32.6±3.3	11576576
2006 Nov. 8	Spitzer/MIPS	70 μm	2.7±0.2	17455360
2004 Oct. 15	Spitzer/MIPS	55 − 95 μm		12260608
2005 Mar. 1	Spitzer/MIPS	55 − 95 μm		11570432
2005 Mar. 4	Spitzer/MIPS	55 − 95 μm		11576576

5.2.2 Optical and NIR photometry

In addition to the already existing photometric data (Acosta-Pulido et al. 2007), new NIR J-, H-, and K_S-band observations were carried out by other members of

our group in 2007 and 2008 (Tab. 5.1). These data could be used to characterize the post-outburst quiescent phase object. The data were obtained using CAIN-2 installed on the 1.52 m Carlos Sanchez Telescope (TCS) at the Teide Observatory (Tenerife, Canary Islands, Spain). We also observed V1647 Ori in the I_J and I_C bands with the 82 cm IAC-80 telescope at the Teide Observatory and the 1 m RCC telescope at the Piszkéstető station of the Konkoly Observatory, respectively. The technique of observation, data reduction and photometric calibration of these data were identical with our previous TCS, IAC-80 and RCC observations of V1647 Ori and are described in detail in Acosta-Pulido et al. (2007).

5.2.3 Spitzer archival data

We found archival Spitzer/IRAC observations of V1647 Ori measured at 3.6, 4.5, 5.8, and 8.0 μm at four different epochs (Table 5.1). The photometric results related to the observation performed on 2004 March 28 have already been published (Muzerolle et al. 2005). These data were re-reduced here, and we obtained somewhat lower flux values at all four wavelengths, due to the different pipeline versions used. The additional three observations were performed in the framework of two different programs (PID 224 and 3716, PI: G. Stringfellow) and were downloaded from the Spitzer Heritage Archive.

Mid-infrared spectra of V1647 Ori were observed with Spitzer/IRS at three different epochs. On 2004 October 21 and on 2005 March 24 the target was measured with the Short-Low (5.2–14.5 μm, R $\sim$ 60–127), Short-High (9.9 – 19.5 μm, R $\sim$ 600) and Long-High (18.7–37.2 μm, R $\sim$ 600) channels, while on 2005 March 11 the Short-Low and the Long-Low (14.0–38.0 μm, R $\sim$ 57–128) channels were used. All these data were published by Quanz et al. (2007), and we consider these spectra for our modelling.

Observations of V1647 Ori were carried out with Spitzer/MIPS (Rieke et al., 2004) in scan map mode on 2004 March 15 and in photometry mode on 2004 October 15 and 2006 November 8. The final photometry and its uncertainty is listed in Table 5.1. The MIPS data in Table 5.1 are colour-corrected (by a factor of 0.91). Our results for 2004 March differ from those of Muzerolle et al. (2005) due to the different pipeline versions and the additional data reduction steps.

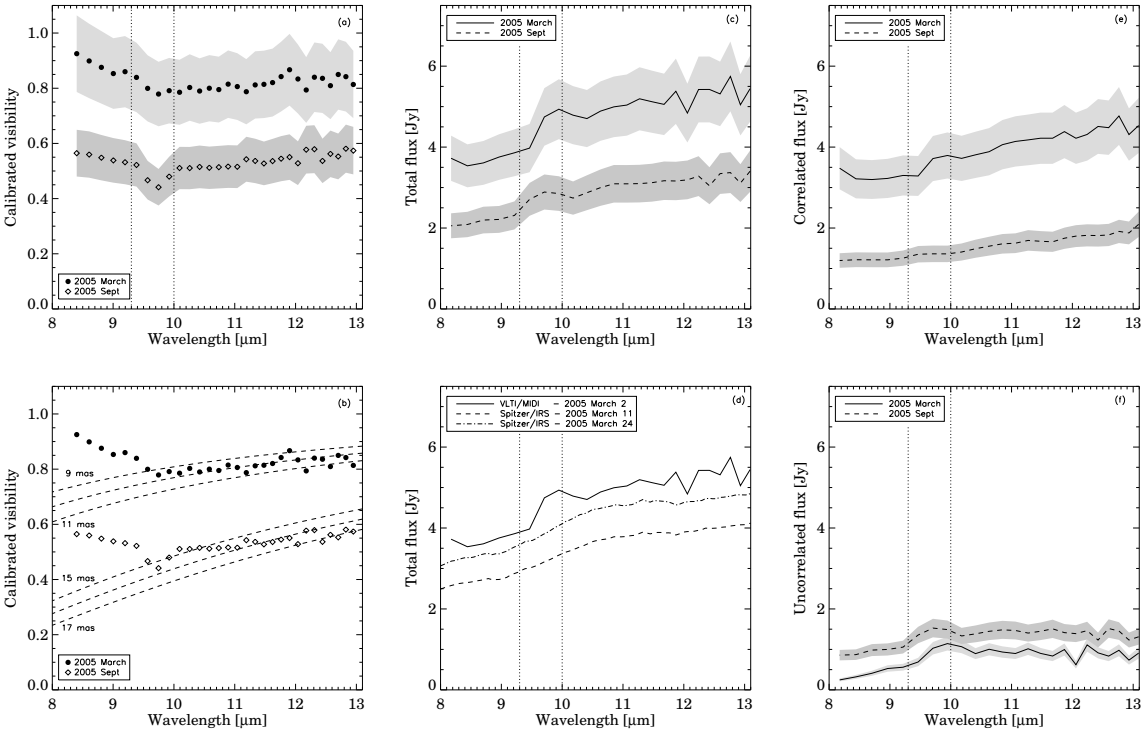

Figure 5.3 – *(a)* Calibrated visibilities and *(b)* Gaussian size estimates. MIDI spectra are shown in *(c)*. The MIDI and Spitzer/IRS spectra from 2005 March are compared in *(d)*. Correlated spectra (i.e. inner disk spectra, panel *e*) and uncorrelated spectra (i.e. outer disk spectra, panel *f*) of V1647 Ori are also shown at two epochs. Note that the baselines of the two observations are very similar, so MIDI data of the two epochs can be compared. The shaded areas mark the 15% errors on panels *a, c, e, f*. The vertical dotted lines show the ozone band which could affect the ground based observations.

V1647 Ori was also observed using the MIPS SED mode. Low resolution far-infrared (55–95 μm; $\lambda/\Delta\lambda \sim 15$–25) spectra were obtained on 2004 October 15 and on 2005 March 1 and 4. Finally, synthetic 8.0, 24 and 70 μm photometry were derived from the IRS and MIPS SED data, by convolving the spectra with the corresponding IRAC or MIPS filter profiles. The results are presented in Table 5.1.

5.3 Results

5.3.1 MIDI results

Fig. 5.3 shows the calibrated visibilities obtained in 2005 March and September. The baselines of the two observations are very similar (Table 5.1), thus the two visibility curves can be directly compared. The difference indicates a significant change in the geometry of the mid-infrared emitting region of V1647 Ori in the 6 months elapsed between the two observations. As a first approximation, we considered Gaussian brightness distributions to estimate the characteristic size of the mid-infrared emitting region defined as the FWHM of the Gaussian. Although the object is much more resolved at the second epoch, thus the Gaussian assumption is less adequate for size estimation, we convert the visibilities to FWHM providing a simple comparison of the interferometric data. Single Gaussians of FWHM = 10 mas and 16 mas, equivalent of 4.0 AU and 6.4 AU at the distance of 400 pc, respectively, fit both visibility datasets well longward of $\sim$10 μm. The object was less resolved at wavelenghts shortward of $\sim$10 μm at both epochs, probably due to an inner warm part of the system. As the shape of the visibility curves is similar to those observed for other YSOs with MIDI (e.g., Leinert et al. 2004; Quanz et al. 2006; Ratzka et al. 2007), we can assume that they have similar circumstellar structures, so the radiation from the inner edge of the disk can dominate at the short wavelengths.

Similarly to Ábrahám et al. (2006), we do not see any sinusoidal variations in the spectrally resolved visibilities potentially caused by a companion. Since the baselines of the two observing runs are very similar, we can only repeat our earlier finding that the shape of the new visibility curve suggests that no companion is present at the measured position angle whose separation is between about 10 and a few hundred AU, and the brightness ratio is larger than 10%.

Our two 8–13 μm MIDI spectra are shown in Fig. 5.3. Although the absolute level of the mid-infrared spectra decreased by a factor of 2 between the two epochs, the shapes of the two spectra are similar. In Fig. 1 *(d)* we also plotted the two IRS spectra obtained in 2005 March. Variations on weekly time-scales are clearly present. Quanz et al. (2007) found weak silicate emission in the IRS spectra. Although the ozone band can affect the spectra at 10μm, this weak feature might also be present

in the MIDI spectra.

The uncorrelated spectrum is calculated as the difference of the total and the correlated ones. The correlated and uncorrelated spectra of an object are dominated by radiation from different circumstellar regions: the inner regions of a few AU size and the outer parts, respectively (van Boekel et al., 2004). In the case of V1647 Ori, most of the mid-infrared emission originates from the inner compact zone of the circumstellar environment, the correlated spectrum being higher than the uncorrelated spectrum. The correlated fluxes decreased significantly between the two MIDI observations, while the uncorrelated fluxes remained practically the same (Fig. 5.3 *f*). These findings suggest that the fading of the mid-infrared emission of V1647 Ori was concentrated to the inner parts. The correlated spectra look featureless; the weak silicate emission seems to be associated with the outer parts of the system.

5.3.2 Optical and infrared light curves

Figure 5.4 shows the light curves of V1647 Ori at five optical and infrared wavelengths (0.8, 2.2, 8.0, 24, and 70 μm) between 2004 and 2007. The overall shape of the I_C light curve, which is the most complete, can be divided into a plateau (2004 February–2005 September), a rapid fading (2005 October–2006 February), and the subsequent quiescent phase. Besides the general slow fading during the plateau phase, short time-scale low-amplitude variations are also observed. The rapid fading started around the epoch of the second MIDI observations. The available data in the K_S band may suggest a light curve similar to that of I_C, but with a smaller amplitude. Although the light curves at 8, 24 and 70 μm are even more sparsely sampled, they are not inconsistent with the shape of the I_C band light curve. We note that at 70 μm, the object became $\sim$20% brighter between the 2004 March peak and 2004 October. During the same period, the IRAC fluxes decreased by a factor of 2. This suggest a time shift between the peak brightnesses at the different wavelengths. The cause of such a shift at 70 μm is unclear.

Comparing the flux values obtained in 2006 to the pre-outburst ones (interpolated in wavelength in Fig. 1 of Ábrahám et al. (2004), we conclude that V1647 Ori returned to quiescence after 2005. The 2007 fluxes at 8 and 24 μm are even lower

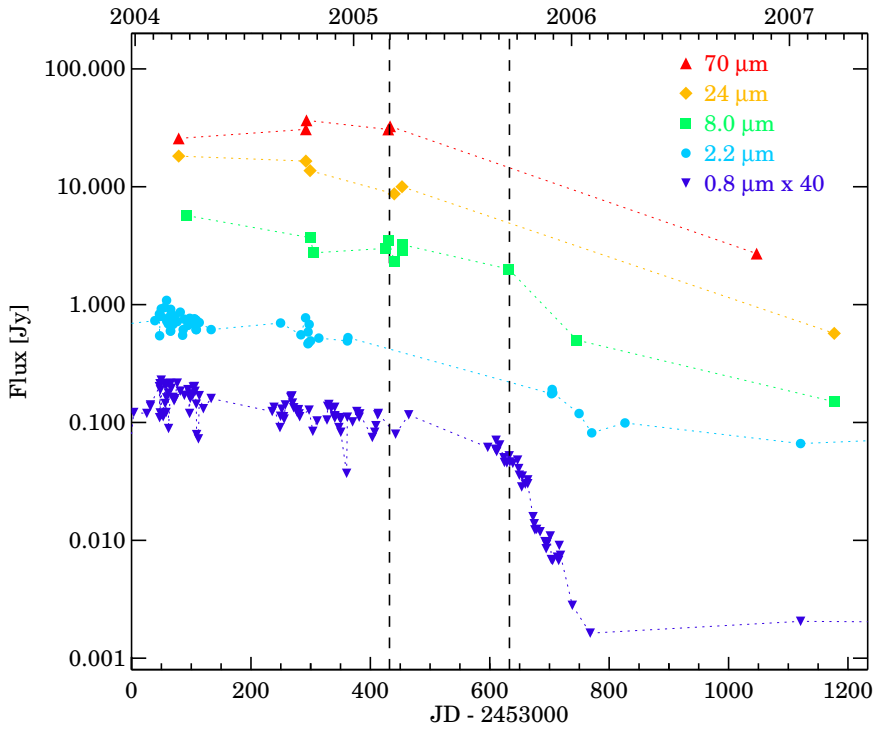

Figure 5.4 – Light curves of V1647 Ori. The vertical dashed lines denote the epochs of the MIDI observations. I_C (0.8μm) and K_S (2.2μm) band data are from Acosta-Pulido et al. (2007) and Mosoni et al. (2012). The I_C data are scaled up by a factor of 40 for the sake of better plotting. 8.0 μm data are from Muzerolle et al. (2005), Ábrahám et al. (2006), Quanz et al. (2007), Mosoni et al. (2012) (obtained from MIDI acqusition data), and Aspin et al. (2008), extrapolated from their N′ band data). 24 μm data are from Mosoni et al. (2012) and Aspin et al. (2008) (extrapolated from their Q_a band data). 70 μm data are from Mosoni et al. (2012).

than the respective pre-outburst values. This can either be due to variability in the quiescent phase (similar as seen in the pre-outburst I_C data of Briceño et al. 2004); or might be related to the beam differences of the different instruments, or differences in the photometric systems, or it might even indicate a different object structure after the outburst.

5.3.3 Spectral energy distribution

We constructed SEDs of V1647 Ori for several different epochs to study its circumstellar environment. These epochs were those of the two MIDI observations (2005 March 2 and 2005 September 19), the quiescent phase, the peak of the outburst

(2004 March) and 2004 October. Due to the lack of simultaneous data, we involved in the SEDs also optical and near-infrared data points obtained within a period of a few weeks of the nominal date. The five SEDs are plotted in Fig. 5.5. The pre- and post-outburst data are plotted together on the quiescent SED. The Spitzer IRS and MIPS SED spectra are also plotted. The absolute errors of both spectra are ∼10%. The steepness of the IRS and MIPS SED spectra (in particular in 2005 March) are significantly different. For reasons related to the radiative transfer modelling, described in Sect. 5.4.1, we consider only data shortward of $\sim 100\,\mu$m. Submillimeter and millimeter data are used only for the estimation of the mass of the system (see Sect. 4.1.1).

5.4 Modelling and Discussion

First we adopted a simple thin-disk model of the V1647 Ori system where the given temperature profile are treated as thin annuli emitting black body radiation of the given temperature (Sect. 2.4). This approach is the same as the one presented in Ábrahám et al. (2006). The results are described in more detail in Appendix B of Mosoni et al. (2012), in the following we present only our conclusion. We modeled the two MIDI epochs (the work of László Mosoni) as described in Ábrahám et al. (2006). We also created such models for the quiescent and the peak states. We found that the characteristic temperature (at 1 AU, which is likely proportional to the mass accretion rate) is the major parameter which changes through the outburst, being highest at the peak and decreasing gradually as the object was fading in 2005 (Mosoni et al. 2012, Table B.1). Although the SED model at the second MIDI epoch is satisfactory, the model cannot reproduce the low visibility values measured in September 2005 (Mosoni et al. 2012, Fig. B.1). Since there was no room to optimize further for the interferometric data we concluded that this type of model could not be confirmed. Therefore we turned to a more physical and complex model.

5.4.1 Radiative transfer modelling

In the following I fit both the SEDs and the visibilities using a radiative transfer code providing a more realistic representation of both the circumstellar environment

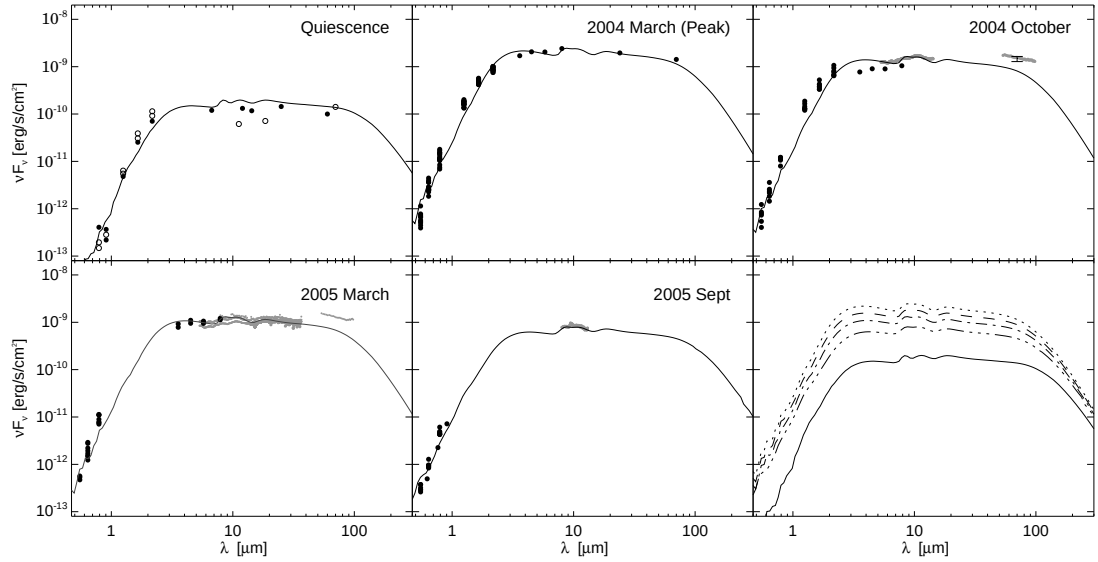

Figure 5.5 – Spectral energy distributions of V1647 Ori at five different epochs. Because of the short timescale variability at the optical and near-infared wavelengths, we present photometry from between 2004-02-01 and 2004-04-30 (2004 March), 2004-10-01 and 2004-10-31 (2004 October), 2005-02-01 and 2005-04-30 (2005 March) and 2005-09-03 and 2005-10-03 (2005 September) in these figures, for the quiescent SED we merged all available quiescent data, filled symbols give pre-outburst, open circles post-outburst measurements. The best fitting models to the SEDs are overplotted with solid lines (see Sect.5.4.1). The last panel shows all the best fitting models. The decrease of the brightness of the object with time, from peak (top) to quiescence (bottom) is continuous.
References: *Quiescence* – Ábrahám et al. (2004); Ábrahám et al. (2006); Aspin et al. (2008); *2004 March (peak)* – Acosta-Pulido et al. (2007); McGehee et al. (2004); Muzerolle et al. (2005); *2004 October* – Acosta-Pulido et al. (2007), Mosoni et al. (2012), Quanz et al. (2007); *2005 March* – Acosta-Pulido et al. (2007), Mosoni et al. (2012), Quanz et al. (2007); *2005 September* – Mosoni et al. (2012), Aspin & Reipurth (2009).

and the heating mechanisms. My strategy for fitting the data was as follows. First I set up a reference model that fits the 2005 March data. I chose this epoch to serve as a starting point because our observational data set is most complete here. Then, I modify this initial setup as necessary to fit the data of the other epochs. The significant change of the MIDI visibilities might indicate structural changes of the inner regions of the circumstellar environment. The case of the 2005 September epoch is discussed separately in Sect. 5.4.3.

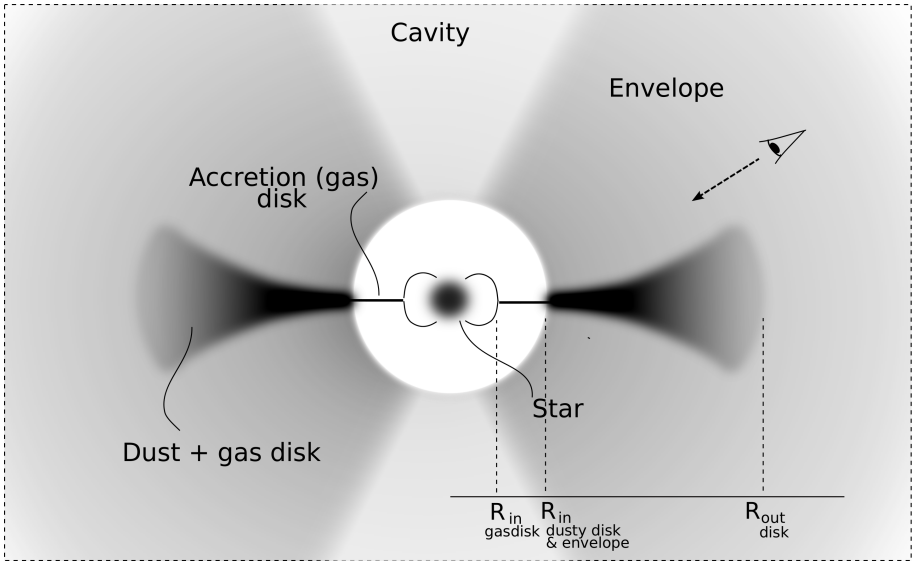

Figure 5.6: Schematic picture of the model geometry of the object (not to scale). The line of sight crosses through the envelope. The inclination of the disk is $\vartheta \approx 60°$, the opening angle of the cavity is 50° (Acosta-Pulido et al. 2007).

5.4.1.1 General overview of the model

For the radiative transfer modelling I use the Monte Carlo code *MC3D* (Wolf et al., 1999, 2003; Schegerer et al., 2008). I assume an axial symmetry of the circumstellar environment, so I use a two-dimensional geometry in polar coordinates (r, θ).

The model system consists of a central star, an inner accretion (gas) disk, and a dusty outer disk embedded in an envelope, from which a cone-shaped cavity is cut (Fig. 5.6). For the structure of the disk I assume the density profile to be like the one used by Wood et al. (2002):

$$\rho_{\rm disk} = \rho_0 \left(\frac{R_*}{\varpi}\right)^{\alpha_{\rm disk}} \exp\left\{-\frac{1}{2}\left[\frac{z}{h(\varpi)}\right]^2\right\},$$

where ϖ is the radial coordinate in the disk midplane, z is the vertical height and ρ_0 is determined from the mass of the disk. The scale height $h(\varpi)$ increases with radius as:

$$h = h_0 \left(\frac{\varpi}{100\,{\rm AU}}\right)^{\beta},$$

where h_0 is the scale height at a radial distance of 100 AU from the center of the

system. The density profile of the envelope is spherically symmetric:

$$\rho_{\rm env} = \rho_{0,\rm env} \left(\frac{R_*}{r} \right)^{\alpha_{\rm env}} .$$

Here r gives the distance from the star, and $\rho_{0,\rm env}$ is the function of $\rho_{0,\rm disk}$. The transition between these two components is assumed to be smooth. In vertical direction the envelope starts where the density of the disk decreases to the density of the envelope. In the cavity I use a density distribution identical to that of the envelope, but a factor of 10^{-6} less dense.

The temperature distribution of the system is determined by the heating sources: the central star, the heated dust grains, both emitting black body radiation, and the accretion, consisting of an α-type disk concentrated to the midplane and a hot spot on the stellar suface (for details of accretion effects see Schegerer et al. 2008). The accretion process is characterized by three parameters, the accretion rate $\dot{M}$, the temperature $T_{\rm spot}$ of the accreting region on the surface of the star, and the magnetic truncation radius $R_{\rm trunc}$. After the calculation of the temperature distribution, the SED and a projected image of the system is produced at an inclination angle ϑ with a ray-tracer.

The temperature $T_{\rm star} = 3800$ K and mass $M_{\rm star} = 0.8\,{\rm M}_\odot$ of the star were taken from Aspin et al. (2008), while the radius $R_{\rm star} = 3.25\,{\rm R}_\odot$ was recalculated from the post-outburst luminosity considering a distance of $d = 400\,{\rm pc}$ (Anthony-Twarog, 1982). These parameters were fixed during the fitting procedure. The circumstellar disk in the model is embedded in a significantly larger envelope that stretches out far beyond the disk, to 3000 AU, in accordance with the mm-images from Tsukagoshi et al. (2005). The inclination of the disk was fixed to be $\vartheta \approx 60^\circ$ and I set the opening angle of the cavity to 50° (Acosta-Pulido et al. 2007), thus the line of sight to the star crosses through the envelope. Although the mid-infrared ice features indicate the presence of foreground material (Vacca et al., 2004; Rettig et al., 2005; Quanz et al., 2007), the ice can also be in the outer regions of the extended envelope around V1647 Ori. Therefore I fixed the interstellar extinction to be $A_{\rm V} = 0$ and assumed that all extinction is circumstellar.

The 10 μm silicate feature is too weak to determine the dust composition via model-fitting. Therefore I considered standard interstellar dust, a mixture of 62.5% astronomical silicate, and 37.5% graphite (the optical parameters were taken from

Weingartner & Draine 2001). The shape of the continuum-subtracted features (Quanz et al., 2007) supports the plausibility of this assumption. I assumed spherical dust grains, with a power-law size distribution: $n(a) \propto a^{-3.5}$, for $a_{\rm min} \leq a \leq a_{\rm max}$, where $n(a)$ is the number of dust particles with a radius a. For the minimum and maximum grain size I used $0.005\,\mu m$ and $0.25\,\mu m$, respectively. The gas-to-dust mass ratio is assumed to be 100, while the grain mass density is set to $\rho_{\rm g} = 2.7\,{\rm gcm}^{-3}$. I found that with the maximum grain size of $0.25\,\mu m$ I underestimate the submm to mm flux in all of our models, unless assuming a disk mass of $\sim 1\,{\rm M}_{\odot}$, which would result in gravitational instabilities. Besides that, the submm–mm slope of the model is steeper than that of the measured data, which leads to the conclusion, that the system possibly contains larger grains than the maximum size used. However, the larger grains are thought to be within the inner regions of the disk closer to the midplane due to sedimentation, affecting the SED significantly only in the (sub-)mm regime, since this region is optically thick at shorter wavelengths. Thus our model can be considered valid shortward of $\sim 100\,\mu$m.

I estimated the mass of the system from the 1.3 mm flux (Lis et al., 1999), using the method described in Beckwith (1999). Assuming $T = 50\,{\rm K}$ and $\kappa_{\nu} = 0.02\,{\rm cm}^2{\rm g}^{-1}$ I found that the total mass of the circumstellar matter is $M_{\rm tot} = 0.045\,{\rm M}_{\odot}$. The estimate is similar to that of Andrews et al. (2004). I considered this estimate as a fixed parameter during the model-fitting.

5.4.1.2 The reference model: 2005 March

As a first step I fitted the available photometric and interferometric data for the 2005 March epoch. I attempted to fit the data with the extreme cases of envelope-only and disk-only models, but I concluded that neither of the two components can be neglected. The parameters of the circumstellar environment are not well defined by the models as the parameters of the envelope and the disk are not independent (eg. Natta 1993). For reducing the degeneracy further system parameters were fixed. I set the outer radius of the disk to 500 AU and the value of $\alpha_{\rm env}$ to -1.5 (Shu, 1977). In the following I present results with these fixed parameters, although the conclusions and the trends seen are also valid for slightly different setups of the disk–envelope system. For further reduction of the number of free parameters, the

Table 5.2 – Parameters of the best fitting model for 2005 March. The fitted parameters are shown in italics.

Parameters	Final model	References for fixed parameters
Stellar parameters		
Temperature ($T_{\rm star}$)	3800 K	Aspin et al. 2008
Mass ($M_{\rm star}$)	0.8 $M_\odot$	Aspin et al. 2008
Radius ($R_{\rm star}$)	3.25 $R_\odot$	Aspin et al. 2008, recalculated
Interstellar visual extinction ($A_{\rm V}$)	0 mag	
Circumstellar disk parameters		
Inner radius of dusty disk ($R_{\rm in,disk}$)	0.75 AU	
Outer radius of dusty disk ($R_{\rm out,disk}$)	500 AU	
Scale height at 100 AU (H_0)	15 AU	
Flaring index (β)	1.2	
Exponent of radial density profile ($\alpha_{\rm disk}$)	-1.75	
Total mass of disk and envelope (M)	0.045 $M_\odot$	estimated
Distance (d)	400 pc	Acosta-Pulido et al. (2007)
Inclination (ϑ)	60 °	Acosta-Pulido et al. (2007)
Circumstellar envelope parameters		
Inner radius of dusty envelope ($R_{\rm in,env}$)	0.75 AU	
Outer radius of dusty envelope ($R_{\rm out,env}$)	3000 AU	Tsukagoshi et al. 2005
Exponent of radial density profile ($\alpha_{\rm env}$)	-1.5	
Parameters for the accretion		
Accretion rate ($\dot{M}$)	3.5×10^{-6} $M_\odot$yr^{-1}	
Magnetic truncation radius ($R_{\rm trunc}$)	5 $R_{\rm star}$	Calvet & Gullbring 1998
Temperature of the hot spot ($T_{\rm spot}$)	6500 K	Calvet & Gullbring 1998

inner radii of the disk and the envelope were prescribed to be identical.

I found that the accretion rate is $3.5 \times 10^{-6}\,M_\odot$/yr and the inner radii of the disk and the envelope are $R_{\rm in} = 0.7$ AU. Since the line-of-sight to the star crosses the envelope but not the disk (Fig. 5.6), the parameters of the envelope (mass, $R_{\rm in}$ and $\alpha_{\rm env}$) strongly determine the fits. The thick envelope increases the extinction in the system in order to decrease the otherwise overestimated optical–NIR model fluxes to the measured values [1], and it also helps reduce the height of the intrinsically strong 10 μm silicate emission feature. The parameters of the best fit model are given in Table 5.2, the model can be seen in the upper panels of Fig. 5.7.

Comparing the disk and envelope parameters of the best fit model with the results of similar modelling efforts of embedded YSOs in the literature (e.g., Whitney et al. 2003) we may conclude that the circumstellar environment of V1647 Ori is rather typical, and no structural features directly linked to the eruptive nature of the object

[1] Note the absence of NIR photometric data in 2005 (Figs. 5.4 and 5.5).

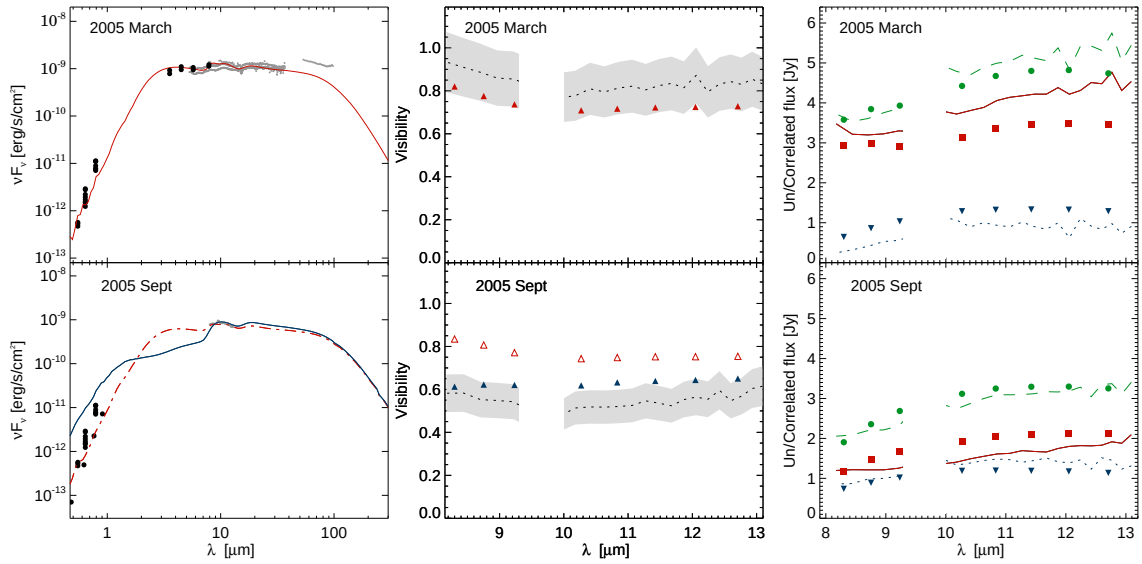

Figure 5.7 – The best fitting models for the 2005 March and September epochs are shown in the *top* and *bottom row*, respectively. The SEDs and the calibrated visibilities are shown in the *left* and *middle columns*, respectively. Model visibilities were calculated at eight different wavelengths. In the *bottom left* panel the dash-dotted red line and in the *bottom middle* panel the open red triangles show the model where only the accretion rate was decreased relative to the reference model. This model fits the SED quite well, but not the visibilities. The blue solid line (*bottom left panel*) and the filled triangles (*bottom middle panel*) show the model where the inner radius of the envelope was also increased. As an alternative interpretation of the mid-infrared fits, the observed mid-infrared total, correlated and uncorrelated MIDI spectra (green dashed, red solid and blue dotted lines, respectively) and the corresponding model values (green filled circles, red diamonds and blue downward pointing open triangles, respectively) are shown in the *right column*. Data probably affected by the atmospheric ozone layer are not shown.

can be identified. The best fit model describes the system with a parameter setup that is plausible for young stellar objects.

5.4.2 Variations during outburst

In order to fit the SEDs of the other epochs, I used the 2005 March model as an initial setup. At first sight, the SEDs differ only in their absolute levels, but their shapes are very similar (Fig. 5.5). Therefore, I attempt to adjust the shift between the levels by the variation of the accretion rate. This way it is possible to test if the geometry of the circumstellar environment may be kept identical and only change the illumination of the system as the outburst proceeds. Besides this I try to

vary only the smallest number of parameters possible between the different epochs and restrict myself to applying modifications that could be the result of a realistic process and may occur in such a short period of time. Significant changes, affecting a large fraction of the disk or a complete restructuring, could happen only on longer timescales (Chiang & Goldreich, 1997).

5.4.2.1 The effect of the varying accretion rate

According to the standard picture of eruptive YSOs (Hartmann & Kenyon, 1996), the accretion is the main energy source in the system in outburst, while its contribution in quiescence is less pronounced. The accretion rate is expected to increase from the pre-outburst phase to the peak of the outburst and decrease during the eruption as the source is fading. The modelling results confirmed our expectations. I found that the accretion was strongest at the peak brightness of 2004 March ($7 \times 10^{-6}\,M_\odot$/yr, see Tab. 5.3), and gradually weakened as the source approached the end of its flare-up, but still accreted strongly in quiescence ($3 \times 10^{-7}\,M_\odot$/yr). The peak accretion rate value found is in the same order of magnitude as the 5–$10 \times 10^{-6}\,M_\odot$/yr values derived from Brγ measurements (Acosta-Pulido et al. 2007) and the simple modelling (Muzerolle et al., 2005). During the plateau phase of the outburst, as the object slowly faded, the model accretion rate slightly decreased. Both observations and modelling indicate that $\sim 10^{-5}\,M_\odot$ material was accreted onto the star during the outburst.

The derived accretion rates fit in the canonical picture of eruptive low-mass YSOs. In quiescence the accretion rate of provided by the model ($3.0 \times 10^{-7}\,M_\odot$/yr) is similar to those of Class I YSOs (10^{-9}–$10^{-7}\,M_\odot$/yr, (White & Hillenbrand, 2004) or Class II objects (10^{-9}–$10^{-6}\,M_\odot$/yr, (Gullbring et al., 1998; Hartmann et al., 1998). During the outburst it is 2.0–7.0 $\times 10^{-6}\,M_\odot$/yr, higher than that of quiescent low-mass YSOs, comparable to that of FUors (10^{-6}–$10^{-4}\,M_\odot$/yr, (Hartmann & Kenyon, 1996). Intermediate values are expected for EXors (Hartmann & Kenyon, 1996). E.g. Juhász et al. (2012) derived $2.2 \times 10^{-7}\,M_\odot$/yr for the prototype EXor, EX Lupi at its outburst peak in 2008.

In the quiescent model I derived a similar accretion rate value as Acosta-Pulido et al. (2007) and Muzerolle et al. (2005) found, i.e., a few times $10^{-7}\,M_\odot$/yr. Aspin

et al. (2008) claimed, based on the strength of the Brγ emission line, that the accretion rate was somewhat higher ($\sim 10^{-6}\,M_\odot$/yr) after the outburst. However, the estimates of the accretion rate derived from the Brγ measurements strongly depends on the applied value of A_V. Aspin et al. (2008) considered higher visual extinction than the previous authors (see Sect. 5.4.2.2).

Lowering the accretion rate to $\sim$4–5% of the peak value, reduced the fluxes considerably at all optical–infrared wavelengths in quiescence. Our model fits the mid-infrared part of the SED well, but the excess of the model in the optical-NIR part of the SED indicates that the accretion rate is not the only parameter which must be adjusted. The best models for the SED fitting with the variable accretion can be seen in Fig. 5.5. Varying parameters of the best fitting models are shown in Table 5.3.

5.4.2.2 Dynamics of the inner disk and envelope

The inner radii of the dusty components in the reference models are at 0.7 AU. Models with these values, but with different accretion rates provided good fit for all three outburst epochs (2004 March and October, 2005 March), thus the geometry of the inner part of the system was unchanged during the plateau phase. The similar setup was fine for the SED fit for the 2005 September epoch (Fig. 5.5), but not for the MIDI interferometric data (see Sect. 5.4.3).

Interestingly, the same geometry clearly failed to reproduce the observations in the quiescent phase. For quiescence, both before and after the outburst, I found the best fit by using $R_{\rm in,qui} = 0.5$ AU. The variation of the inner radii of the disk and the envelope indicates that a dynamical process worked right after the outburst and enlarged the inner dust-free hole from 0.5 AU to 0.7 AU on a few months time-scale. The derived $R_{\rm in} = 0.5$ and 0.7 AU radii correspond to $\sim$1000 K and $\sim$1500 K in quiescent state and at the peak brightness phase, respectively. The temperature value at the epoch of the peak brightness is at the canonical dust sublimation temperature ($\sim$ 1400–1600 K). However, moving the inner radii of the quiescent model inward to the corresponding sublimation radii, the model underestimates the optical data points due to the increased extinction. Although similar deviations of the radii were found at other eruptive young systems (e.g. Juhász et al. 2012; Eisner & Hillenbrand

2011), the cause of this larger inner radius is not clear.

During the outburst the temperatures were the highest at the peak, so this epoch defines the radius up to which dust had to evaporate. The variation of the inner radii of the disk and the envelope suggests that the physical mechanism enlarging the inner dust-free hole from 0.5 to 0.7 AU is the evaporation of dust due to the increased heating from the central source. The intensified wind from the center of the system might have also played a role in these changes (Reipurth & Aspin, 2004).

In order to fit the observed changes in the optical-NIR wavelength colors better, I also had to modify the parameters describing the accretion characteristics. At the outburst peak, the hot spot covers a large fraction ($\sim$50%) of the stellar surface. In quiescence, the hot spot is much smaller, i.e., it covers $\lesssim$1% of the surface. Similar results were determined for other eruptive YSOs (EX Lupi, Juhász et al. 2012, and V1118 Ori, Audard et al. 2010). Calvet & Gullbring (1998) found fractions of 20% in strongly accreting systems, and typically 1% for T Tau systems. These parts of the surface are the sources of a given fraction of the accretion luminosity. Therefore these surface fractions correspond to 6500 K and 15000 K hot spot temperatures at the outburst peak and quiescence, respectively.

5.4.2.3 Burst of luminosity or drop of extinction?

Due to such a structural change described previously, the extinction of the system should also change. The increased accretion luminosity and the varying extinction determine the total brightening of the object. When the increased accretion temperature evaporates dust particles and creates a larger inner hole, the line-of-sight extinction decreases, which leads to an additional apparent brightening of the object. Since the density in the envelope decreases with radius, most of the extinction comes from the innermost parts. Therefore, dust evaporation at the inner edge of the envelope can significantly change the total extinction towards the central star. Similarly, the gradual fading of the central source may allow re-condensation of dust grains in regions where evaporation took place previously, resulting in an extra dimming. Kun et al. (2011) claim that such a re-condensation was observed at another YSO, PV Cep.

For the understanding of the outburst, it is essential to separate to which ex-

tent those two agents contributed to the brightening of V1647 Ori throughout the eruption. Some authors (e.g., McGehee et al. 2004; Reipurth & Aspin 2004) concluded that only part of the brightness variation of V1647 Ori was due to extinction variation, e.g., dust-clearing. From the models, I derived a change of the extinction $\Delta A_{\rm V} \approx 4.5$ mag or $\Delta A_{\rm I_C} \approx 2.6$ mag. Compared to the largest measured variation in $\rm I_C$ (6.0 mag, Acosta-Pulido et al. 2007 and Aspin & Reipurth 2009), it leaves more than 3 mag for the intrinsic brightening in $\rm I_C$ having accretion-related origin.

There are a number of different attempts in the literature to derive the value of extinction and its variation during the outburst. Our model-extinction result for the quiescent phase of $A_{\rm V} \approx 23.4$ mag is in good agreement with the value of $A_{\rm V} \approx 19$ mag derived by Aspin et al. (2008). The object moved along the reddening path in the NIR colour-colour diagram during the outburst. The excursion corresponds to $\Delta A_{\rm V} \approx 5$ mag (e.g., Reipurth & Aspin 2004), which is close to our results. However, with different methods, Aspin et al. (2008) derived $\Delta A_{\rm V} \approx 10$ mag. Since the optical extinction values are poorly defined over the outburst, we do not aim at fitting those with our model, only attempt a qualitative check of this parameter. Our modelling indicated that the extinction is larger in quiescence than at peak brightness.

Table 5.3 – Varied model parameters and the derived visual extinction values for different epochs.

Parameters	2004		2005	2003/06
	Mar	Oct	Mar	quiescent
$\dot{M}$ ($\rm M_\odot yr^{-1} \times 10^{-6}$)	7.0	5.0	3.5	0.3
$R_{\rm in}$ (AU)	0.7	0.7	0.7	0.5
$A_{\rm V}$ (mag)	18.9	18.9	18.9	23.4

5.4.3 2005 September: The puzzling MIDI data

For the 2005 March and September epochs the MIDI visibilities give further constraints for the system parameters. We attempted to fit the 2005 September SED and visibility values using the same method followed above. We kept the inner radii unchanged ($R_{\rm in} = 0.7$ AU) and applied a 40% change in the accretion rate between the two MIDI epochs (i.e., from $3.5 \times 10^{-6}\,\rm M_\odot/yr$ to $2.0 \times 10^{-6}\,\rm M_\odot/yr$). Due to the

fading of the central source the mid-infrared emitting region is smaller and results in slightly increased visibilities. This is just the opposite of what the measurements show (shown with dash-dotted line in Fig. 5.7 lower left panel). Thus, although for fitting the SEDs our first strategy of changing only the accretion rate and the inner radii of the dust disk and the envelope works, it cannot account for the changes in the visibilities.

5.4.3.1 Variable puffed-up inner rim

The geometry of the circumstellar environment also had to undergo changes in the inner regions of the disk-envelope system in order to explain the lowering of the visibility points. The change has to take place in the inner regions of the system, because the dynamical timescales for changing the structure of the environment further out is much larger than the half-year elapsed between the two MIDI observations.

An effect that might help to explain the changes in the visibility data is if we suppose that due to the enhanced accretion, the scale height of the regions close to the inner edge of the disk increases in the first phase of the outburst. By introducing such a region to the system and varying the scale height of the inner part of the disk, we also see variations in the visibilities: they are higher if the scale height increases. A higher inner rim means an additional hot component in the inner part of the system, which increases visibilities. We tested several geometries of the disk to see how large the effect is, and we found that this process could only account for approximately one quarter of the observed decrease. Therefore we do not discuss these models further.

5.4.3.2 A blown-up spherical cavity

Another straightforward idea is to increase the inner radii of the dusty components from March to September, which we expect to have the effect of increasing the mid-infrared emitting region, i.e., making the source more resolved. The inner radii of the envelope and the disk were changed previously and seem to be the parameters which could vary the easiest (compared to disk scale height or density profile exponents). However, any transportation mechanism which removes material is much more effective on the significantly less dense envelope, and would move its

inner radius much further out. Therefore we do not consider any change in the disk in the following.

The expected structural changes can either occur relatively slowly during the March-September interval or in a few weeks time (cf. the light curves in Fig. 5.4). Even in the latter case such a change of the envelope seems to be plausible. To test the assumption I changed the density distribution in the models and moved the inner radius of the envelope outwards. According to the setup that fits the visibilities, the dusty envelope starts only at 3.0 AU, and the matter removed from the inner regions is piled up in a thin shell close to the inner edge of the envelope. By moving the inner edge outwards, however the infrared flux increased slightly, so I had to adjust further the accretion rate and lower it by an additional 20% to $1.6 \times 10^{-6}\,\mathrm{M}_{\odot}/\mathrm{yr}$. Moving matter outwards, has the additional effect of reducing the extinction, thus increasing the optical–NIR flux. As the results show in Fig. 5.7, improving the fit to the visibilities made the SED-fit somewhat worse[2]. The extinction in this model dropped down to A_V =11.5 mag, which would have led to an unobserved brightening of V1647 Ori (cf. Fig. 2). I need to mention here, that in order to have the effect of reduced visibilities, we do not need to remove *all* of the material from the inner envelope. By reducing the density in the inner part of the envelope by a factor of at least ~ 4, I was able to fit the visibilities. However the more matter I left in the 'wiped-out' region, the further out its outer radius had to be moved. These models also resulted in the explained drop of extinction of about the same magnitude as if we removed all matter from the inner regions up to 3.0 AU. Although the accretion luminosity decreased during this period, it could hardly compensate the effect of ΔA_{V}. The uncertainty of the optical part of our model for 2005 September prevents us from doing an analysis of the evolution of the extinction at this epoch.

We attempt to find the mechanism which can produce the dramatic variation of the envelope radius between March and September 2005. During most of this period the object was slowly fading thus we would expect the decrease of the inner (dust evaporation) radii both of the disk and the envelope rather than any increase. Combet & Ferreira (2008) showed that at the accretion rate of $10^{-6}\,\mathrm{M}_{\odot}/\mathrm{yr}$, a strong disk wind, which can be the source of an outflow, is launched from the inner disk

[2]Similar compromise was made in other interferometric studies, e.g., di Folco et al. 2009.

up to 2–3 AU. Thus, the disk wind might be responsible for the clearing of the inner envelope. However, during the 2005 March–September period the wind is expected to become weaker since its strength should be proportional to the accretion activity. Furthermore, the wind which was present from the beginning of the outburst and had no such effect before, might only have cleared out the cone in the reflection nebula when the outburst started (Reipurth & Aspin, 2004). Therefore the stellar or disk wind could likely not produce this clearing.

Another possibility is that some temporary outflow changed the inner structure of the system, and moved the inner edge of the envelope outwards. Spectroscopic observations from early 2006 showed evidence of a short outflow activity (Brittain et al., 2007). Furthermore, detection of forbidden optical lines indicated the presence of shocked gas in early 2006 (Fedele et al., 2007). These lines can be tracers of a Herbig-Haro object (HHO). Although HHOs are thought to be related to mass accretion, they are not typical in the environment of eruptive YSOs (Hartmann & Kenyon, 1996). However, Eisloffel & Mundt (1997) identified V1647 Ori as the driving source of HH23 – presumably ejected some thousands of years ago – which is located 155″north of the young star and is close to the axis of the nebula. If such an event is responsible for the change of the inner radius of the envelope, based on the beforementioned findings, it should be connected to the final decrease of the accretion rate. However, Brittain et al. (2007) proposed, that the re-structuring of the inner disk producing the (CO) outflow might have occured later.

During an outflow activity or the appearance of a HHO, the disk structure can be very different from that of a standard accretion disk. There is a significant difference in all parameters between those of a standard accretion disk and a jet emitting disk (Combet & Ferreira, 2008). Reproducing such events are beyond the limits of our static modelling and can be a source of discrepancy.

By 2006 February the object returned to its quiescent brightness at all wavelengths. This suggests that the structural changes in the circumstellar environment of V1647 Ori should have been reversible on the time-scale of some months. It means that the material should have filled up the evacuated cavity on this timescale via accretion, requiring an inward radial velocity of 10–20 km/s. In our modelling it means that the inner radii of both the disk and the envelope should have moved

back close to the quiescent values. Matter of the disk and the envelope might have moved inwards due to the accretion and thus could fill the cleared regions. However, the dynamical timescale at ∼3 AU is about 7 years, much longer than half a year. Therefore dust re-condensation might also have played a role here.

5.4.3.3 The disappearance of a warm halo

In the next scenario we again consider a large inner cavity in the envelope as in Sect. 5.4.3.2 ($R_{in,env} = 3.0$ AU while $R_{in,disk} = 0.7$ AU), but we assume that the cavity has been produced at the early phases of the outburst by e.g. stellar or disk winds (see e.g., Clarke et al. 2005). If dust was lifted from the disk above it by wind (Vinković & Jurkić, 2007; Sitko et al., 2008), the dust could fill the inner cavity of the envelope. The warm dust halo (which in our models cannot be distinguished from the inner envelope), present in the system during the plateau phase, makes V1647 Ori look more compact at the first MIDI epoch. The apparent change of the visibility data could then be due to the waning wind. As the accretion process and thus the wind gets weaker, less and less dust is fed into the cavity, while the dust moved there previously is blown further outwards. In this case most of the dust, which made the object compact in 2005 March, is cooled below the temperatures corresponding to the mid-infrared wavelengths. By 2005 September the cavity is practically cleared. Without carrying out new modelling, we can consider the results of the radiative transfer modelling described above. Such scenario could explain transition between 2005 March and September seen in the data and also the short time-scale variability of the mid-infrared emission.

5.4.3.4 An out-of-equilibrium system

At last, we further speculate to find other alternatives for our series of static models. Between 2005 March and September, the heated disk area should shrink gradually because of the fading of the central illuminating source. On the contrary, the visibilities of V1647 Ori apparently did not follow such a scenario. The above hypothesis would predict a smaller, thus less resolved source at our second MIDI epoch. Our measurements, however, revealed the opposite behaviour: the visibilities decreased between the first and the second epochs. Since the shapes of the two visibility curves

are similar (Fig. 1.), and their ratio is almost independent of the wavelength (≈1.4–1.5), a simple qualitative picture might explain the data. One could assume, that the system consists of two components: one compact central and an extended component (e.g., approximated by a Gaussian brightness distribution like in Sect. 5.3.1). If the resolved component did not change between the two MIDI epochs, but the emission of the central unresolved source had significantly dropped in the same period, the emission of the system became less peaked, i.e. relatively more resolved. This way we might get a simplistic picture what caused the decrease of the measured visibilities.

The constancy of the extended emission component could easily be explained if the $\sim$10 μm flux arised from optically thick regions, whose temperature is not adjusted rapidly to the changing central illumination field. Although we see variations of the mid-IR brightness of the system on weekly timescales, that of an optically thick component could not change significantly since the corresponding timescales (Chiang & Goldreich, 1997) exceed even the difference between the epochs of the MIDI observations. However, according to Muzerolle et al. (2005), the contribution of an optically thick accretion disk to the mid-infrared emission of V1647 Ori in outburst is small, and the $\sim$10 μm flux mainly arises from an envelope. In such an envelope the temperature of the dust grains must be quickly adjusted to the external radiation field. This suggestion is supported by the fact that the mid-infrared flux of V1647 Ori had increased remarkably in less than a few months, between the beginning of the eruption and the Spitzer measurements in March 2004. Thus the invariability of the extended emitting component in the simple picture above is not straightforward to explain.

A qualitative argument leads to a possible solution in which the decrease seen in the MIDI visibilities are due to the fading of the central source which is not followed by the fading of the outer regions immediately. However such effect should be confirmed by dynamical modelling and is beyond the scope of the steady-state radiative transfer model used.

5.5 Conclusions

We performed interferometric and photometric observations of V1647 Ori during its 2003–2006 outburst in order to investigate the temporal evolution of its circumstellar structure and physical processes related to the eruption. Besides the general fading of the object, shown by the multi-wavelength photometric data and archival mid-infrared spectroscopy, short timescale variations were also observed. Optical–infrared SEDs at five epochs were compiled. The radiative transfer modelling, with a smoothly decreasing accretion rate as a major varying parameter, provided good fits of the SEDs at different stages of the outburst. It is important to note that the inner radii of the dust disk and envelope also had to increase during the transition from quiescence to the outburst peak. The latter finding is a clear evidence of dynamical variations in the inner circumstellar environment of V1647 Ori. Such dust clearing is likely caused by the evaporation of the dust grains due to the outburst heat.

High angular resolution spatial information were also considered in the model-fitting procedure. VLTI/MIDI data obtained at two epochs, during both the slow and rapid fading stages, show a considerable change of the circumstellar structure. In constrast to our expectations, based on our model sequence, the object looked more resolved at the second epoch. One possible explanation can be a rapid removal of dust from the inner 3 AU of the envelope, possibly caused by wind or outflow processes. In one case this spherical cavity is produced at the end of the outburst phase (the blown-up cavity scenario), or alternatively at the beginning (the warm dust halo scenario). Finally, we may also see V1647 Ori in a non-equilibrium situation in 2005 September, when the sudden fading of the central source was not yet followed by the fading of the optically thick circumstellar material.

In general, our modelling showed that the circumstellar environment of V1647 Ori can be described by a disk and envelope system with parameters which are typical of embedded low-mass YSOs. This finding supports the hypothesis that eruptive YSOs are not peculiar objects, but represent an important phase in the evolution of all low-mass YSOs.

Chapter 6

Summary

In this thesis, I investigated both the quiescent and outburst conditions in the circumstellar environments of two eruptive sources, V1647 Ori, and the prototype of EXors, EX Lupi. I interpreted optical–infrared observations of the sources via model-fitting. In the following I summarize my goals, methods and emphasize my most important findings.

6.1 Scientific aims

My PhD research focused on two groups of questions. One topic concerned the general significance of young eruptive sources. My goal was to find answers to the following open issues: Do outburst periods occur during the early evolution of *all* low-mass young stars? In which stage of disk evolution can eruptive phenomena occur? Do EXors/FUors have any characteristics that would set them apart from normal T Tauri stars? Altogether we know about somewhat less than 30 EXors/FUors. Still, eruptive phenomena cannot be considered rare. If we take into account the short-lived nature of the bursts, then according to statistical considerations, most low-mass young stars may undergo these stages during their evolution, and furthermore, the bursts have to be repetitive. However, besides statistics, the quiescent properties of eruptive stars have to be examined, in order to find answers to these still open issues. If the eruptive sources in their low-state indeed show distinctive characteristics, that points to the fact that eruptive phenomena are only

important in the evolution of a subgroup of stars. However, if no distinct features can be found in the quiescent circumstellar disk–envelope system of the sources, it implies that EXors have a non-exceptional status among regular YSOs. Eruptive phases thus may occur during the early evolution of all Sun-like stars, and have a general significance in the birth process of low-mass stars and their planets. In order to contribute to this issue, I studied whether the prototype of EXors, EX Lupi is exceptional among regular low-mass T Tauri stars. My analysis focused on the structure and properties of the circumstellar disk, I compared the circumstellar environment of the source with those of classical T Tauri stars.

I also examined the immediate surroundings of two young stars in outburst. Eruptions affect the stars themselves, their circumstellar environments, and consequently also the formation of their planetary systems. The extra accretion energy heats up the whole system, and the increased accretion is accompanied by powerful winds and outflows. These events modify the geometrical and thermal structure of the disk and also the dust composition of young stellar systems on the time-scales of weeks – months. The nature of these modifications was the other main topic of my research. During the recent, 2008 eruption of EX Lupi in situ crystallization was observed, and I examined in which regions of the circumstellar disk crystals could form. Besides the outburst of EX Lupi, I followed the temporal evolution of the inner circumstellar structure during the recent eruption of V1647 Ori via radiative transfer modelling of multiepoch measurements. I was also interested whether the observed temporal changes are related to the varying illumination of the disk by its central region, or are due to the restructuring of the circumstellar environment.

6.2 Methodology

In order to study the properties of the immediate environment of young eruptive stars, I constructed the spectral energy distribution of the sources both in outburst and quiescence. I compiled the SEDs from ground-based and space-borne observations covering the optical–infrared wavelength regime. I used both literature data and new measurements. In the case of V1647 Ori, multiepoch measurements made a complex, temporal analysis possible. The SEDs were complemented by mid-infrared

interferometric data collected on two epochs, which helped the investigation of the inner regions of the circumstellar environment.

Depicting the nature of the sources from observations can be complicated. Thus, I compared observations with simulations based on recent theoretical models describing disk and envelope properties. For this purpose, sophisticated numerical radiative transfer codes serve as basic tools. I modelled simultaneously continuum measurements at the optical–far-infrared wavelengths range, and in the case of V1647 Ori mid-infrared interferometric data, for delivering a detailed, quantitative, physical picture of the studied sources. I utilized for this purpose two of the leading continuum radiative transfer codes called *RADMC* (Dullemond & Dominik, 2004) and *MC3D* (Wolf et al. 1999, Wolf 2002). Both codes use the Monte Carlo method and the Bjorkmann–Wood algorithm for solving the radiative transfer problem in various dusty environments. They can treat complex density configurations, and include accretion characteristics as well. For all of the models during my PhD work, I used two dimensional, axisymmetric density distributions consisting of a circumstellar disk, and in the case of V1647 Ori an envelope too. Spectra and images were calculated from the model-temperature distribution obtained as the result of the radiative transfer calculations, which I compared to measurements. Based on the parameters of the best fitting model I gave a characterization of the system, and drew conclusions about the processes forming the given configuration.

6.3 Theses

EX Lupi in quiescence

(Sipos et al., 2009, *A&A*, 507, 881)

(1) I examined the properties of the SED of EX Lupi, constructed from all available optical–infrared measurements of the quiescent phase, and compared it with those of other non-eruptive young stellar objects. My results are listed below.

   (a) During quiescence I found an indication of an intrinsic variability of the source of less than 25% in the optical–mid-infrared wavelength regime.

(b) In general, the shape of the SED is similar to those of typical classical T Tau stars, but above 7 μm EX Lup is brighter than the Taurus median by a factor of $\sim$2.5. The relative flux contribution from shorter and longer wavelengths is a parameter that may distinguish EX Lup from the majority of classical T Tau stars.

(2) Based on the detailed modelling of the quiescent disk structure of EX Lup, I found that a modestly flaring disk model with a total mass of 0.025 $M_\odot$ and with inner and outer radii of 0.2 and 150 AU, respectively, was able to reproduce the observed SED. The parameters characterizing the source are similar to typical values for classical T Tauri stars. The inner radius of the dust free inner hole is larger by a factor of $\sim$3.5 than the dust sublimation radius.

(3) I concluded that the large dust-free inner gap encircling EX Lupi points to a clearing mechanism, typical of T Tauri stars being in a later stage of disk evolution. These disks, classified as 'evolved' or 'transitional' are present among T Tauris of various ages and masses. EX Lupi might be in a phase preceding this transitional period. However, more explanations can be invoked for what resulted in the inner hole to form. It might be connected to the eruption mechanism or can be the result of binarity, photoevaporation or magnetic field effects as well.

EX Lupi in outburst

(Ábrahám et al. 2009, *Nature*, 459, 224; Juhász et al. 2012, *ApJ*, 744, 118)

(4) I simulated both the quiescent and outburst temperature distribution of the disk of EX Lupi and concluded that the newly discovered crystals in the disk of EX Lupi were formed through a mechanism that is active above $\sim$900 K. Based on the temperature distribution in the disk, I determined the possible crystal-forming regions within the outburst-disk. Crystal-formation took place in the surface layer of the disk, up to a radial distance of $\sim$0.5 AU from the central star. The temperature exceeded the threshold value of 1000 K, necessary for crystallization via thermal annealing only here. In the midplane the temperatures were below this threshold value, just like in the entire quiescent disk, preventing the crystallization process to be activated.

Dynamics during outburst
VLTI observations of the young eruptive star V1647 Ori

(Mosoni et al. 2012, submitted to *A&A*)

(5) I gave a detailed description of the circumstellar environment of V1647 Ori based on the SED and interferometric visibilities via modelling, and concluded that the young stellar system consists of a disk and an envelope, with system parameters typical of embedded low-mass YSOs. This finding supports the hypothesis that eruptive sources are not peculiar objects, but represent an important phase in the evolution of all low-mass stellar systems.

(6) I compared the compiled optical–infrared SEDs of V1647 Ori at five epochs, before, during and after its 2003–2006 flare-up. My findings are the following.

   (a) The accretion to the star from the circumstellar disk was the strongest at the epoch of the peak brightness ($7 \times 10^{-6}\,\mathrm{M}_{\odot}/\mathrm{yr}$), and weakened gradually as the outburst proceeded. In quiescence it dropped to ∼4–5% of the maximal accretion rate, but still accreted strongly ($3 \times 10^{-7}\,\mathrm{M}_{\odot}/\mathrm{yr}$).

   (b) The inner radii of the dust disk and envelope also had to increase during the transition from quiescence to the outburst peak. The variation of the inner radii of the disk–envelope system indicates that a dynamical process worked right after the outburst, and enlarged the dust-free inner hole from 0.5 to 0.7 AU on a few months time-scale. Due to such a structural change, the extinction of the system also changed by $A_{\mathrm{I_C}} = 2.6\,\mathrm{mag}$. Thus I concluded that the increased accretion luminosity and the varying extinction together determined the total brightening of the object.

(7) Based on high angular resolution spatial information from two epochs during the outburst, I found that the circumstellar structure changed considerably, the object looked more resolved at the second epoch. I attributed this change to a rapid removal of dust from the inner 3 AU of the envelope. This was possibly caused by an outflow or alternatively by the disappearance of a warm halo around the central object. The observed changes, however may also indicate that we saw V1647 Ori in a non-equilibrium situation in 2005 September, when

the sudden fading of the central source was not yet followed by the fading of the optically thick circumstellar material.

Notes: This outburst has already been discussed in the PhD Thesis of Ágnes Kóspál and the DSc Thesis of Péter Ábrahám. However, in my work I used different methods for the interpretation of the data, and examined the object from a new perspective. Thus, my results are completely independent from their findings.

6.4 Conclusions

My thesis contributes to the better understanding of young eruptive stars. Both my results connected to EX Lup and to V1647 Ori indicate, that these outbursting sources do not form a special subgroup of peculiar stars. Instead, they are representatives of regular young stars, being in an important phase of the star formation process. The dust free inner hole discovered around EX Lup was a surprising result. It implies that the protoplanetary disk of EX Lup might be at a later stage of disk evolution than what is usually assumed for EXors, as similar inner holes are characteristic of objects at the end of their Class II stage. Further research, concentrating to this inner hole, will probably be able to resolve what might have lead to the clearing of the gap. Comparison of EX Lup with other EXors at infrared wavelengths would be important. It may answer the question of whether an inner gap in the dusty disk is characteristic of the EXor phenomenon, possibly connecting the hole to the eruption mechanism, and we could learn to what extent EX Lup is a good representative of eruptive stars.

I presented models of two sources in outburst, and showed, that the temperature structure of the circumstellar environment is modified, resulting in the case of EX Lup crystal formation, and in the case of V1647 Ori an enlargement of the inner radius of the dusty components. This result also confirmed that the brightening of the object, was only partly due to the enhanced accretion, a decrease in the extinction contributed as well.

These results demonstrated the adequacy and effectiveness of radiative transfer modelling tools for studying the circumstellar environment of young eruptive stars quantitavely. I showed that due to the intrinsic variability of the sources, different

observations should be as simultaneous as possible. Interferometric visibility curves served in the case of V1647 Ori, and pointed to a mechanism acting in the innermost regions of the disk, which we had no indication of, when examining the SEDs only. I also met the limitations of the static radiative transfer modelling approach, as a possible non-equilibrium situation would have required dynamical treatment. However, as we are still far from being able to build a comprehensive picture of the eruptive phenomenon, other eruptions will likely be studied in a similar way. Combining multiepoch multiwavelength photometric data supplemeted with interferometric, high-angular resolution observations and interpreting them via detailed model fitting, will certainly further deepen our knowledge about FUor/EXor outbursts.

Acknowledgements

During my PhD, I encountered lots of helpful people, whose support I would like to thank here. First of all, I thank my supervisors, Péter Ábrahám and Mária Kun for providing the opportunity to work in the Konkoly Infrared Space Astronomy Group (KISAG) of the Konkoly Observatory of the Hungarian Academy of Sciences, and introducing me to the topic of star formation. Péter Ábrahám recommended me to deal with eruptive young stars, which I am really grateful for. I benefitted a lot from having discussions with him and also with Mária Kun, who has an incredibly thorough knowledge of the field of early stellar evolution, which she was happy to share.

Besides my supervisors, I would like to express here, how much I appreciated the help of three outstanding scientists and people: László Mosoni, Attila Juhász and Kees Dullemond. Without their tireless assistance I wouldn't have been able to finish my PhD. They provided me a really inspiring working environment in Heidelberg, and formed my view on how to do research. They helped me through lots of difficulties I met during my PhD, and made me really like what I am doing now.

I also thank Ágnes Kóspál and Attila Moór for regularly doing the data reduction part necessary for my research, and often helping my work with their advice.

Sebastian Wolf and Alexander Schegerer were kind to give me the first radiative transfer code I used, *MC3D* and taught me how to use it.

I acknowledge Thomas Henning too, who hosted me at the Max-Planck Institut für Astronomie in Heidelberg, and thus provided me an oppotunity to interact with lots of interesting scientist in a really inspiring atmosphere.

I thank for providing me computing facilities: Csaba Kiss, Ulrich Hiller, Zsolt Sándor

and Róbert Kulyassa.

For careful proofreading and helping the thesis improve I am grateful to Mária Kun, Ágnes Kóspál, László Mosoni, Péter Ábrahám, Attila Moór, László Szabados and Máté Maródi.

Róbert Kulyassa, Attila Moór, Attila Juhász, András Pál and Csaba Kiss often helped me with technical problems, saving me lots of time, thanks for the effort.

I would also like to mention all the colleagues who contributed to research projects I participated in: Jose Acosta-Pulido, Roy van Boekel, Jeroen Bouwman, Albert Jones, Christoph Leinert, Sascha Quanz, Thorsten Ratzka, Zsolt Regály, Johny Setiawan, Aurora Sicilia-Aguilar and Gyula Szokoly.

I a thank every present and former member of the KISAG that I could be one of them, it was a pleasure working with you. I'm glad that I had so nice office and almost office-mates: Andris, Ági, Csaba, Attila, Elza, Niki, Judit, Laci, Wes, thanks for making my stay there fun.

Frithjof, Andris, Juliet and Flo, thanks that you were friends for me in Heidelberg and made me feel at home there.

I thank both the Konkoly Observatory and The Max Planck Institut für Astronomie that they provided a facility where I could work, and the staff working there for administrative or technical help.

And finally I would like to express how grateful I am for the support and of my friends, and my family: Nóri, Szandi, Anya and Apa, and above all Robi. Without them this work wouldn't have been possible.

References

Ábrahám, P., Juhász, A., Dullemond, C. P., Kóspál, Á., van Boekel, R., Bouwman, J., Henning, T., Moór, A., Mosoni, L., Sicilia-Aguilar, A., & Sipos, N. (2009). Episodic formation of cometary material in the outburst of a young Sun-like star. *Nature*, *459*, 224–226.

Ábrahám, P., Kóspál, Á., Csizmadia, S., Moór, A., Kun, M., & Stringfellow, G. (2004). The infrared properties of the new outburst star IRAS 05436-0007 in quiescent phase. *A&A*, *419*, L39–L42.

Ábrahám, P., Kóspál, Á., Csizmadia, S., et al. (2004a). Long-term evolution of FU Orionis objects at infrared wavelengths. *A&A*, *428*, 89–97.

Ábrahám, P., Mosoni, L., Henning, T., Kóspál, Á., Leinert, C., Quanz, S. P., & Ratzka, T. (2006). First AU-scale observations of V1647 Orionis with VLTI/MIDI. *A&A*, *449*, L13–L16.

Acosta-Pulido, J. A., Kun, M., Ábrahám, P., Kóspál, Á., Csizmadia, S., Kiss, L. L., Moór, A., Szabados, L., Benkő, J. M., Barrena Delgado, R., Charcos-Llorens, M., Eredics, M., Kiss, Z. T., Manchado, A., Rácz, M., Ramos Almeida, C., Székely, P., & Vidal-Núñez, M. J. (2007). The 2004-2006 Outburst and Environment of V1647 Ori. *AJ*, *133*, 2020–2036.

Adams, F. C., & Shu, F. H. (1986). Infrared spectra of rotating protostars. *ApJ*, *308*, 836–853.

Andre, P., & Montmerle, T. (1994). From T Tauri stars to protostars: Circumstellar material and young stellar objects in the rho Ophiuchi cloud. *ApJ*, *420*, 837–862.

Andre, P., Ward-Thompson, D., & Barsony, M. (1993). Submillimeter continuum observations of Rho Ophiuchi A - The candidate protostar VLA 1623 and prestellar clumps. *ApJ*, *406*, 122–141.

Andrews, S. M., Rothberg, B., & Simon, T. (2004). Mid-Infrared and Submillimeter Observations of the Illuminating Source of MCNeil's Variable Nebula. *ApJ*, *610*, L45–L48.

Anthony-Twarog, B. J. (1982). The H-beta distance scale for B stars - The Orion association. *AJ*, *87*, 1213–1222.

Armitage, P. J. (2011). Dynamics of Protoplanetary Disks. *ARA&A*, *49*, 195–236.

Armitage, P. J., Livio, M., & Pringle, J. E. (2001). Episodic accretion in magnetically layered protoplanetary discs. *MNRAS*, *324*, 705–711.

Aspin, C., Beck, T. L., & Reipurth, B. (2008). V1647 Orionis: One Year Into Quiescence. *AJ*, *135*, 423–440.

Aspin, C., & Reipurth, B. (2009). V1647 Orionis: Optical Photometric and Spectroscopic Monitoring Through the 2003-2006 Outburst. *AJ*, *138*, 1137–1158.

Audard, M., Stringfellow, G. S., Güdel, M., Skinner, S. L., Walter, F. M., Guinan, E. F., Hamilton, R. T., Briggs, K. R., & Baldovin-Saavedra, C. (2010). A multi-wavelength study of the young star V1118 Orionis in outburst. *A&A*, *511*, A63.

Bailey, J. (1998). Detection of pre-main-sequence binaries using spectro-astrometry. *MNRAS*, *301*, 161–167.

Barrado y Navascués, D., & Martín, E. L. (2003). An Empirical Criterion to Classify T Tauri Stars and Substellar Analogs Using Low-Resolution Optical Spectroscopy. *AJ*, *126*, 2997–3006.

Bastian, U., & Mundt, R. (1979). UBV photometry of T Tauri stars and related objects. *A&AS*, *36*, 57–60.

Beckwith, S. V. W. (1999). Circumstellar Disks. In C. J. Lada & N. D. Kylafis (Ed.) *NATO ASIC Proc. 540: The Origin of Stars and Planetary Systems*, (p. 579).

Berger, J. P., & Segransan, D. (2007). An introduction to visibility modeling. *New A Rev.*, *51*, 576–582.

Bjorkman, J. E., & Wood, K. (2001). Radiative Equilibrium and Temperature Correction in Monte Carlo Radiation Transfer. *ApJ*, *554*, 615–623.

Bonnell, I., & Bastien, P. (1992). A binary origin for FU Orionis stars. *ApJ*, *401*, L31–L34.

Born, M., & Wolf, E. (1999). *Principles of Optics*.

Bouwman, J., Meeus, G., de Koter, A., Hony, S., Dominik, C., & Waters, L. B. F. M. (2001). Processing of silicate dust grains in Herbig Ae/Be systems. *A&A*, *375*, 950–962.

Briceño, C., Vivas, A. K., Hernández, J., Calvet, N., Hartmann, L., Megeath, T., Berlind, P., Calkins, M., & Hoyer, S. (2004). McNeil's Nebula in Orion: The Outburst History. *ApJ*, *606*, L123–L126.

Brittain, S., Rettig, T. W., Simon, T., Balsara, D. S., Tilley, D., Gibb, E., & Hinkle, K. H. (2007). Post-Outburst Observations of V1647 Orionis: Detection of a Brief Warm Molecular Outflow. *ApJ*, *670*, L29–L32.

Calvet, N., & Gullbring, E. (1998). The Structure and Emission of the Accretion Shock in T Tauri Stars. *ApJ*, *509*, 802–818.

Castelli, F., & Kurucz, R. L. (2003). New Grids of ATLAS9 Model Atmospheres. In N. Piskunov, W. W. Weiss, & D. F. Gray (Ed.) *Modelling of Stellar Atmospheres*, vol. 210 of *IAU Symposium*, (p. 20).

Chiang, E. I., & Goldreich, P. (1997). Spectral Energy Distributions of T Tauri Stars With Passive Circumstellar Disks. *ApJ*, *490*, 368–376.

Clarke, C., Lodato, G., Melnikov, S. Y., & Ibrahimov, M. A. (2005). The photometric evolution of FU Orionis objects: disc instability and wind-envelope interaction. *MNRAS*, *361*, 942–954.

Colangeli, L., Henning, T., Brucato, J. R., Clément, D., Fabian, D., Guillois, O., Huisken, F., Jäger, C., Jessberger, E. K., Jones, A., Ledoux, G., Manicó, G., Mennella, V., Molster, F. J., Mutschke, H., Pirronello, V., Reynaud, C., Roser, J., Vidali, G., & Waters, L. B. F. M. (2003). The role of laboratory experiments in the characterisation of silicon-based cosmic material. *A&A Rev.*, *11*, 97–152.

Combet, C., & Ferreira, J. (2008). The radial structure of protostellar accretion disks: influence of jets. *A&A*, *479*, 481–491.

Cutri, R. M., et al. (2003). *Explanatory Supplement to the 2MASS All Sky Data Release (Pasadena, Caltech).*

Dahm, S. E. (2008). A Spectroscopic Examination of Accretion Diagnostics for Near Solar Mass Stars in IC 348. *AJ*, *136*, 521–547.

D'Alessio, P., Calvet, N., Hartmann, L., Lizano, S., & Cantó, J. (1999). Accretion Disks around Young Objects. II. Tests of Well-mixed Models with ISM Dust. *ApJ*, *527*, 893–909.

D'Angelo, C. R., & Spruit, H. C. (2010). Episodic accretion on to strongly magnetic stars. *MNRAS*, *406*, 1208–1219.

Delplancke, F., & Mosoni, L. (2009). Proceedings: VLTI Summer School. *New A Rev.*, *53*.

DENIS Consortium (2005). The DENIS database (DENIS Consortium, 2005). *VizieR Online Data Catalog*, *10*, 2002.

di Folco, E., Dutrey, A., Chesneau, O., Wolf, S., Schegerer, A., Leinert, C., & Lopez, B. (2009). The flared inner disk of the Herbig Ae star AB Aurigae revealed by VLTI/MIDI in the N-band. *A&A*, *500*, 1065–1076.

Dorschner, J., Begemann, B., Henning, T., Jaeger, C., & Mutschke, H. (1995). Steps toward interstellar silicate mineralogy. II. Study of Mg-Fe-silicate glasses of variable composition. *A&A*, *300*, 503.

Dullemond, C. P., & Dominik, C. (2004). Flaring vs. self-shadowed disks: The SEDs of Herbig Ae/Be stars. *A&A*, *417*, 159–168.

Dullemond, C. P., Hollenbach, D., Kamp, I., & D'Alessio, P. (2007). Models of the Structure and Evolution of Protoplanetary Disks. *Protostars and Planets V*, (pp. 555–572).

Dullemond, C. P., & Monnier, J. D. (2010). The Inner Regions of Protoplanetary Disks. *ARA&A*, *48*, 205–239.

Eisloffel, J., & Mundt, R. (1997). Parsec-Scale Jets From Young Stars. *AJ*, *114*, 280–287.

Eisner, J. A., & Hillenbrand, L. A. (2011). Resolving the Sub-AU-scale Gas and Dust Distribution in FU Orionis Sources. *ApJ*, *738*, 9.

Eisner, J. A., Hillenbrand, L. A., White, R. J., Bloom, J. S., Akeson, R. L., & Blake, C. H. (2007). Near-Infrared Interferometric, Spectroscopic, and Photometric Monitoring of T Tauri Inner Disks. *ApJ*, *669*, 1072–1084.

Evans, N., Calvet, N., Cieza, L., Forbrich, J., Hillenbrand, L., Lada, C., Merín, B., Strom, S., & Watson, D. (2009). The Diskionary: A Glossary of Terms Commonly Used for Disks and Related Objects, First Edition. *ArXiv e-prints, 0901.1691*.

Fedele, D., van den Ancker, M. E., Petr-Gotzens, M. G., & Rafanelli, P. (2007). Optical and infrared properties of V1647 Orionis during the 2003-2006 outburst. II. Temporal evolution of the eruptive source. *A&A*, *472*, 207–217.

Furlan, E., Hartmann, L., Calvet, N., D'Alessio, P., Franco-Hernández, R., Forrest, W. J., Watson, D. M., Uchida, K. I., Sargent, B., Green, J. D., Keller, L. D., & Herter, T. L. (2006). A Survey and Analysis of Spitzer Infrared Spectrograph Spectra of T Tauri Stars in Taurus. *ApJS*, *165*, 568–605.

Gail, H.-P. (2001). Radial mixing in protoplanetary accretion disks. I. Stationary disc models with annealing and carbon combustion. *A&A*, *378*, 192–213.

Gammie, C. F. (1996). Layered Accretion in T Tauri Disks. *ApJ*, *457*, 355.

Ghez, A. M., McCarthy, D. W., Patience, J. L., & Beck, T. L. (1997). The Multiplicity of Pre-Main-Sequence Stars in Southern Star-forming Regions. *ApJ*, *481*, 378.

Glass, I. S., & Penston, M. V. (1974). An infrared survey of RW Aurigae stars. *MNRAS*, *167*, 237–249.

Gorti, U., & Hollenbach, D. (2009). Photoevaporation of Circumstellar Disks By Far-Ultraviolet, Extreme-Ultraviolet and X-Ray Radiation from the Central Star. *ApJ*, *690*, 1539–1552.

Goto, M., Regály, Z., Dullemond, C. P., van den Ancker, M., Brown, J. M., Carmona, A., Pontoppidan, K., Ábrahám, P., Blake, G. A., Fedele, D., Henning, T., Juhász, A., Kóspál, Á., Mosoni, L., Sicilia-Aguilar, A., Terada, H., van Boekel, R., van Dishoeck, E. F., & Usuda, T. (2011). Fundamental Vibrational Transition of CO During the Outburst of EX Lupi in 2008. *ApJ*, *728*, 5.

Grankin, K. N., Melnikov, S. Y., Bouvier, J., Herbst, W., & Shevchenko, V. S. (2007). Results of the ROTOR-program. I. The long-term photometric variability of classical T Tauri stars. *A&A*, *461*, 183–195.

Gras-Velázquez, À., & Ray, T. P. (2005). Weak-line T Tauri stars: circumstellar disks and companions. I. Spectral energy distributions and infrared excesses. *A&A*, *443*, 541–556.

Green, J. D., Hartmann, L., Calvet, N., Watson, D. M., Ibrahimov, M., Furlan, E., Sargent, B., & Forrest, W. J. (2006). Spitzer IRS Observations of FU Orionis Objects. *ApJ*, *648*, 1099–1109.

Guenther, E. W., Esposito, M., Mundt, R., Covino, E., Alcalá, J. M., Cusano, F., & Stecklum, B. (2007). Pre-main sequence spectroscopic binaries suitable for VLTI observations. *A&A*, *467*, 1147–1155.

Gullbring, E., Hartmann, L., Briceno, C., & Calvet, N. (1998). Disk Accretion Rates for T Tauri Stars. *ApJ*, *492*, 323.

Güsten, R., Nyman, L. Å., Schilke, P., Menten, K., Cesarsky, C., & Booth, R. (2006). The Atacama Pathfinder EXperiment (APEX) - a new submillimeter facility for southern skies -. *A&A*, *454*, L13–L16.

Hallenbeck, S. L., Nuth, J. A., & Daukantas, P. L. (1998). Mid-Infrared Spectral Evolution of Amorphous Magnesium Silicate Smokes Annealed in Vacuum: Comparison to Cometary Spectra. *Icarus*, *131*, 198–209.

Hanner, M. S., Lynch, D. K., & Russell, R. W. (1994). The 8-13 micron spectra of comets and the composition of silicate grains. *ApJ*, *425*, 274–285.

Harker, D. E., & Desch, S. J. (2002). Annealing of Silicate Dust by Nebular Shocks at 10 AU. *ApJ*, *565*, L109–L112.

Hartmann, L. (2009). *Accretion Processes in Star Formation: Second Edition*. Cambridge University Press.

Hartmann, L., Calvet, N., Gullbring, E., & D'Alessio, P. (1998). Accretion and the Evolutiion of T Tauri Disks. *ApJ*, *495*, 385.

Hartmann, L., & Kenyon, S. J. (1996). The FU Orionis phenomenon. *ARA&A*, *34*, 207–240.

Henning, T., & Mutschke, H. (1997). Low-temperature infrared properties of cosmic dust analogues. *A&A*, *327*, 743–754.

Herbig, G. H. (1977). Eruptive phenomena in early stellar evolution. *ApJ*, *217*, 693–715.

Herbig, G. H. (1989). *ESO Workshop on Low-Mass Star Formation and Pre-Main Sequence Objects (ESO, Garching)*, *233*.

Herbig, G. H. (2007). EX Lupi: History and Spectroscopy. *AJ*, *133*, 2679–2683.

Herbig, G. H. (2008). History and Spectroscopy of EXor Candidates. *AJ*, *135*, 637–648.

Herbig, G. H., Aspin, C., Gilmore, A. C., Imhoff, C. L., & Jones, A. F. (2001). The 1993-1994 Activity of EX Lupi. *PASP*, *113*, 1547–1553.

Herbig, G. H., Suntzeff, N., & Blanco, B. (1992). The Photometric Range of EX Lupi. *Information Bulletin on Variable Stars*, *3755*, 1.

Herbst, W., Williams, E. C., & Hawley, W. P. (2004). A Photometric Study of Stars in the MBM 12 Association. *AJ*, *127*, 1594–1601.

Hughes, J., Hartigan, P., Krautter, J., & Kelemen, J. (1994). The stellar population of the Lupus clouds. *AJ*, *108*, 1071–1090.

Jaeger, C., Molster, F. J., Dorschner, J., Henning, T., Mutschke, H., & Waters, L. B. F. M. (1998). Steps toward interstellar silicate mineralogy. IV. The crystalline revolution. *A&A*, *339*, 904–916.

Johns-Krull, C. M. (2007). The Magnetic Fields of Classical T Tauri Stars. *ApJ*, *664*, 975–985.

Jones, A. F. A. L. (2008). EX Lupi. *Central Bureau Electronic Telegrams*, *1217*, 1.

Juhász, A., Dullemond, C. P., van Boekel, R., Bouwman, J., Ábrahám, P., Acosta-Pulido, J. A., Henning, T., Kóspál, A., Sicilia-Aguilar, A., Jones, A., Moór, A., Mosoni, L., Regály, Z., Szokoly, G., & Sipos, N. (2012). The 2008 Outburst of EX Lup – Silicate Crystals in Motion. *ApJ*, *744*, 118.

Juhász, A., Henning, T., Bouwman, J., Dullemond, C. P., Pascucci, I., & Apai, D. (2009). Do We Really Know the Dust? Systematics and Uncertainties of the Mid-Infrared Spectral Analysis Methods. *ApJ*, *695*, 1024–1041.

Kaufer, A., Stahl, O., Tubbesing, S., Nørregaard, P., Avila, G., Francois, P., Pasquini, L., & Pizzella, A. (1999). Commissioning FEROS, the new high-resolution spectrograph at La-Silla. *The Messenger*, *95*, 8–12.

Kemper, F., Vriend, W. J., & Tielens, A. G. G. M. (2004). The Absence of Crystalline Silicates in the Diffuse Interstellar Medium. *ApJ*, *609*, 826–837.

Kemper, F., Vriend, W. J., & Tielens, A. G. G. M. (2005). Erratum: "The Absence of Crystalline Silicates in the Diffuse Interstellar Medium" . *ApJ*, *633*, 534–534.

Kessler, M. F., Steinz, J. A., Anderegg, M. E., Clavel, J., Drechsel, G., Estaria, P., Faelker, J., Riedinger, J. R., Robson, A., Taylor, B. G., & Ximénez de Ferrán, S. (1996). The Infrared Space Observatory (ISO) mission. *A&A*, *315*, L27–L31.

Koike, C., Chihara, H., Tsuchiyama, A., Suto, H., Sogawa, H., & Okuda, H. (2003). Compositional dependence of infrared absorption spectra of crystalline silicate. II. Natural and synthetic olivines. *A&A*, *399*, 1101–1107.

Kóspál, Á., Ábrahám, P., Goto, M., Regály, Z., Dullemond, C. P., Henning, T., Juhász, A., Sicilia-Aguilar, A., & van den Ancker, M. (2011). Near-infrared Spectroscopy of EX Lupi in Outburst. *ApJ*, *736*, 72.

Kóspál, Á., Ábrahám, P., Prusti, T., Acosta-Pulido, J., Hony, S., Moór, A., & Siebenmorgen, R. (2007). The outburst of the eruptive young star OO Serpentis between 1995 and 2006. *A&A*, *470*, 211–219.

Kun, M., Szegedi-Elek, E., Moór, A., Kóspál, Á., Ábrahám, P., Apai, D., Kiss, Z. T., Klagyivik, P., Magakian, T. Y., Mező, G., Movsessian, T. A., Pál, A., Rácz, M., & Rogers, J. (2011). Inner disc rearrangement revealed by dramatic brightness variations in the young star PV Cep. *MNRAS*, *413*, 2689–2695.

Lada, C. J. (1987). Star formation - From OB associations to protostars. In M. Peimbert & J. Jugaku (Ed.) *Star Forming Regions*, vol. 115 of *IAU Symposium*, (pp. 1–17).

Leinert, C., Graser, U., Richichi, A., Schöller, M., Waters, L. F. B. M., Perrin, G., Jaffe, W., Lopez, B., Glazenborg-Kluttig, A., Przygodda, F., Morel, S., Biereichel, P., Haddad, N., Housen, N., & Wallander, A. (2003). MIDI combines light from the VLTI: the start of 10 μm interferometry at ESO. *The Messenger*, *112*, 13–18.

Leinert, C., van Boekel, R., Waters, L. B. F. M., Chesneau, O., Malbet, F., Köhler, R., Jaffe, W., Ratzka, T., Dutrey, A., Preibisch, T., Graser, U., Bakker, E., Chagnon, G., Cotton, W. D., Dominik, C., Dullemond, C. P., Glazenborg-Kluttig, A. W., Glindemann, A., Henning, T., Hofmann, K.-H., de Jong, J., Lenzen, R., Ligori, S., Lopez, B., Meisner, J., Morel, S., Paresce, F., Pel, J.-W., Percheron, I., Perrin, G., Przygodda, F., Richichi, A., Schöller, M., Schuller, P., Stecklum, B., van den Ancker, M. E., von der Lühe, O., & Weigelt, G. (2004). Mid-infrared sizes of circumstellar disks around Herbig Ae/Be stars measured with MIDI on the VLTI. *A&A*, *423*, 537–548.

Lemke, D., Klaas, U., Abolins, J., Abraham, P., Acosta-Pulido, J., Bogun, S., Castaneda, H., Cornwall, L., Drury, L., Gabriel, C., Garzon, F., Gemuend, H. P., Groezinger, U., Gruen, E., Haas, M., Hajduk, C., Hall, G., Heinrichsen, I., Herbstmeier, U., Hirth, G., Joseph, R., Kinkel, U., Kirches, S., Koempe, C., Kraetschmer, W., Kreysa, E., Krueger, H., Kunkel, M., Laureijs, R., Luetzow-Wentzky, P., Mattila, K., Mueller, T., Pacher, T., Pelz, G., Popow, E., Rasmussen, I., Rodriguez Espinosa, J., Richards, P., Russell, S., Schnopper, H., Schubert, J., Schulz, B., Telesco, C., Tilgner, C., Tuffs, R., Voelk, H., Walker,

H., Wells, M., & Wolf, J. (1996). ISOPHOT - capabilities and performance. *A&A*, *315*, L64–L70.

Li, M. P., Zhao, G., & Li, A. (2007). On the crystallinity of silicate dust in the interstellar medium. *MNRAS*, *382*, L26–L29.

Lis, D. C., Menten, K. M., & Zylka, R. (1999). Dust Continuum Imaging of the HH 24 Region in L1630. *ApJ*, *527*, 856–865.

Lisse, C. M., VanCleve, J., Adams, A. C., A'Hearn, M. F., Fernández, Y. R., Farnham, T. L., Armus, L., Grillmair, C. J., Ingalls, J., Belton, M. J. S., Groussin, O., McFadden, L. A., Meech, K. J., Schultz, P. H., Clark, B. C., Feaga, L. M., & Sunshine, J. M. (2006). Spitzer Spectral Observations of the Deep Impact Ejecta. *Science*, *313*, 635–640.

Lodato, G., & Clarke, C. J. (2004). Massive planets in FU Orionis discs: implications for thermal instability models. *MNRAS*, *353*, 841–852.

Lombardi, M., Lada, C. J., & Alves, J. (2008). Hipparcos distance estimates of the Ophiuchus and the Lupus cloud complexes. *A&A*, *480*, 785–792.

Luhman, K. L., Allen, P. R., Espaillat, C., Hartmann, L., & Calvet, N. (2010). The Disk Population of the Taurus Star-Forming Region. *ApJS*, *186*, 111–174.

Lynden-Bell, D., & Pringle, J. E. (1974). The evolution of viscous discs and the origin of the nebular variables. *MNRAS*, *168*, 603–637.

Malbet, F., & Perrin, G. (2007). Proceedings of the Euro Summer School "Observation and Data Reduction with with the VLT Interferometer". *New A Rev.*, *51*.

McGehee, P. M., Smith, J. A., Henden, A. A., Richmond, M. W., Knapp, G. R., Finkbeiner, D. P., Ivezić, v., & Brinkmann, J. (2004). The V1647 Orionis (IRAS 05436-0007) Protostar and Its Environment. *ApJ*, *616*, 1058–1064.

McKee, C. F., & Ostriker, E. C. (2007). Theory of Star Formation. *ARA&A*, *45*, 565–687.

McLaughlin, D. B. (1946). The nova-like variable star HV 11976. *AJ*, *52*, 109–+.

McNeil, J. W., Reipurth, B., & Meech, K. (2004). IRAS 05436-0007. *IAU Circ.*, *8284*, 1.

Melo, C. H. F. (2003). The short period multiplicity among T Tauri stars. *A&A*, *410*, 269–282.

Min, M., Dullemond, C. P., Dominik, C., de Koter, A., & Hovenier, J. W. (2009). Radiative transfer in very optically thick circumstellar disks. *A&A*, *497*, 155–166.

Min, M., Hovenier, J. W., & de Koter, A. (2005). Modeling optical properties of cosmic dust grains using a distribution of hollow spheres. *A&A*, *432*, 909–920.

Mosoni, L., Sipos, N., Ábrahám, P., Moór, A., Kóspál, A., Henning, T., Juhász, A., Kun, M., Leinert, C., Quanz, S., Ratzka, T., Schegerer, A., van Boekel, R., & Wolf, S. (2012). Dynamics during outburst: VLTI observations of the young eruptive star V1647 Ori during its 2003-2006 outburst. *A&A*, *submitted*.

Mundt, R., & Bastian, U. (1980). UBV photometry of young emission-line objects. *A&AS*, *39*, 245–250.

Muzerolle, J., Hartmann, L., & Calvet, N. (1998). A Br γ Probe of Disk Accretion in T Tauri Stars and Embedded Young Stellar Objects. *AJ*, *116*, 2965–2974.

Muzerolle, J., Megeath, S. T., Flaherty, K. M., Gordon, K. D., Rieke, G. H., Young, E. T., & Lada, C. J. (2005). The Outburst of V1647 Orionis Revealed by Spitzer. *ApJ*, *620*, L107–L110.

Natta, A. (1993). The temperature profile of T Tauri disks. *ApJ*, *412*, 761–770.

Natta, A., Testi, L., Muzerolle, J., Randich, S., Comerón, F., & Persi, P. (2004). Accretion in brown dwarfs: An infrared view. *A&A*, *424*, 603–612.

Nguyen, D. C., Jayawardhana, R., van Kerkwijk, M. H., Brandeker, A., Scholz, A., & Damjanov, I. (2009). Disk Braking in young Stars: Probing Rotation in Chamaeleon I and Taurus-Auriga. *ApJ*, *695*, 1648–1656.

Pascucci, I., Wolf, S., Steinacker, J., Dullemond, C. P., Henning, T., Niccolini, G., Woitke, P., & Lopez, B. (2004). The 2D continuum radiative transfer problem. Benchmark results for disk configurations. *A&A*, *417*, 793–805.

Pilbratt, G. L., Riedinger, J. R., Passvogel, T., Crone, G., Doyle, D., Gageur, U., Heras, A. M., Jewell, C., Metcalfe, L., Ott, S., & Schmidt, M. (2010). Herschel Space Observatory. An ESA facility for far-infrared and submillimetre astronomy. *A&A*, *518*, L1.

Pinte, C., Harries, T. J., Min, M., Watson, A. M., Dullemond, C. P., Woitke, P., Ménard, F., & Durán-Rojas, M. C. (2009). Benchmark problems for continuum radiative transfer. High optical depths, anisotropic scattering, and polarisation. *A&A*, *498*, 967–980.

Pojmanski, G. (2002). The All Sky Automated Survey. Catalog of Variable Stars. I. 0 h - 6 hQuarter of the Southern Hemisphere. *Acta Astron.*, *52*, 397–427.

Preibisch, T., Ossenkopf, V., Yorke, H. W., & Henning, T. (1993). The influence of ice-coated grains on protostellar spectra. *A&A*, *279*, 577–588.

Quanz, S. P., Henning, T., Bouwman, J., Ratzka, T., & Leinert, C. (2006). FU Orionis: The MIDI VLTI Perspective. *ApJ*, *648*, 472–483.

Quanz, S. P., Henning, T., Bouwman, J., van Boekel, R., Juhász, A., Linz, H., Pontoppidan, K. M., & Lahuis, F. (2007). Evolution of Dust and Ice Features around FU Orionis Objects. *ApJ*, *668*, 359–383.

Ratzka, T., Leinert, C., Henning, T., Bouwman, J., Dullemond, C. P., & Jaffe, W. (2007). High spatial resolution mid-infrared observations of the low-mass young star TW Hydrae. *A&A*, *471*, 173–185.

Reipurth, B., & Aspin, C. (2004). IRAS 05436-0007 and the Emergence of McNeil's Nebula. *ApJ*, *606*, L119–L122.

Rettig, T. W., Brittain, S. D., Gibb, E. L., Simon, T., & Kulesa, C. (2005). CO Emission and Absorption toward V1647 Orionis (McNeil's Nebula). *ApJ*, *626*, 245–252.

Rieke, G. H., Young, E. T., Engelbracht, C. W., Kelly, D. M., Low, F. J., Haller, E. E., Beeman, J. W., Gordon, K. D., Stansberry, J. A., Misselt, K. A., Cadien, J., Morrison, J. E., Rivlis, G., Latter, W. B., Noriega-Crespo, A., Padgett, D. L., Stapelfeldt, K. R., Hines, D. C., Egami, E., Muzerolle, J., Alonso-Herrero, A., Blaylock, M., Dole, H., Hinz, J. L., Le Floc'h, E., Papovich, C., Pérez-González, P. G., Smith, P. S., Su, K. Y. L., Bennett, L., Frayer, D. T., Henderson, D., Lu, N., Masci, F., Pesenson, M., Rebull, L., Rho, J., Keene, J., Stolovy, S., Wachter, S., Wheaton, W., Werner, M. W., & Richards, P. L. (2004). The Multiband Imaging Photometer for Spitzer (MIPS). *ApJS*, *154*, 25–29.

Rutten, R. J. (2003). *Radiative Transfer in Stellar Atmospheres*. Lecture Notes Utrecht University, 255 pages, 2003.

Schegerer, A. A., Wolf, S., Ratzka, T., & Leinert, C. (2008). The T Tauri star RY Tauri as a case study of the inner regions of circumstellar dust disks. *A&A*, *478*, 779–793.

Servoin, J. L., & Piriou, B. (1973). Infrared Reflectivity and Raman Scattering of Mg2SiO4 Single Crystal. *Physica Status Solidi B Basic Research*, *55*, 677–686.

Shakura, N. I., & Sunyaev, R. A. (1973). Black holes in binary systems. Observational appearance. *A&A*, *24*, 337–355.

Shu, F. H. (1977). Self-similar collapse of isothermal spheres and star formation. *ApJ*, *214*, 488–497.

Sicilia-Aguilar, A., Hartmann, L., Calvet, N., Megeath, S. T., Muzerolle, J., Allen, L., D'Alessio, P., Merín, B., Stauffer, J., Young, E., & Lada, C. (2006). Disk Evolution in Cep OB2: Results from the Spitzer Space Telescope. *ApJ*, *638*, 897–919.

Sicilia-Aguilar, A., Merín, B., Hormuth, F., Ábrahám, P., Henning, T., Kun, M., Patel, N., Juhász, A., Brandner, W., Hartmann, L. W., Csizmadia, S., & Moór, A. (2008). The Rapid Outbursting Star GM Cep: An EXor in Tr 37? *ApJ*, *673*, 382–399.

Sipos, N., Ábrahám, P., Acosta-Pulido, J., Juhász, A., Kóspál, Á., Kun, M., Moór, A., & Setiawan, J. (2009). EX Lupi in quiescence. *A&A*, *507*, 881–889.

Sipos, N., & Kóspál, A. (2012). The inner disks of EXors. *A&A*, *in prep*.

Sitko, M. L., Carpenter, W. J., Kimes, R. L., Wilde, J. L., Lynch, D. K., Russell, R. W., Rudy, R. J., Mazuk, S. M., Venturini, C. C., Puetter, R. C., Grady, C. A., Polomski, E. F., Wisnewski, J. P., Brafford, S. M., Hammel, H. B., & Perry, R. B. (2008). Variability of Disk Emission in Pre-Main-Sequence and Related Stars. I. HD 31648 and HD 163296: Isolated Herbig Ae Stars Driving Herbig-Haro Flows. *ApJ*, *678*, 1070–1087.

Tsukagoshi, T., Kitamura, Y., Kawabe, R., Saito, M., Yokogawa, S., & Kurono, Y. (2005). Millimeter Continuum Observations of McNeil's Nebula Object. *PASJ*, *57*, L21–L24.

Vacca, W. D., Cushing, M. C., & Simon, T. (2004). Near-Infrared Spectroscopy of MCNeil's Nebula Object. *ApJ*, *609*, L29–L32.

van Boekel, R., Min, M., Leinert, C., Waters, L. B. F. M., Richichi, A., Chesneau, O., Dominik, C., Jaffe, W., Dutrey, A., Graser, U., Henning, T., de Jong, J., Köhler, R., de Koter, A., Lopez, B., Malbet, F., Morel, S., Paresce, F., Perrin, G., Preibisch, T., Przygodda, F., Schöller, M., & Wittkowski, M. (2004). The building blocks of planets within the 'terrestrial' region of protoplanetary disks. *Nature*, *432*, 479–482.

Vinković, D., & Jurkić, T. (2007). Relation between the Luminosity of Young Stellar Objects and Their Circumstellar Environment. *ApJ*, *658*, 462–479.

Vorobyov, E. I., & Basu, S. (2006). The Burst Mode of Protostellar Accretion. *ApJ*, *650*, 956–969.

Vorobyov, E. I., & Basu, S. (2010). The Burst Mode of Accretion and Disk Fragmentation in the Early Embedded Stages of Star Formation. *ApJ*, *719*, 1896–1911.

Weingartner, J. C., & Draine, B. T. (2001). Dust Grain-Size Distributions and Extinction in the Milky Way, Large Magellanic Cloud, and Small Magellanic Cloud. *ApJ*, *548*, 296–309.

Werner, M. W., Roellig, T. L., Low, F. J., Rieke, G. H., Rieke, M., Hoffmann, W. F., Young, E., Houck, J. R., Brandl, B., Fazio, G. G., Hora, J. L., Gehrz, R. D., Helou, G., Soifer, B. T., Stauffer, J., Keene, J., Eisenhardt, P., Gallagher, D., Gautier, T. N., Irace, W., Lawrence, C. R., Simmons, L., Van Cleve, J. E., Jura, M., Wright, E. L., & Cruikshank, D. P. (2004). The Spitzer Space Telescope Mission. *ApJS*, *154*, 1–9.

White, R. J., & Basri, G. (2003). Very Low Mass Stars and Brown Dwarfs in Taurus-Auriga. *ApJ*, *582*, 1109–1122.

White, R. J., & Hillenbrand, L. A. (2004). On the Evolutionary Status of Class I Stars and Herbig-Haro Energy Sources in Taurus-Auriga. *ApJ*, *616*, 998–1032.

Whitney, B. A., Wood, K., Bjorkman, J. E., & Cohen, M. (2003). Two-dimensional Radiative Transfer in Protostellar Envelopes. II. An Evolutionary Sequence. *ApJ*, *598*, 1079–1099.

Williams, J. P., & Cieza, L. A. (2011). Protoplanetary Disks and Their Evolution. *ARA&A*, *49*, 67–117.

Wolf, S., & Garcia, P. (2008). Circumstellar Disks and Planets at Very High Angular Resolution, Proceedings of the VLTI Euro Summer School Held in Porto, Portugal, 28 May-8 June 2007. *New A Rev.*, *52*.

Wolf, S., Henning, T., & Stecklum, B. (1999). Multidimensional self-consistent radiative transfer simulations based on the Monte-Carlo method. *A&A*, *349*, 839–850.

Wolf, S., Henning, T., & Stecklum, B. (2003). MC3D-simulating polarization maps and more. In S. Fineschi (Ed.) *Society of Photo-Optical Instrumentation Engineers (SPIE) Conference Series*, vol. 4843 of *Society of Photo-Optical Instrumentation Engineers (SPIE) Conference Series*, (pp. 524–532).

Wood, K., Lada, C. J., Bjorkman, J. E., Kenyon, S. J., Whitney, B., & Wolff, M. J. (2002). Infrared Signatures of Protoplanetary Disk Evolution. *ApJ*, *567*, 1183–1191.

Zhu, Z., Hartmann, L., Gammie, C., & McKinney, J. C. (2009). Two-dimensional Simulations of FU Orionis Disk Outbursts. *ApJ*, *701*, 620–634.